# A non-Gaussian probabilistic approach for the equivalent static loads of wind effects in structural dynamics from wind tunnel measurements

Wafaa Kassir

UNIVERSITÉ PARIS-EST

Année 2017

THÈSE

pour obtenir le grade de

DOCTEUR DE L'UNIVERSITÉ PARIS-EST

**Discipline : Génie Civil**

présentée et soutenue publiquement par

Wafaa Kassir

le 7 septembre 2017

Title :

# A non-Gaussian probabilistic approach for the equivalent static loads of wind effects in structural dynamics from wind tunnel measurements

**JURY**

| | | |
|---|---|---|
| M Roger OHAYON | Professeur, CNAM | Président du jury |
| M Geert LOMBAERT | Professeur, KU Leuven | Rapporteur |
| M Roger GHANEM | Professeur, University of Southern California | Rapporteur |
| M Denis DUHAMEL | Professeur, Ecole des Ponts ParisTech | Examinateur |
| M Christian SOIZE | Professeur, UPEM | Directeur de thèse |
| M Jean-Vivien HECK | CSTB | Co-encadrant |
| M Fabrice DE OLIVEIRA | CSTB | Co-encadrant |
| M Jean-Marc JAEGER | Setec-TPI | Invité |
| M Adrien ESCOFFIER | Elioth | Invité |

# Short abstract

A novel probabilistic approach is presented for estimating the equivalent static wind loads that produce a static response of the structure, which is ”equivalent” in a probabilistic sense, to the extreme dynamical responses due to the unsteady pressure random field induced by the wind. This approach has especially been developed for the case for which a large number of unsteady pressure sensors are carried out on complex structures (such stadium roofs) in a boundary layer wind tunnel, but for which the time duration of the measurements are not sufficient for estimating the extreme value statistics of responses. The measured unsteady pressure random field is non-Gaussian. The method proposed is adapted to complex structures described by finite element model, for which the quasi-static part of the responses is important with respect to the dynamical part. The proposed approach is experimentally validated with a relatively simple application and is then applied to a stadium roof structure for which experimental measurements of unsteady pressures have been performed in a boundary layer wind tunnel.

# Long abstract

In order to estimate the equivalent static wind loads, which produce the extreme quasi-static and dynamical responses of structures submitted to random unsteady pressure field induced by the wind effects, a new probabilistic method is proposed. This method allows for computing the equivalent static wind loads for structures with complex aerodynamic flows such as stadium roofs, for which the pressure field is non-Gaussian, and for which the dynamical response of the structure cannot simply be described by using only the first elastic modes (but require a good representation of the quasi-static responses). Usually, the wind tunnel measurements of the unsteady pressure field applied to a structure with complex geometry are not sufficient for constructing a statistically converged estimation of the extreme values of the dynamical responses. Such a convergence is necessary for the estimation of the equivalent static loads in order to reproduce the extreme dynamical responses induced by the wind effects taking into account the non-Gaussianity of the random unsteady pressure field. In this work, (1) a generator of realizations of the non-Gaussian unsteady pressure field is constructed by using the realizations that are measured in the boundary layer wind tunnel; this generator based on a polynomial chaos representation allows for generating a large number of independent realizations in order to obtain the convergence of the extreme value statistics of the dynamical responses, (2) a reduced-order model with quasi-static acceleration terms is constructed, which allows for accelerating the convergence of the structural dynamical responses by using only a small number of elastic

modes of the structure, (3) a novel probabilistic method is proposed for estimating the equivalent static wind loads induced by the wind effects on complex structures that are described by finite element models, preserving the non-Gaussian property and without introducing the concept of responses envelopes. The proposed approach is experimentally validated with a relatively simple application and is then applied to a stadium roof structure for which experimental measurements of unsteady pressures have been performed in boundary layer wind tunnel.

**Keywords:** Equivalent static wind loads; Non-Gaussian unsteady pressure field; Polynomial chaos expansion; Quasi-static responses; Stochastic dynamics; Extreme value statistics.

# Résumé court

Une nouvelle approche probabiliste est présentée pour estimer les forces statiques équivalentes du vent qui produisent une réponse statique de la structure, qui est ”équivalente” au sens probabiliste, aux réponses dynamiques extrêmes induites par le champ aléatoire des pressions instationnaires dues aux effets du vent. Cette approche a été spécialement développée pour le cas où un grand nombre de capteurs de pression instationnaire sont utilisés pour les mesures sur des structures complexes (telles que des toitures de stade) dans une soufflerie à couche limite turbulente, mais pour laquelle la durée des mesures n'est pas suffisante pour estimer correctement les statistiques des valeurs extrêmes des réponses. Le champ aléatoire de pression instationnaire mesuré est non gaussien. La méthode proposée est adaptée à des structures complexes décrites par un modèle éléments finis, pour lesquelles la partie quasi-statique des réponses est importante par rapport à la partie dynamique. L'approche proposée est validée expérimentalement sur un exemple relativement simple et est ensuite appliquée à une structure de toiture de stade pour laquelle des mesures expérimentales des pressions instationnaires ont été effectuées dans une soufflerie à couche limite turbulente.

# Résumé long

Afin d'estimer les forces statiques équivalentes du vent, qui produisent les réponses quasi-statiques et dynamiques extrêmes dans les structures soumises au champ de pression instationnaire induit par les effets du vent, une nouvelle méthode probabiliste est proposée. Cette méthode permet de calculer les forces statiques équivalentes du vent pour les structures avec des écoulements aérodynamiques complexes telles que les toitures de stade, pour lesquelles le champ de pression n'est pas gaussien et pour lesquelles la réponse dynamique de la structure ne peut

être simplement décrite en utilisant uniquement les premiers modes élastiques (mais nécessitent une bonne représentation des réponses quasi-statiques). Généralement, les mesures en soufflerie du champ de pression instationnaire appliqué à une structure dont la géométrie est complexe ne suffisent pas pour construire une estimation statistiquement convergée des valeurs extrêmes des réponses dynamiques de la structure. Une telle convergence est nécessaire pour l'estimation des forces statiques équivalentes afin de reproduire les réponses dynamiques extrêmes induites par les effets du vent en tenant compte de la non-gaussianité du champ de pression aléatoire instationnaire. Dans ce travail, (1) un générateur de réalisation du champ de pression instationnaire non gaussien est construit en utilisant les réalisations qui sont mesurées dans la soufflerie à couche limite turbulente; ce générateur basé sur une représentation en chaos polynomiaux permet de construire un grand nombre de réalisations indépendantes afin d'obtenir la convergence des statistiques des valeurs extrêmes des réponses dynamiques, (2) un modèle d'ordre réduit avec des termes d'accélération quasi-statique est construit et permet d'accélérer la convergence des réponses dynamiques de la structure en n'utilisant qu'un petit nombre de modes élastiques, (3) une nouvelle méthode probabiliste est proposée pour estimer les forces statiques équivalentes induites par les effets du vent sur des structures complexes décrites par des modèles éléments finis, en préservant le caractère non gaussien et sans introduire le concept d'enveloppes des réponses. L'approche proposée est validée expérimentalement avec une application relativement simple et elle est ensuite appliquée à une structure de toiture de stade pour laquelle des mesures expérimentales de pressions instationnaires ont été effectuées dans la soufflerie à couche limite turbulente.

**Mots clé:** Force statique équivalente du vent, Champ de pression instationnaire non gaussien, Représentation en chaos polynomiaux, Réponses quasi-statiques, Dynamique stochastique, Statistiques des valeurs extrêmes.

# Acknowledgement

First of all, I would like to express my sincere gratitude to my advisor Professor Christian Soize for the continuous support of my Ph.D study and related research, for his patience, motivation, and immense knowledge. His guidance helped me in all the time of research and writing of this thesis. I could not have imagined having a better advisor and mentor for my Ph.D study.
Besides my advisor, I would like to thank the rest of my thesis co-supervisors: Jean-Vivien Heck and Fabrice De Oliveira, for their insightful comments and encouragement, but also for their valuable and indispensable contribution in this thesis.
My sincere thanks also goes to Professor Roger Ghanem and to Professor Geert Lombaert for having accepted to participate in the thesis jury and to report on my work. I would like to thank also Professor Roger Ohayon, Professor Denis Duhamel, Mr. Jean-Marc Jaeger and Mr. Adrien Escoffier for accepting to be in the thesis jury.
A very special gratitude goes out to all my colleagues at CSTB and my labmates at UPEM for the stimulating discussions, for the time we worked together, and for all the fun we have had in the last three years.
My dear friends Mohamad, Julie, Alexandre, Darine, Salam, Rabab, Alex, Zak, Perla, and Ali thank you very much for being always there for me. I am so blessed to have you.
Finally, I must express my very profound gratitude to my beloved parents for their selfless love, unfailing support, and continuous encouragement over the years. Thank you, this accomplishment would not have been possible without you.

# Contents

# Notations

| | |
|---|---|
| $\mathbb{e}$ | Principal equivalent static force |
| $\underline{\mathbf{f}}$ | External force mean value |
| $\mathbb{f}^{e,s}$ | Total equivalent static force |
| $\mathbf{f}^{e,s}$ | Centered equivalent static force |
| $g_{\text{gauss}}$ | Gust loading factor computed with the Gaussian hypothesis |
| $g+$ | Non-Gaussian Gust loading factor for a maximum |
| $g-$ | Non-Gaussian Gust loading factor for a minimum |
| $[\widehat{\mathbb{h}}_N^c(\omega)]$ | Frequency response function of order $N$ without quasi-static term |
| $[\widehat{\mathbb{h}}_N^{c,acc}(\omega)]$ | Frequency response function of order $N$ with quasi-static term |
| $m$ | Number of degrees of freedom |
| $m_{\mathbb{e}}$ | Number of the principal equivalent static forces |
| $m_{\text{exp}}$ | Dimension of the vector-valued unsteady pressure |
| $m_f$ | Number of the equivalent static forces |
| $m_u$ | Dimension of the observation vector |
| $n_r$ | Number of experimental realizations |
| $n_p$ | Number of time steps in the time window |
| $\underline{\mathbf{p}}$ | Vector of the unsteady pressure mean value |
| $\mathbf{p}^{\text{MV}}$ | Vector of the centered equivalent static pressure |
| $\mathbf{q}^{\text{MV}}$ | Centered equivalent static generalized coordinates associated with $\mathbf{p}^{\text{MV}}$ |
| $t$ | Time in s |
| $\underline{\mathbf{u}}$ | Observation mean value |

| | |
|---|---|
| $\mathbb{u}^{e,s}$ | Equivalent static observation |
| $\mathbf{u}^{e,s}$ | Centered equivalent static observation |
| $\underline{v}$ | Mean wind profile |
| $\underline{\mathbf{y}}$ | Displacement mean value |
| $\mathbf{y}^{e,s}$ | Equivalent static displacement |
| | |
| $[A_c]$ | Controlability matrix |
| $[A_o]$ | Observability matrix |
| $[D]$ | Damping matrix |
| $\mathbf{F}$ | External forces vector |
| $\mathbb{F}^e$ | Total equivalent force |
| $\mathbf{F}^e$ | Centered equivalent force |
| $\mathbf{H}$ | Coordinates of the KL expansion of $\mathbf{P}$ |
| $[K]$ | Stiffness matrix |
| $[M]$ | Mass matrix |
| $N$ | Number of modes used in the reduced-order model |
| $N_d$ | Maximum degree of the normalized Hermite polynomial used in the PCE of $\mathbf{H}$ |
| $N_g$ | Length of the Gaussian germ used in the PCE of $\mathbf{H}$ |
| $N_{\text{KL}}$ | Reduction order of the KL expansion of $\mathbf{P}$ |
| $N_{\text{PCA}}$ | Reduction order of the PCA of $\mathbf{P}(T)$ |
| $\mathbb{P}$ | Total pressure vector-valued stochastic process |
| $\mathbf{P}$ | Centered pressure vector-valued stochastic process |
| $\mathbb{P}^{\text{exp}}$ | Total experimental pressure vector-valued stochastic process |
| $\mathbf{P}^{\text{exp}}$ | Centered experimental pressure field |

| | |
|---|---|
| $\mathbb{Q}$ | Generalized coordinates associated with $\mathbb{P}$ |
| $\mathbf{Q}$ | Centered generalized coordinates associated with $\mathbf{P}$ |
| $[S_{\mathbf{P}}(w)]$ | Matrix-valued spectral density function of $\mathbf{P}$ |
| $[S_{\mathbf{P}^{\exp}}(w)]$ | Matrix-valued spectral density function of $\mathbf{P}^{\exp}$ |
| $T$ | Time window duration in s |
| $T_{\text{tot}}$ | Total duration of measurements in s |
| $\mathbb{U}$ | Observation vector associated with $\mathbb{P}$ |
| $\mathbf{U}$ | Centered observation vector associated with $\mathbf{P}$ |
| $\mathbb{U}_{\max}$ | Maximum of $\mathbb{U}(t)$ on $[0\,,T]$ |
| $\mathbf{U}_{\max}$ | Maximum of $\mathbf{U}$ on $[0\,,T]$ |
| $\underline{\mathbf{U}}_{\max}$ | Mean value of $\mathbf{U}_{\max}$ |
| $\mathbb{U}_{\min}$ | Minimum of $\mathbb{U}(t)$ on $[0\,,T]$ |
| $\mathbf{U}_{\min}$ | Minimum of $\mathbf{U}$ on $[0\,,T]$ |
| $\underline{\mathbf{U}}_{\min}$ | Mean value of $\mathbf{U}_{\min}$ |
| $\mathbf{X}$ | Centered displacement vector associated with $\mathbf{P}$ |
| $\mathbf{Y}$ | Displacement vector associated with $\mathbb{P}$ |
| | |
| $\boldsymbol{\eta}^{e,s}$ | Equivalent static coordinates of $\mathbf{H}$ |
| $[\lambda_N]$ | Diagonal matrix of eigenvalues |
| $\nu$ | Number of the generated independent realizations |
| $\nu_c$ | Cutoff frequency in Hz |
| $\nu_e$ | Sampling frequency in Hz |
| $\xi$ | Damping rate |
| $[\varphi^N]$ | Matrix of modes |
| $\omega$ | Frequency in rad/s |

| | |
|---|---|
| $\omega_c$ | Cutoff frequency in rad/s |
| $\Delta t$ | Sampling time step in s |
| $[\Phi_N^c]$ | Modal controlability matrix |
| $[\Phi_N^o]$ | Modal observability matrix |
| $\mathscr{B}$ | Frequency band of analysis |
| $\mathscr{D}$ | Domain associated with the observation |
| $\mathscr{D}^c$ | Centered domain associated with the observation |
| $\mathscr{D}_{\text{inf}}$ | Lower bound of $\mathscr{D}$ |
| $\mathscr{D}_{\text{sup}}$ | Upper bound of $\mathscr{D}$ |
| $\mathscr{D}^c_{\text{inf}}$ | Lower bound of $\mathscr{D}^c$ |
| $\mathscr{D}^c_{\text{sup}}$ | Upper bound of $\mathscr{D}^c$ |
| DOF | Degree Of Freedom |
| FRF | Frequency Response Function |
| KL | Karhunen-Loève expansion |
| PCA | Principal Component Analysis |
| PCE | Polynomial Chaos Expansion |
| PDF | Probability Density Function |
| PSD | Power Spectral Density |

**Deterministic variable:** A deterministic scalar variable is denoted by a lower case letter such as $x$.

**Deterministic vector:** A deterministic vector is denoted by a boldface, lower case letter such as in $\mathbf{x} = (x_1, \ldots, x_n)$.

**Random variable:** A random scalar variable is denoted by an upper case letter such as $X$.

**Random vector:** A random vector is denoted by a boldface, upper case letter such as in $\mathbf{X} = (X_1, \ldots, X_n)$.

**Deterministic matrix:** A deterministic matrix is denoted by an upper (or lower) case letter between brackets such as $[A]$ (or $[a]$).

**Random matrix:** A random matrix is denoted by a boldface, upper case letter between brackets such as $[\mathbf{A}]$.

| | |
|---|---|
| $\mathbf{x}$ | $\mathbf{x} = (x_1, \ldots, x_n)$: vector in $\mathbb{R}^n$ or in $\mathbb{C}^n$. |
| $\overline{x}_j$ | Complex conjugate of the complex number $x_j$. |
| $\mathrm{tr}\{[A]\}$ | Trace of matrix $[A]$. |
| $[A]^T$ | Transpose of matrix $[A]$. |
| $[A]^*$ | Transpose conjugate of matrix $[A]$ (adjoint matrix). |
| $[I_n]$ | Identity (or unit) matrix in $\mathbb{M}_n$. |
| $\delta_{jk}$ | Kronecker's symbol such that $\delta_{jk} = 0$ if $j \neq k$ and $\delta_{jk} = 1$ if $j = k$. |
| $\mathbb{1}_B(\mathbf{x})$ | Indicator function of a set $B$ defined by $\mathbb{1}_B(\mathbf{x}) = 1$ if $\mathbf{x} \in B$ and $\mathbb{1}_B(\mathbf{x}) = 0$ if $\mathbf{x} \notin B$. |
| $i$ | Pure imaginary complex number satisfying $i^2 = -1$. |

| | |
|---|---|
| $\mathbb{C}$ | Set of all the complex numbers |
| $\mathbb{R}$ | Set of all the real numbers |
| $\mathbb{R}^+$ | Set $[0\,, +\infty[$ of all the positive and zero real numbers. |
| $\mathbb{R}^n$ | Euclidean vector space of dimension $n$. |
| $\mathbb{N}$ | Set of all the integers $0, 1, 2, \ldots$. |

| | |
|---|---|
| $\mathbb{N}^*$ | Set of all the positive integers $1, 2, \ldots$. |
| $\mathbb{M}_{n,m}(\mathbb{R})$ | Set of all the $(n \times m)$ real matrices. |
| $\mathbb{M}_{n,m}(\mathbb{C})$ | Set of all the $(n \times m)$ complex matrices. |
| $\mathbb{M}_n(\mathbb{R})$ | Set of all the $(n \times n)$ real matrices. |
| $\mathbb{M}_n(\mathbb{C})$ | Set of all the $(n \times n)$ complex matrices. |
| $\mathbb{M}_n^+(\mathbb{R})$ | Set of all the positive-definite symmetric $(n \times n)$ real matrices. |
| $\mathbb{M}_n^{+0}(\mathbb{R})$ | Set of all the semipositive-definite symmetric $(n \times n)$ real matrices. |

| | |
|---|---|
| $E$ | Mathematical expectation. |
| $(\Theta, \mathcal{T}, \mathscr{P})$ | Probability space. |
| $\mathbf{L}^2(\omega, \mathbb{R}^n)$ | Vector space (Hilbert space) of all the square integrable functions defined on a subset $\omega$ of $\mathbb{R}^d$ with values in $\mathbb{R}^n$. |

| | |
|---|---|
| $< \mathbf{x}, \mathbf{y} >_{\mathbb{R}^n}$ | Euclidean inner product $\sum_{j=1}^n x_j y_j$ in $\mathbb{R}^n$. |
| $< \mathbf{x}, \mathbf{y} >_{\mathbb{C}^n}$ | Hermitian inner product $\sum_{j=1}^n x_j y_j$ in $\mathbb{C}^n$. |
| $\|[A]\|_F$ | Frobenius norm $\sqrt{\text{tr}\{[A]^T[A]\}}$ for any real matrix $[A]$. |
| $\|[A]\|_F$ | Frobenius norm $\sqrt{\text{tr}\{[A]^*[A]\}}$ for any complex matrix $[A]$. |

# Chapter 1

# Introduction and objectives

## 1.1 Industrial context

Design of structures subjected to wind effects for which the unsteady aerodynamic flow is complex, requires first the knowledge of the unsteady pressure field generated by the wind on the structure as a function of its environment. For a structure with complex geometry, such as the roof of a stadium, for instance, the unsteady pressure field is measured in a boundary layer wind tunnel with a turbulent incident flow. This framework is the one used in this work. For such situations, the number of unsteady pressure sensors is relatively large (of the order of one thousand) and the acquisition time is necessarily limited by many factors. This implies that the knowledge of the measured unsteady pressures is generally not sufficient to estimate converged statistics. It is therefore necessary to develop models that allow the knowledge of the unsteady measured pressures to be increased by using numerical simulations. Finally, the computation of the stresses in the structural elements of the structure subjected to the unsteady pressure field taking into account the dynamical effects must be carried out. This step induces a large amount of calculations and analyses for the design and the justification of the structure, which is not always compatible with the time constraints imposed to the study offices. Consequently, it is important to develop methodologies and numerical methods that allow for computing the equivalent static loads, which induce the extreme values that are used for design. When the structure behavior and the aerodynamic flow are relatively simple, methods for computing the equivalent static loads have been successfully developed and are available in the literature. In the case of complex structures with complex aerodynamic flows such as stadium roofs, efficient and robust methods had to be improved / developed.

## 1.2 Industrial objectives

The industrial objective is to develop an efficient and robust method, validated on a simple structure and on a complex structure such as a stadium roof, to compute the equivalent static forces that induce the same extreme stresses, such as those induced by the unsteady aerodynamic effects of wind, with the following assumptions:

- the unsteady pressure field induced by the wind is measured in a wind tunnel,
- the structure has a linear behavior,
- the dynamic effects must be taken into account.

## 1.3 State of the art

The framework of this work requires knowledge about:

- random signal processing to analyze the wind tunnel measurements of unsteady pressures applied to the structure;
- stochastic dynamics and associated numerical methods for linear behavior structures subjected to wind loads;
- probabilistic and statistical methods for the construction of equivalent static loads;
- probabilistic modeling of the wind speed in the 0-300 meters boundary layer for validating the methodology on a simple example for which unsteady pressure measurements in a wind tunnel are not available.

**Random signal processing**
The random signal processing is extremely developed in the literature. This work does not require any special development and only uses standard methods [85, 92, 93, 97, 116].

**Dynamic linear responses of structures subjected to wind loads in a Gaussian framework and experimental measurements**
Once the first stochastic models of wind were developed, they were used to calculate the linear stochastic dynamical responses of tall buildings, introducing reduced modal models of the structure and computing estimates of extreme value

statistics related to the random dynamical responses. These estimates are based on the use of sample paths statistics of Gaussian processes that have allowed the "gust loading factor" concept to be introduced. Davenport [29] was the pioneer. Numerous studies have then been made by using the same assumptions but by improving models and conducting many experimental validations in full scale and in turbulent-boundary-layer wind tunnels, such as [5, 6, 29, 32, 33, 39, 41, 59, 71, 74, 77, 78, 107, 121, 122, 131, 132, 134, 136, 137]. In addition, a lot of works have been performed for exceptional structures such as, for instance, the wind effects on super-tall buildings [143, 84, 141, 65], on super long-span cable bridges [142], and on silo groups [57, 58].

**Probabilistic and statistical methods for the construction of the equivalent static loads**

Relatively early, late 60's and early 70's, research have been done to develop methods for calculating the equivalent static loads producing the same extreme dynamical responses of structures subjected to wind effects. The first proposed approaches were then widely developed with many applications in civil engineering structures, such as [9, 18, 19, 21, 24, 42, 52, 60, 62, 75, 73, 76, 81, 98, 105, 125, 130, 140, 145, 146, 144, 94].

Several works were carried out to take into account the non-Gaussian property of the random responses for estimating the gust loading factor. Such a non-Gaussianity is mainly due either to the aerodynamic drag ([77, 108, 109]) or to the unsteady pressure field applied to the buildings, which is a nonlinear function of the velocity field (see for instance [107, 133]). Some works related to the calculation of linear and nonlinear structural responses use representations of the stochastic responses such as the Principal Component Analysis or the Proper Orthogonal Decomposition [20, 126]. Recently, some correction terms have been introduced to take into account the non-Gaussianity of the unsteady pressure field in order to calculate the extreme value statistics [10, 83, 8] using an orthogonal polynomial expansion of probability density functions (method that was already used in the 70s).

**Modeling of wind in the 0-300 meters boundary layer**

The modeling of the wind speed by a stochastic process in the 0-300 meters boundary layer, which allows for taking into account the turbulence and for calculating its dynamic effects on structures from experimental measurements, began in the 1960's with the Davenport works [30, 31], which then gave rise to numerous studies to improve the stochastic models based on full scale experimental measurements, such as [7, 38, 51, 55, 101, 104, 106, 107].

## 1.4 Scientific objectives

It is assumed that the number of unsteady pressure sensors, which are required for performing experimental measurements of the unsteady pressure field applied to a structure with complex geometry, is relatively high (about $1{,}000$). Under this hypothesis, the number of time trajectories measured by the set of sensors over a sufficiently long duration (about $10$ minutes in scale $1$) remains limited (about $100$). Under these conditions, the measurements do not allow us to construct a statistically converged estimation of the extreme values of the dynamical responses, what are necessary for the determination of the equivalent static forces in order to reproduce the wind action on the structure taking into account the non-Gaussianity of the random unsteady pressure field. The scientific objectives of this thesis are the following:

- construction of a generator of a non-Gaussian vector-valued stochastic process in high dimension (number of pressure sensors) for which a small number of realizations are available (wind tunnel pressure measurements);
- construction of a time-domain reduced-order model in linear structural dynamics, including a term of quasi-static acceleration that allows us to ensure the convergence of the stochastic responses by using only a small number of elastic modes;
- construction of the equivalent static forces based on a non-Gaussian probabilistic model and on extreme value statistics.
- Validation of the developed methods.

## 1.5 Proposed approach in the thesis

A new probabilistic approach is proposed to estimate the equivalent static forces of wind, which produce a static response of the structure, which is "equivalent" in a probabilistic sense, to the dynamical responses due to the random unsteady pressure field induced by wind. The subject concerning the estimation of the equivalent static forces (that represent the wind effects on structures) has widely been developed since 1970 (see [105, 24, 75, 73]) and have given rise to many works and applications [18, 19, 21, 42, 60, 62, 76, 98, 130, 145, 146, 144], and more recently to [9, 52, 81, 125, 140]. The approach proposed in this thesis is based on the following assumptions and methods:

- the stochastic process of the spatially discretized unsteady pressure field is assumed to be non-Gaussian;

- a representation of the non-Gaussian stochastic process that models the discretized unsteady pressure field is constructed using the polynomial chaos expansion method. This representation is identified in inverse using the wind tunnel measurements. We then obtain a generator of realizations of the pressure random field, which allows for generating additional realizations to those measured in the wind tunnel;
- the reduced dynamical model of the structure includes a quasi-static correction term that allows the convergence of the stochastic dynamical responses to be obtained by using only a small number of elastic modes;
- the equivalent static forces are estimated by a maximum likelihood principle conditioned by the extreme values of the observations (internal forces, displacement, etc.) in the structure.

## 1.6 Novelties with respect to the state of the art

With respect to the existing methods, the novelties of the approach proposed in this thesis, are the following.

- A quasi-static correction term is introduced in the construction of the reduced-order model, for three-dimensional structures that exhibit, in the frequency band of analysis, a numerous local modes interwined with global modes. Such a quasi-static correction term allows for limiting the number of modes to those whose eigenfrequencies belong to the frequency band of analysis while ensuring a perfect convergence of the reduced-order model.
- The non-Gaussianity of the unsteady pressure field is taken into account for estimating the extreme values statistics of the time responses. The centered unsteady pressure field is represented by a centered vector-valued stochastic process $\mathbf{P} = \{\mathbf{P}(t), t \in [0\,, T]\}$ that corresponds to its spatial discretization. The non-Gaussian character of stochastic process $\mathbf{P}$ is not described by a given prior probability model for which its hyperparameter would be identified with the experiments. Non-Gaussian stochastic process $\mathbf{P}$ is constructed by using a general nonparametric probability model based on the use of a Karhunen-Loève expansion for which the non-Gaussian random coordinates are represented by a polynomial chaos expansion whose coefficients are identified with measurements performed in a boundary layer wind tunnel. Consequently, absolutely no hypotheses are introduced *a priori* and in addition, not only the non-Gaussian marginal probability distribution of order 1 is taken into account, but all the system of the non-Gaussian probability distributions of stochastic process $\mathbf{P}$ is indirectly constructed.

- This non-Gaussian probability model of stochastic process **P** is used for generating a large number of additional realizations that are required for estimating extreme values statistics of the non-Gaussian time responses.

- A set of observations is defined corresponding to internal forces and/or displacements in given finite elements of the computational model. For each given subset of the set of observations, an equivalent static force is estimated. The principal static forces are therefore classically deduced of the set of the equivalent static forces.

- A novel approach is also proposed for estimating equivalent static forces associated with a subset of observations, which is based on the use of the maximum likelihood principle applied to an adapted random vector of the formulation. The proposed approach ensures to preserve the phases of time responses for all the components of the observations subset. This formulation avoids the use of the classical method based on the responses envelopes that generally yields an overestimate of the equivalent static forces.

- For each given subset of observations, the extreme value statistics of the time responses are directly estimated from the realizations of the responses for which the number of realizations can arbitrarily be large due to the existence of the generator of the non-Gaussian stochastic process **P**, which has been developed. The gust loading factors are thus deduced from these extreme value statistics, but their values are not used for estimating the equivalent static forces.

Such novelties introduced for estimating the equivalent static forces are particularly useful for studying the wind effects on stadium roofs

- for which the flow can present large swirls and eddies due to flow separations, which induce non-Gaussianity of the unsteady pressure field,

- for which the probability model of stochastic process **P** cannot *a priori* be constructed or simulated by the computational fluid dynamics with sufficient accuracy, but requires unsteady measurements in boundary layer wind tunnel,

- for which the dynamics cannot be represented with few modes but requires the introduction of a quasi-static term in order to accelerate the convergence rate of the reduced-order model.

## 1.7 Organization of the thesis

The thesis is organized as follows:

- Chapter 1: Introduction and objectives.
- Chapter 2: Stochastic modeling, model reduction, and stationary stochastic response.
- Chapter 3: Time discretization. Signal processing aspects for the numerical model and the experimental measurements.
- Chapter 4: Generator of realizations of the non-Gaussian process **P**.
- Chapter 5: Estimation of the equivalent static forces.
- Chapter 6: Application to a simple structure and experimental validation.
- Chapter 7: Application to a stadium structure with wind tunnel pressure measurements.
- Chapter 8: Conclusions.

# Chapter 2

# Stochastic modeling, model reduction, and stationary stochastic response

## 2.1 Framework of the methodology proposed

The methodology proposed is in the framework of stochastic structural dynamics consisting in analyzing the stationary response of a weakly damped linear structure subjected to external forces that is modeled by a second-order stationary non-Gaussian stochastic process $\mathbb{P} = \{\mathbb{P}(t), t \in \mathbb{R}\}$. The frequency band of analysis, $\mathscr{B}$, associated with the stationary response is defined by

$$\mathscr{B} = [0, \omega_c] \,, \tag{2.1}$$

where $\omega_c$ (rad/s) is the cutoff frequency.
If process $\mathbb{P}$ was Gaussian then it would be completely defined by its mean function (that is a constant vector $\underline{\mathbf{p}}$) and by the matrix-valued spectral density function [36, 53, 77] of the centered process $\{\mathbf{P}(t), t \in \mathbb{R}\}$ such that $\mathbb{P}(t) = \underline{\mathbf{p}} + \mathbf{P}(t)$. The stationary response being a linear or an affine transformation of $\mathbb{P}$, this stochastic response would be Gaussian and then it would be characterized by its mean function that is a constant vector and by the matrix-valued spectral density function of the centered stationary stochastic response. In such a case, it would be sufficient to use spectral analysis in the frequency domain of the second-order stationary stochastic processes to fully define the stationary Gaussian response [97, 77]. Statistics of sample paths of the stochastic response could then be calculated by using the S.O Rice formulas and the extreme values theory for Gaussian processes [26, 77, 80, 99, 100]. However, as we consider the non-Gaussian case, the method mentioned above is not usable (see for instance [36, 53, 77, 111]).

Obviously, it is important to calculate, as for the Gaussian case, the power spectral density function of the stationary non-Gaussian stochastic response, using the spectral analysis method, firstly to analyze the stochastic dynamical system and secondly, to construct predictions of some statistical quantities as we will see. As the theoretical results on statistics on sample paths of Gaussian processes cannot be used, and as the probability distribution of the stationary stochastic response is not Gaussian, statistics on sample paths must be estimated using realizations of the stationary stochastic responses. For that, it is then necessary to generate independent realizations of stochastic process $\mathbf{P}$ from a stochastic modeling of $\{\mathbf{P}(t), t \in \mathbb{R}\}$, which is identified by using experimental measurements, and to solve the linear dynamics equation in time domain.

## 2.2 Computational model of the linear structural dynamics in the time domain

It is assumed that the structure is fixed (no rigid body displacement). The computational model for the linear dynamics of the structure [3, 28, 44, 64, 91, 147] is written as

$$[M]\,\ddot{\mathbf{Y}}(t) + [D]\,\dot{\mathbf{Y}}(t) + [K]\,\mathbf{Y}(t) = \mathbf{F}(t)\,, t \in \mathbb{R}\,, \tag{2.2}$$

where

- $m$ is the number of degree of freedom (DOF);
- $\mathbf{Y}(t) = (Y_1(t), \ldots, Y_m(t))$ is the displacement vector (translations and/or rotations);
- $\dot{\mathbf{Y}}(t)$ and $\ddot{\mathbf{Y}}(t)$ are the velocity and acceleration vectors associated with $\mathbf{Y}(t)$;
- $\mathbf{F}(t) = (F_1(t), \ldots, F_m(t))$ is the vector of external forces applied (forces and/or bending moments) modeled by a stationary stochastic process;
- the mass matrix $[M]$ is an $(m \times m)$ real positive-definite matrix;
- the damping matrix $[D]$ is an $(m \times m)$ real positive-definite matrix;
- the stiffness matrix $[K]$ is an $(m \times m)$ real positive-definite matrix.

**Remark**.

1. Matrices $[D]$ and $[K]$ are definite positive because there are no rigid body displacements.

2. Matrices $[D]$ and $[K]$ are constant, that corresponds to a model for which the behavior of the constitutive materials of the structure are elastic dissipative (viscoelastic type without memory) [43, 91, 129].

3. As we search the stationary stochastic solution, we are interested in the construction of $\mathbf{Y}(t)$ that verifies, for all $t$ in $\mathbb{R}$, Eq. (2.2). Consequently, we are not interested in an evolution problem for $t > 0$ with initial conditions for displacement and velocity at time $t = 0$.

4. In general, in structural dynamics, the computational model defined by Eq. (2.2) corresponds to a finite element model.

## 2.3 Controlability and observability of the dynamical system

### 2.3.1 Controlability

For the considered applications, all the DOFs are not subjected to external forces but only $m_c < m$ DOFs. We then introduced the matrix $[O_c] \in \mathbb{M}_{m,m_c}(\mathbb{R})$ such that

$$\mathbf{F}(t) = [O_c]\,\mathbf{F}^c(t) \quad , \quad t \in \mathbb{R}\,, \tag{2.3}$$

where

$$\mathbf{F}^c(t) = (F^c_1(t), \ldots, F^c_{m_c}(t))\,, \tag{2.4}$$

is the vector of the external forces that are effectively applied. By assumption, the null space of $[O_c]$ is reduced to $\{0\}$, that is to say, $[O_c]\,\mathbf{f} = \mathbf{0}$ implies $\mathbf{f} = \mathbf{0}$.
In the context of the considered application that is related to the response of complex structures (such as stadium roofs [137]) subjected to wind effects, the loads applied at time $t$ are represented by the vector $\mathbb{P}(t)$ with values in $\mathbb{R}^{m_{\text{exp}}}$, which corresponds to measurements of pressures or differential pressures at some points of the structure [136, 137],

$$\mathbb{P}(t) = (\mathbb{P}_1(t), \ldots, \mathbb{P}_{m_{\text{exp}}}(t))\,. \tag{2.5}$$

It is assumed that $\mathbf{F}^c(t)$ depends linearly on $\mathbb{P}(t)$. Under this hypothesis, we can write

$$\mathbf{F}^c(t) = [B_c]\,\mathbb{P}(t) \quad , \quad t \in \mathbb{R}\,, \tag{2.6}$$

in which $[B_c] \in \mathbb{M}_{m_c,m_{\text{exp}}}(\mathbb{R})$ is a given matrix. By combining Eqs. (2.3) and (2.6) yields

$$\mathbf{F}(t) = [A_c]\,\mathbb{P}(t) \quad , \quad t \in \mathbb{R}\,, \tag{2.7}$$

in which $[A_c]$ is the controlability matrix defined by

$$[A_c] = [O_c]\,[B_c] \in \mathbb{M}_{m,m_{\text{exp}}}(\mathbb{R})\,. \tag{2.8}$$

By assumption, the null space of $[A_c]$ is reduced to $\{0\}$, that is to say, $[A_c]\,\mathfrak{p} = \mathbf{0}$ implies $\mathfrak{p} = \mathbf{0}$.

### 2.3.2 Observability

The observations of the structure can be displacement components, internal forces, components of a stress tensor, components of a strain tensor, etc. For the application under consideration, for which the equivalent static loads induced by the wind effects have to be calculated, observations must be introduced (see for instance [56]) in order to construct the equivalent static forces in a probabilistic framework.
Let $\mathbb{U}$ be a given observation in a structural element, with values in $\mathscr{D}$ that is a subset of $\mathbb{R}^{m_u}$ with $m_u \geq 1$. Let $T$ be a fixed time. The equivalent static force associated with $\mathbb{U}$ , $T$, and $\mathscr{D}$, is constructed in order to maximize the probability that $\mathbb{U}(T)$ belongs to given domain $\mathscr{D}$. Therefore the computed equivalent static force depends on $\mathbb{U}(T)$ and $\mathscr{D}$. Then, as we will see, all the equivalent static forces will be concatenated in order to construct an algebraic basis that spans a subspace of the computed equivalent static forces ("fusion methodology"). This basis allows for generating any load case associated with the set of all the observations subsets $\{\mathbb{U}(T), \mathscr{D}\}$.
In order to not overburden the notations, we do not introduce an indexation related to the observations and their associated domains. The latter will only be introduced for the "fusion" methodology of the equivalent forces introduced for several observations. For a given observation $\mathbb{U}(t)$, the observation matrix $[A_o] \in \mathbb{M}_{m_u,m}(\mathbb{R})$ is introduced such that

$$\mathbb{U}(t) = (\mathbb{U}_1(t), \ldots, \mathbb{U}_{m_u}(t))\,, \tag{2.9}$$

is written as

$$\mathbb{U}(t) = [A_o]\,\mathbf{Y}(t)\,. \tag{2.10}$$

By assumption, the null space of $[A_o]$ is reduced to $\{0\}$, that is to say, $[A_o]\,\mathbf{y} = \mathbf{0}$ implies $\mathbf{y} = \mathbf{0}$. Let $\mathbb{U}_{\max}$ be the maximum of $\mathbb{U}(t)$ on $[0, T]$,

$$\mathbb{U}_{\max} = \max_{t\in[0,T]} \mathbb{U}(t)\,, \tag{2.11}$$

and let $\mathbb{U}_{\min}$ be the minimum of $\mathbb{U}(t)$ on $[0, T]$,

$$\mathbb{U}_{\min} = \min_{t\in[0,T]} \mathbb{U}(t)\,, \tag{2.12}$$

where $[0, T]$ is the time window corresponding to the duration on which the dynamical system is observed, and which will be defined in Chapter 3. Domain $\mathscr{D}$, associated with $\mathbb{U}$, is generally an unbounded subset of $\mathbb{R}^{m_u}$. The criterion for that observation $\mathbb{U}(T)$ belongs to domain $\mathscr{D}$ is then written as,

$$\mathbb{U}(T) \in \mathscr{D} \subset \mathbb{R}^{m_u} . \tag{2.13}$$

**Remarks**.

1. Often, domain $\mathscr{D}$ will be a separable domain, which means that $\mathscr{D}$ is written as a Cartesian product of subsets of $\mathbb{R}$, that is to say is written as $\mathscr{D} = \mathscr{D}_1 \times \ldots \times \mathscr{D}_{m_u}$ in which $\mathscr{D}_k \subset \mathbb{R}$.

2. Considering the methodology that will be implemented to construct the equivalent static force associated with Eq. (2.13), domain $\mathscr{D}$ will most often be defined with respect to the mean value of $\mathbb{U}_{\max}$ or $\mathbb{U}_{\min}$, which is detailed in Appendix A for a separable domain.

## 2.4 Reduced-order model in time domain

In order to reduce the numerical costs, a reduced-order model, suitable for the frequency band of analysis $\mathscr{B} = [0, \omega_c]$, is classically constructed in the time domain. Taking into account the linearity of the dynamical system, the usual methodology for constructing the reduced-order model consists in projecting Eq. (2.2) on the subspace $\mathscr{C}_N \subset \mathbb{R}^m$, generated by $N$ elastic modes of the undamped system associated with the $N$ smallest eigenfrequencies that belong to $\mathscr{B}$ [22, 87]. However, for structures for which the static deformation induced by the considered static loads, do not belong to $\mathscr{C}_N$ for the value of $N$ defined above, it is necessary to significantly increase the value of $N$ for obtaining an accurate convergence of the dynamical response computed with the reduced-order model. In such a case, numerous elastic modes whose eigenfrequencies are much higher than the cut-off frequency $\omega_c$ of the frequency band of analysis should be added. To avoid increasing too much the value of $N$ (which penalizes numerical costs for probabilistic estimation of the equivalent static forces in the non-Gaussian framework), a quasi-static term is added in the modal representation in order to accelerate the convergence with respect to $N$ (see [91]).

### 2.4.1 Modes (elastic modes)

The matrix $[\varphi_N] \in \mathbb{M}_{m,N}(\mathbb{R})$ of the modes $\varphi^1, \ldots, \varphi^N \in \mathbb{R}^m$ (also called elastic modes), associated with the first $N$ eigenfrequencies $\omega_1, \ldots, \omega_N$ such that

$$0 < \omega_1 \leq \omega_1 \leq \ldots \leq \omega_N , \tag{2.14}$$

is constructed as the solution to the generalized eigenvalue problem [17],

$$[K]\,[\varphi_N] = [M]\,[\varphi_N]\,[\lambda_N]\,, \tag{2.15}$$

where $[\lambda_N]$ is the diagonal matrix of the eigenvalues $0 < \lambda_1 \leq \lambda_2 \leq \ldots \leq \lambda_N$ such that $\lambda_j = \omega_j^2$. We have the usual orthogonality properties (see for instance, [3, 91]),

$$[\varphi_N]^T[M][\varphi_N] = [I_N]\,, \tag{2.16}$$

$$[\varphi_N]^T[K][\varphi_N] = [\lambda_N]\,. \tag{2.17}$$

Note that the normalization of the modes are chosen with respect to the mass matrix (see Eq. (2.16)).

### 2.4.2 Reduced-order model in time domain

**(i) Reduced-order model without quasi-static acceleration term**

**(i-1) Construction of the reduced-order model**
By projecting Eq. (2.2) on subspace $\mathscr{C}_N$ of $\mathbb{R}^m$ and by using Eqs. (2.7), (2.16), and (2.17) yield the reduced-order model of order $N$ that is written, for all $t \in \mathbb{R}$, as

$$\mathbf{Y}^N(t) = [\varphi_N]\,\mathbf{Q}(t)\,, \tag{2.18}$$

$$\ddot{\mathbf{Q}}(t) + [D_N]\,\dot{\mathbf{Q}}(t) + [\lambda_N]\,\mathbf{Q}(t) = [\phi_N^c]\,\mathbb{P}(t)\,. \tag{2.19}$$

in which

- $[D_N]$ is the $(N \times N)$ real positive-definite matrix that is written as $[D_N] = [\varphi_N]^T[D]\ [\varphi_N]$. It is assumed that the dissipation of the structure is described by the modal damping rates, $\xi_1, \ldots, \xi_N$. Therefore, $[D_N]$ is a diagonal matrix [22, 3, 44], which is written as

$$[D_N]_{\alpha\beta} = 2\xi_\alpha\omega_\alpha\delta_{\alpha\beta} \quad , \quad 0 < \xi_\alpha < 1\,. \tag{2.20}$$

- Using the definition given by Eq. (2.8) of controlability matrix $[A_c] \in \mathbb{M}_{m,m_{\text{exp}}}(\mathbb{R})$ and using Eq. (2.7), the modal controlability matrix $[\phi_N^c]$ (see [88]) is written as

$$[\phi_N^c] = [\varphi_N]^T\,[A_c] \in \mathbb{M}_{N,m_{\text{exp}}}(\mathbb{R})\,. \tag{2.21}$$

- $\mathbf{Q}(t) = (\mathbb{Q}_1(t), \ldots, \mathbb{Q}_N(t))$ with values in $\mathbb{R}^N$, is the vector of the generalized coordinates.

- $\mathbf{Y}^N(t) = (Y_1^N(t), \ldots, Y_m^N(t))$ with values in $\mathbb{R}^m$, is the approximation of order $N$ of $\mathbf{Y}(t)$.

**(i-2) Convergence analysis with respect to $N$**

Let $\omega \mapsto [\widehat{\mathbb{h}}_N^c(\omega)]$ be the frequency response function (FRF), defined on $\mathbb{R}$ with values in $\mathbb{M}_{m,m_{\text{exp}}}(\mathbb{C})$, of the linear filter [93, 97, 110] defined by Eqs. (2.18) and (2.19), for which the input is $\mathbb{P}$ and the output is $\mathbf{Y}^N$. This function is such that, for all $\omega$ in $\mathbb{R}$,

$$[\widehat{\mathbb{h}}_N^c(\omega)] = [\varphi_N]\,[\widehat{h}_N(\omega)]\,[\phi_N^c] \in \mathbb{M}_{m,m_{\text{exp}}}(\mathbb{C})\,, \tag{2.22}$$

in which $[\widehat{h}_N(\omega)]$ is the $(N \times N)$ complex diagonal matrix that is such that

$$[\widehat{h}_N(\omega)]_{\alpha\beta} = \delta_{\alpha\beta}(-\omega^2 + 2i\omega\xi_\alpha\omega_\alpha + \omega_\alpha^2)^{-1}\,. \tag{2.23}$$

For $N = m$, $[\widehat{\mathbb{h}}_m^c(\omega)]$ is the frequency response function, rewritten as $[\widehat{\mathbb{h}}^c(\omega)]$, of the filter defined by Eqs. (2.2) and (2.7) for which the input is $\mathbb{P}$ and the output is $\mathbf{Y}$. For any external excitation and for all $\omega$ in $\mathscr{B} = [0, \omega_c]$, the convergence of the reduced-order model with respect to $N$ can be analyzed by studying the graph of the function $N \mapsto \text{err}_{\text{ROM}}(N)$ defined by

$$\text{err}_{\text{ROM}}(N) = \frac{\int_{\mathscr{B}} \|\widehat{\mathbb{h}}^c(\omega) - \widehat{\mathbb{h}}_N^c(\omega)\|_M^2 d\omega}{\int_{\mathscr{B}} \|\widehat{\mathbb{h}}^c(\omega)\|_M^2 d\omega}\,, \tag{2.24}$$

where the norm $\|.\|_M$ is such that

$$\|\widehat{\mathbb{h}}^c(\omega)\|_M^2 = \text{tr}\{[\widehat{\mathbb{h}}^c(\omega)]^*\,[M]\,[\widehat{\mathbb{h}}^c(\omega)]\}\,, \tag{2.25}$$

where $[\widehat{\mathbb{h}}^c(\omega)]^* = \overline{[\widehat{\mathbb{h}}^c(\omega)]}^T$ (conjugate transpose). It should be noted that the right-hand side of Eq. (2.24) is not efficient for its computation because the $(m \times m_{\text{exp}})$ complex matrix $[\widehat{\mathbb{h}}^c(\omega)]$ is a full matrix. The convergence criterion $\text{err}_{\text{ROM}}(N)$ defined by Eq. (2.24) can then be replaced by the analysis of the graph of the function $N \mapsto \|\widehat{\mathbb{h}}_N^c\|_{\mathbf{L}^2(\mathscr{B})}$ such that

$$\|\widehat{\mathbb{h}}_N^c\|_{\mathbf{L}^2(\mathscr{B})} = \sqrt{\int_{\mathscr{B}} \|\widehat{\mathbb{h}}_N^c(\omega)\|_M^2 d\omega}\,. \tag{2.26}$$

Convergence is obtained when the function $N \mapsto \|\widehat{\mathbb{h}}_N^c\|_{\mathbf{L}^2(\mathscr{B})}$ becomes constant. In practice, the $(m \times m_{\text{exp}})$ complex full matrix $[\widehat{\mathbb{h}}_N^c(\omega)]$ is not constructed and we use the following expression deduced from Eqs. (2.16), (2.22), and (2.25),

$$\|\widehat{\mathbb{h}}_N^c\|_{\mathbf{L}^2(\mathscr{B})} = \sqrt{\int_{\mathscr{B}} \|[\widehat{h}_N(\omega)]\,[\phi_N^c]\|_F^2 d\omega}\,, \tag{2.27}$$

where $\|C\|_F^2 = \text{tr}\{[C]^*\,[C]\}$ for any complex matrix $[C]$, and where $[\widehat{h}_N(\omega)]$ is a $(N \times N)$ complex diagonal matrix that is defined by Eq. (2.23).

**(ii) Reduced-order model with a quasi-static acceleration term**

**(ii-1) Construction of the reduced-order model**

A quasi-static acceleration term can be added to the reduced-order model presented in paragraph 2.4.2 (i) to accelerate the convergence with respect to $N$. Following the method proposed in [91], the reduced-order model is written, for all $t$ in $\mathbb{R}$, as

$$\mathbf{Y}^N(t) = [\mathscr{S}_N^c]\,\mathbb{P}(t) + [\varphi_N]\mathbb{Q}(t)\,, \tag{2.28}$$

$$\ddot{\mathbb{Q}}(t) + [D_N]\,\dot{\mathbb{Q}}(t) + [\lambda_N]\,\mathbb{Q}(t) = [\phi_N^c]\,\mathbb{P}(t)\,, \tag{2.29}$$

in which $[\mathscr{S}_N^c]$ is the $(m \times m_{\text{exp}})$ real full matrix such that

$$[\mathscr{S}_N^c] = [K]^{-1}\,[A_c] - [\widehat{\mathbb{h}}_N^c(0)] \in \mathbb{M}_{m,m_{\text{exp}}}(\mathbb{R})\,, \tag{2.30}$$

where $[\widehat{\mathbb{h}}_N^c(0)]$ is the $(m \times m_{\text{exp}})$ real matrix given by Eq. (2.22) for $\omega = 0$. It should be noted that the matrix $[K]^{-1}$, which is a full matrix, is never explicitly constructed. The rectangular matrix $[\mathscr{S}_N^c]$ is computed by $[\mathscr{S}_N^c] = [A_1] - [\widehat{\mathbb{h}}_N^c(0)]$ in which the matrix $[A_1]$ is computed by solving the linear system of equations, $[K]\,[A_1] = [A_c]$.

**(ii-2) Convergence study with respect to $N$**

The FRF associated with the linear filter defined by Eqs. (2.28) and (2.29), for which the input is $\mathbb{P}$ and the output is $\mathbf{Y}^N$, is denoted by $\omega \mapsto [\widehat{\mathbb{h}}_N^{c,\text{acc}}(\omega)]$ from $\mathbb{R}$ into $\mathbb{M}_{m,m_{\text{exp}}}(\mathbb{C})$, such that, for all $\omega$ in $\mathbb{R}$,

$$[\widehat{\mathbb{h}}_N^{c,\text{acc}}(\omega)] = [\mathscr{S}_N^c] + [\widehat{\mathbb{h}}_N^c(\omega)]\,, \tag{2.31}$$

in which $[\widehat{\mathbb{h}}_N^c(\omega)]$ is the matrix in $\mathbb{M}_{m,m_{\text{exp}}}(\mathbb{C})$ defined by Eq. (2.22), and where $[\mathscr{S}_N^c]$ is the matrix in $\mathbb{M}_{m,m_{\text{exp}}}(\mathbb{R})$ defined by Eq. (2.30). By reusing the analysis carried out in Section 2.4.2 (i-2), the convergence of the "accelerated" reduced-order model with respect to $N$ in band $\mathscr{B}$, is studied by analyzing the graph of the function $N \mapsto \|\widehat{\mathbb{h}}_N^{c,\text{acc}}\|_{\mathbf{L}^2(\mathscr{B})}$ such that

$$\|\widehat{\mathbb{h}}_N^{c,\text{acc}}\|_{\mathbf{L}^2(\mathscr{B})} = \sqrt{\int_{\mathscr{B}} \|\widehat{\mathbb{h}}_N^{c,\text{acc}}(\omega)\|_M^2 d\omega}\,, \tag{2.32}$$

in which

$$\|\widehat{\mathbb{h}}_N^{c,\text{acc}}(\omega)\|_M^2 = \text{tr}\{[\widehat{\mathbb{h}}^{c,\text{acc}}(\omega)]^*\,[M]\,[\widehat{\mathbb{h}}^{c,\text{acc}}(\omega)]\}\,. \tag{2.33}$$

An appropriate numerical analysis that allows the explicit construction of the full $(m \times m)$ complex matrix $[\widehat{\mathbb{h}}_N^{c,\text{acc}}(\omega)]$ to be done is used to compute Eq. (2.32) and is given in Appendix B.

## 2.5 Observations and instantaneous equivalent force expressed with the reduced-order model

In this section, the reduced-order model with the quasi-static acceleration term is used. To obtain the model without this term, it is sufficient to do $[\mathscr{S}_N^c] = [0]$ in the equations.

### 2.5.1 Introduction of the centered quantities and the centered reduced-order model

For all fixed $t$, random vector $\mathbb{P}(t)$, with values in $\mathbb{R}^{m_{\text{exp}}}$, is written as

$$\mathbb{P}(t) = \underline{\mathbf{p}} + \mathbf{P}(t)\,, \tag{2.34}$$

in which $\underline{\mathbf{p}}$ is the mean vector in $\mathbb{R}^{m_{\text{exp}}}$ and where $\mathbf{P}(t)$ is the centered random vector. For all fixed $t$, the response $\mathbf{Y}(t)$ with values in $\mathbb{R}^m$ can be written as

$$\mathbf{Y}(t) = \underline{\mathbf{y}} + \mathbf{X}(t)\,, \tag{2.35}$$

where the static response $\underline{\mathbf{y}} \in \mathbb{R}^m$ is such that

$$[K]\,\underline{\mathbf{y}} = \underline{\mathbf{f}} \quad , \quad \underline{\mathbf{f}} = [A_c]\,\underline{\mathbf{p}} \in \mathbb{R}^m\,. \tag{2.36}$$

From Section 2.4.2 (ii), it can be deduced that the reduced-order model with the quasi-static acceleration term, which allows for computing the centered stochastic process $\mathbf{X}$, is written (by using the same notation $\mathbf{X}(t)$ instead of $\mathbf{X}^N(t)$), for all $t$ in $\mathbb{R}$, as

$$\mathbf{X}(t) = [\mathscr{S}_N^c]\,\mathbf{P}(t) + [\varphi_N]\,\mathbf{Q}(t)\,, \tag{2.37}$$

$$\ddot{\mathbf{Q}}(t) + [D_N]\,\dot{\mathbf{Q}}(t) + [\lambda_N]\,\mathbf{Q}(t) = [\phi_N^c]\,\mathbf{P}(t)\,. \tag{2.38}$$

### 2.5.2 Observability

In this section, observation $\mathbb{U}(t)$ with values in $\mathbb{R}^{m_u}$ (defined by Eq. (2.10)) is expressed by using the approximation of $\mathbf{X}(t)$ constructed with Eqs. (2.35) to (2.38). We recall that the modal controlability (defined by Eq. (2.21)) is written as,

$$[\phi_N^c] = [\varphi_N]^T\,[A_c] \in \mathbb{M}_{N,m_{\text{exp}}}(\mathbb{R})\,. \tag{2.39}$$

The modal observability is defined as follows,

$$[\phi_N^o] = [A_o]\,[\varphi_N] \in \mathbb{M}_{m_u,N}(\mathbb{R})\,. \tag{2.40}$$

Using Eqs. (2.22), (2.23), (2.30), and (2.40), it can be seen that the matrix $[\mathscr{U}_N^{oc}] = [A_o][\mathscr{S}_N^c] \in \mathbb{M}_{m_u, m_{\exp}}(\mathbb{R})$, in which $[\mathscr{S}_N^c]$ is defined by Eq. (2.30), can be written as

$$[\mathscr{U}_N^{oc}] = [A_o]\,[K]^{-1}\,[A_c] - [\phi_N^o]\,[\lambda_N]^{-1}\,[\phi_N^c]\,. \tag{2.41}$$

For all $t$ in $\mathbb{R}$, observation $\mathbb{U}(t)$ can be written (keeping the notation $\mathbb{U}(t)$ instead of $\mathbb{U}^N(t)$), as

$$\mathbb{U}(t) = \underline{\mathbf{u}} + \mathbf{U}(t)\,, \tag{2.42}$$

$$\mathbf{U}(t) = [\mathscr{U}_N^{oc}]\,\mathbf{P}(t) + [\phi_N^o]\,\mathbf{Q}(t)\,, \tag{2.43}$$

where $\mathbf{Q}(t)$ verifies Eq. (2.38), that is to say

$$\ddot{\mathbf{Q}}(t) + [D_N]\,\dot{\mathbf{Q}}(t) + [\lambda_N]\,\mathbf{Q}(t) = [\phi_N^c]\,\mathbf{P}(t)\,, \tag{2.44}$$

and where

$$\underline{\mathbf{u}} = [A_o]\,\underline{\mathbf{y}} \in \mathbb{R}^{m_u}\,. \tag{2.45}$$

### 2.5.3 Instantaneous equivalent force

At time $t$, the equivalent force $\mathbb{F}^e(t)$ in $\mathbb{R}^m$ is defined by

$$\mathbb{F}^e(t) = [K]\,\mathbf{Y}(t)\,, \tag{2.46}$$

and can be rewritten, using Eqs. (2.35) and (2.36), as

$$\mathbb{F}^e(t) = \underline{\mathbf{f}} + \mathbf{F}^e(t)\,, \tag{2.47}$$

$$\mathbf{F}^e(t) = [K]\,\mathbf{X}(t)\,. \tag{2.48}$$

By substituting $\mathbf{X}(t)$ by its approximation defined by Eqs. (2.37) and (2.38) (keeping again the notation $\mathbf{F}^e(t)$ instead of $\mathbf{F}^{e,N}(t)$) yields,

$$\mathbf{F}^e(t) = [\mathscr{F}_N^c]\,\mathbf{P}(t) + [\mathcal{F}_N^{\mathbf{Q}}]\mathbf{Q}(t)\,, \tag{2.49}$$

where $\mathbf{Q}(t)$ verifies Eq. (2.38), that is to say

$$\ddot{\mathbf{Q}}(t) + [D_N]\,\dot{\mathbf{Q}}(t) + [\lambda_N]\,\mathbf{Q}(t) = [\phi_N^c]\,\mathbf{P}(t)\,, \tag{2.50}$$

in which $[\mathcal{F}_N^{\mathbf{Q}}]$ is the rectangular matrix such that

$$[\mathcal{F}_N^{\mathbf{Q}}] = [K]\,[\varphi_N] \in \mathbb{M}_{m,N}(\mathbb{R})\,, \tag{2.51}$$

and where $[\mathscr{F}_N^c] = [K]\,[\mathscr{S}_N^c] \in \mathbb{M}_{m,m_{\exp}}(\mathbb{R})$ is the matrix such that

$$[\mathscr{F}_N^c] = [A_c] - [\mathcal{F}_N^{\mathbf{Q}}]\,[\lambda_N]^{-1}\,[\phi_N^c] \in \mathbb{M}_{m,m_{\exp}}(\mathbb{R})\,. \tag{2.52}$$

**Remark**. Matrix $[\mathcal{F}_N^{\mathbf{Q}}]$ can easily be computed with a finite element code (black box) introducing successively, for $\alpha = 1, \ldots, N$, the Dirichlet condition $\mathbf{y} = \boldsymbol{\varphi}^\alpha$ to the computational model that corresponds to the static problem $[K]\,\mathbf{y} = \mathbf{f}$. The static response gives the reactions $\mathbf{f} = \mathcal{F}^\alpha$ that are the columns of matrix $[\mathcal{F}_N^{\mathbf{Q}}]$.

### 2.5.4 Synthesis and global notation

For all fixed $t$, let

$$\mathbf{W}(t) = (\mathbf{X}(t), \mathbf{U}(t), \mathbf{F}^e(t)) \in \mathbb{R}^{m_w} , \tag{2.53}$$

in which

$$m_w = m + m_u + m = 2m + m_u . \tag{2.54}$$

Equations (2.37), (2.43), and (2.49) can globally be written as,

$$\mathbf{W}(t) = [\mathscr{W}_N]\, \mathbf{P}(t) + [\mathcal{Q}_N]\, \mathbf{Q}(t) , \tag{2.55}$$

where $[\mathscr{W}_N]$ is the $(m_w \times m_{\text{exp}})$ real matrix and $[\mathcal{Q}_N]$ is the $(m_w \times N)$ real matrix, defined by

$$[\mathscr{W}_N] = \begin{bmatrix} [\mathscr{S}_N^c] \\ [\mathscr{U}_N^{oc}] \\ [\mathscr{F}_N^c] \end{bmatrix} \quad , \quad [\mathcal{Q}_N] = \begin{bmatrix} [\varphi_N] \\ [\phi_N^o] \\ [\mathcal{F}_N^{\mathbf{Q}}] \end{bmatrix} , \tag{2.56}$$

and where the forced response $\{\mathbf{Q}(t), t \in \mathbb{R}\}$ that verifies

$$\ddot{\mathbf{Q}}(t) + [D_N]\, \dot{\mathbf{Q}}(t) + [\lambda_N]\, \mathbf{Q}(t) = [\phi_N^c]\, \mathbf{P}(t) \quad , \quad \forall t \in \mathbb{R} , \tag{2.57}$$

is written as

$$\mathbf{Q}(t) = \int_{-\infty}^{t} [h_N(t-\tau)][\phi_N^c]\mathbf{P}(\tau) d\tau , \tag{2.58}$$

in which $[h_N(t)]$ is the $(N \times N)$ real diagonal matrix such that

$$[h_N(t)]_{\alpha\beta} = \delta_{\alpha\beta} \mathbb{1}_{\mathbb{R}^+}(t) \frac{1}{\omega_{D,\alpha}} e^{-\xi_\alpha \omega_\alpha t} \sin(\omega_{D,\alpha} t) , \tag{2.59}$$

in which $\mathbb{1}_{\mathbb{R}^+}(t)$ is equal to 0 if $t \notin \mathbb{R}^+$ and is equal to 1 if $t \in \mathbb{R}^+$, and where $\omega_{D,\alpha} = \omega_\alpha \sqrt{1 - \xi_\alpha^2}$, because $\xi_\alpha$ is assumed to be less than 1.

## 2.6 Stochastic modeling of the pressure vector

For fixed time $t$, in Section 2.3.1, $\mathbb{P}(t)$ with values in $\mathbb{R}^{m_{\text{exp}}}$ has been defined as measured pressures and differential pressures at several locations of the structure, and in Section 2.5.1, $\mathbf{P}(t)$ with values in $\mathbb{R}^{m_{\text{exp}}}$ has been defined the centered random vector associated with $\mathbb{P}(t)$ (see Eq. (2.34)). In this section, we detail the construction of the probability model of stochastic process $\{\mathbb{P}(t), t \in \mathbb{R}\}$ indexed by $\mathbb{R}$ with values in $\mathbb{R}^{m_{\text{exp}}}$ (total unsteady pressure) and its counter part $\{\mathbf{P}(t), t \in \mathbb{R}\}$ (centered unsteady pressure).
Total unsteady pressure $\{\mathbb{P}(t), t \in \mathbb{R}\}$ is modeled by a stochastic process, defined

on a probability space $(\Theta, \mathcal{T}, \mathscr{P})$, which is assumed to be second-order, stationary, and non-Gaussian [36, 53, 77, 97, 110]. The mean function of $\mathbb{P}$ is then a constant vector $\underline{\mathbf{p}} \in \mathbb{R}^{m_{\text{exp}}}$, such that

$$\underline{\mathbf{p}} = E\{\mathbb{P}(t)\}\,, \tag{2.60}$$

in which $E$ is the mathematical expectation [89]. In these conditions, the centered unsteady pressure $\{\mathbf{P}(t), t \in \mathbb{R}\}$ is such that

$$\mathbf{P}(t) = \mathbb{P}(t) - \underline{\mathbf{p}} \quad , \quad \forall t \in \mathbb{R}\,. \tag{2.61}$$

Stochastic process $\{\mathbf{P}(t), t \in \mathbb{R}\}$ is

- defined on $(\Theta, \mathcal{T}, \mathscr{P})$,
- indexed by $\mathbb{R}$ with values in $\mathbb{R}^{m_{\text{exp}}}$,
- stationary,
- of second-order: $E\{\|\mathbf{P}(t)\|^2_{\mathbb{R}^{m_{\text{exp}}}}\} < +\infty \quad , \quad \forall t$,
- centered: $E\{\mathbf{P}(t)\} = 0$,
- non-Gaussian.

The covariance function $(t, t') \mapsto [C_{\mathbf{P}}(t, t')]$ of stationary stochastic process $\mathbf{P}$, defined on $\mathbb{R} \times \mathbb{R}$, with values in $\mathbb{M}_{m_{\text{exp}}}(\mathbb{R})$, depends only on $t - t'$ and can be written as

$$[C_{\mathbf{P}}(t - t')] = E\{\mathbf{P}(t)\mathbf{P}(t')^T\}\,, \tag{2.62}$$

in which $\tau \mapsto [C_{\mathbf{P}}(\tau)]$ is defined on $\mathbb{R}$. The following hypotheses and the justification of their introduction in regards to the problem that has to be solved are introduced.

- Function $\tau \mapsto [C_{\mathbf{P}}(\tau)]$ is continous on $\mathbb{R}$ and tends to $0$ when $|\tau| \to +\infty$, which means that stochastic process $\mathbf{P}$ is mean-square continous. This hypothesis allows [53, 97, 110] for carrying out the spectral analysis of the process by assuming the existence of a matrix-valued spectral density function $\omega \mapsto [S_{\mathbf{P}}(\omega)]$ from $\mathbb{R}$ into $\mathbb{M}_{m_{\text{exp}}}(\mathbb{C})$, such that

  $$[C_{\mathbf{P}}(\tau)] = \int_{\mathbb{R}} e^{i\omega\tau}[S_{\mathbf{P}}(\omega)]d\omega \quad , \quad \forall \tau \in \mathbb{R}\,. \tag{2.63}$$

  We then have

  $$E\{\|\mathbf{P}(t)\|^2_{\mathbb{R}^{m_{\text{exp}}}}\} = \text{tr}[C_{\mathbf{P}}(0)] = \int_{\mathbb{R}} \text{tr}[S_{\mathbf{P}}(\omega)]d\omega\,, \tag{2.64}$$

  where $\omega \mapsto \text{tr}[S_{\mathbf{P}}(\omega)]$ from $\mathbb{R}$ into $\mathbb{R}^+$ is the total power spectral density function of vector-valued stochastic process $\mathbf{P}$.

- The continuity of function $\tau \mapsto [C_{\mathbf{P}}(\tau)]$ on $\mathbb{R}$, implies that for all fixed $T$,

$$\frac{1}{T^2}\int_0^T \int_0^T \|[C_{\mathbf{P}}(t-t')]\|_F^2 \, dt \, dt' < +\infty \, . \tag{2.65}$$

  The property given by Eq. (2.65) will allow [110] for constructing a finite statistical reduction $\{\mathbf{P}^{N_{\text{KL}}}(t), t \in [0,T]\}$ of $\{\mathbf{P}(t), t \in [0,T]\}$ using the truncated Karhunen-Loève expansion [72, 82]. This representation will be developed in Chapter 4, and will be necessary for constructing a polynomial chaos expansion [47] of non-Gaussian stochastic process $\{\mathbf{P}^{N_{\text{KL}}}(t), t \in [0,T]\}$. Then, this PCE will be the generator of independent realizations that will be used in the Monte Carlo procedure for the stochastic solver and for estimating non-Gaussian probability density functions of random quantities such as the observations, the generalized coordinates, etc., in order to estimate the equivalent static forces by the maximum likelihood principle (see Chapter 5). As we will see, the PCE of non-Gaussian stochastic process $\{\mathbf{P}^{N_{\text{KL}}}(t), t \in [0,T]\}$ will be constructed by solving an inverse statistical problem based on the experimental measurements carried out in a boundary layer wind tunnel (see Chapter 4).

## 2.7 Matrix-valued spectral density function of centered stationary process W

Since $\{\mathbf{P}(t), t \in \mathbb{R}\}$ with values in $\mathbb{R}^{m_{\text{exp}}}$ is a second-order, centered, stationary, and non-Gaussian stochastic process, it can be deduced that $\{\mathbf{W}(t), t \in \mathbb{R}\}$ with values in $\mathbb{R}^{m_w}$, which is defined by Eqs. (2.55) to (2.59), is also a second-order, centered, stationary, and non-Gaussian stochastic process [53, 97, 110]. In addition, its covariance function $\tau \mapsto [C_{\mathbf{W}}(\tau)] = E\{\mathbf{W}(t+\tau)\mathbf{W}(t)^T\}$ from $\mathbb{R}$ into $\mathbb{M}_{m_w}(\mathbb{R})$ admits the spectral representation

$$[C_{\mathbf{W}}(\tau)] = \int_{\mathbb{R}} e^{i\omega\tau}[S_{\mathbf{W}}(\omega)]d\omega \quad , \quad \forall \tau \in \mathbb{R} \, , \tag{2.66}$$

in which $[S_{\mathbf{W}}(\omega)]$ is the matrix-valued spectral density function with values in $\mathbb{M}_{m_w}(\mathbb{C})$ of stochastic process **W**.

The frequency response function $\omega \mapsto [\widehat{\mathbb{h}}_N^{\mathbf{W}}(\omega)]$, from $\mathbb{R}$ into $\mathbb{M}_{m_{\text{exp}},m_w}(\mathbb{C})$, of the linear filter defined by Eqs. (2.55) to (2.59), for which the input is **P** and the output is **W**, is written, for all $\omega$ in $\mathbb{R}$, as

$$[\widehat{\mathbb{h}}_N^{\mathbf{W}}(\omega)] = [\mathscr{W}_N] + [\mathcal{Q}_N]\,[\widehat{h}_N(\omega)]\,[\phi_N^c] \, , \tag{2.67}$$

in which $[\mathscr{W}_N]$ and $[\mathcal{Q}_N]$ are the matrices defined by Eq. (2.56), where $[\widehat{h}_N(\omega)]$ is the $(N \times N)$ diagonal complex matrix defined by Eq. (2.23), and where $[\phi^c_N]$ is the matrix defined by Eq. (2.21). Based on the spectral analysis of stationary second-order processes [53, 97, 110], matrix $[S_{\mathbf{W}}(\omega)]$ is written, for all $\omega$ in $\mathbb{R}$, as

$$[S_{\mathbf{W}}(\omega)] = [\widehat{\mathbb{h}}^{\mathbf{W}}_N(\omega)]\,[S_{\mathbf{P}}(\omega)]\,[\widehat{\mathbb{h}}^{\mathbf{W}}_N(\omega)]^*\,, \tag{2.68}$$

where $[S_{\mathbf{P}}(\omega)]$ is defined in Eq. (2.63).

The calculation of $[S_{\mathbf{W}}(\omega)]$ defined by Eq. (2.68) with $[\widehat{\mathbb{h}}^{\mathbf{W}}_N(\omega)]$ defined by Eq. (2.67) is performed by using the following methodology. Matrix $[S_{\mathbf{W}}(\omega)]$ is written as

$$[S_{\mathbf{W}}(\omega)] = [S^S_{\mathbf{W}}(\omega)] + [S^D_{\mathbf{W}}(\omega)]\,, \tag{2.69}$$

in which the dynamical part $[S^D_{\mathbf{W}}(\omega)]$ and the quasi-static part $[S^S_{\mathbf{W}}(\omega)]$ are computed as follows.

**(i) Dynamic part.** Matrix $[S^D_{\mathbf{W}}(\omega)]$ is written as

$$[S^D_{\mathbf{W}}(\omega)] = [\mathcal{Q}_N]\,[\mathscr{S}_{\mathbf{Q}}(\omega)]\,[\mathcal{Q}_N]^T\,, \tag{2.70}$$

in which $[\mathscr{S}_{\mathbf{Q}}(\omega)] \in \mathbb{M}_N(\mathbb{C})$ is such that

$$[\mathscr{S}_{\mathbf{Q}}(\omega)] = [\widehat{h}_N(\omega)]\,[\mathscr{S}_{\mathbf{P}}(\omega)]\,\overline{[\widehat{h}_N(\omega)]}\,, \tag{2.71}$$

and where $[\mathscr{S}_{\mathbf{P}}(\omega)] \in \mathbb{M}_N(\mathbb{C})$ is such that

$$[\mathscr{S}_{\mathbf{P}}(\omega)] = [\phi^c_N]\,[S_{\mathbf{P}}(\omega)]\,[\phi^c_N]^T\,. \tag{2.72}$$

**(ii) Quasi-static part.** Matrix $[S^S_{\mathbf{W}}(\omega)]$ is computed by

$$[S^S_{\mathbf{W}}(\omega)] = [S^S_1(\omega)] + [S^S_2(\omega)] + [S^S_2(\omega)]^*\,, \tag{2.73}$$

where

$$[S^S_1(\omega)] = [\mathscr{W}_N]\,[S_{\mathbf{P}}(\omega)]\,[\mathscr{W}_N]^T\,, \tag{2.74}$$

$$[S^S_2(\omega)] = [\mathscr{W}_N]\,[S_{\mathbf{P}}(\omega)]\,[\phi^c_N]^T\,\overline{[\widehat{h}_N(\omega)]}\,[\mathcal{Q}_N]^T\,. \tag{2.75}$$

**Remark**. If quasi-static acceleration term is not considered, matrix $[\mathscr{S}^c_N] = [0]$ and then $[\mathscr{W}_N] = [0]$. In this case $[S_{\mathbf{W}}(\omega)] = [S^D_{\mathbf{W}}(\omega)]$.

# Chapter 3

# Time discretization. Signal processing aspects for the computational model and the experimental measurements

It is recalled that the objective is the construction of the equivalent static forces from the unsteady pressure measurements $\mathbb{P}$ carried out in a boundary layer wind tunnel on a rigid model of the structure and from a computational structure dynamics model.
The acquisition and signal processing parameters used to analyze the measurements must therefore be reused by the stochastic solver of the computational model that therefore requires a time discretization.
It is also recalled that the non-Gaussian character of stationary process $\{\mathbb{P}(t), t \in \mathbb{R}\}$ leads us to formulate the computational model in the time domain, even if the second-order quantities, such as the matrix-valued spectral density functions, are obviously estimated and/or computed in the frequency domain.
In this chapter,

- the notations and the values for the signal processing parameters are defined;
- the estimates used for the second-order quantities are recalled;
- the approximation formulas of the filter that allows the stochastic responses to be computed are presented.

## 3.1 Notations and signal processing parameters

In this chapter, at time $t$, the experimental pressure vector is denoted by $\mathbb{P}^{\text{exp}}(t)$ (instead of $\mathbb{P}(t)$). The restriction $\{\mathbb{P}^{\text{exp}}(t)\,, t \in [0,T]\}$ to $[0,T]$ of stationary stochastic process $\{\mathbb{P}^{\text{exp}}(t)\,, t \in \mathbb{R}\}$ is introduced and is assumed to be defined to another probability space denoted as $(\Theta^{\text{exp}}, \mathcal{T}^{\text{exp}}, \mathscr{P}^{\text{exp}})$. The total duration of the time acquisition of measurements is $T_{\text{tot}}$ and the experimental unsteady pressure vector is a deterministic function denoted by $t \mapsto \mathbb{p}^{\text{exp}}(t)$ from $[0, T_{\text{tot}}]$ into $\mathbb{R}^{m_{\text{exp}}}$ (this deterministic function is used below for constructing independent realizations of stochastic process $\{\mathbb{P}^{\text{exp}}(t)\,, t \in [0,T]\}$).
The parameters related to acquisition and signal processing of experimental measurements of stochastic process $\mathbb{P}^{\text{exp}}$ are the following [85, 92, 93, 97, 116],

- dimension of vector $\mathbb{P}^{\text{exp}}(t)$: $m_{\text{exp}}$;
- cutoff frequency: $\nu_c$ (Hz) and $\omega_c = 2\pi\nu_c$ (rad/s);
- sampling frequency: $\nu_e = 2\,\nu_c$ (Hz) (Sahnnon's theorem);
- sampling time step: $\Delta t = 1/\nu_e$ (s);
- measurements total duration: $T_{\text{tot}}$ (s);
- time window: $[0\,, T]$ (s);
- number of independent realizations of stochastic process $\mathbb{P}^{\text{exp}}$ : $n_r$;
- number of time steps for the time sampling of $[0\,, T]$: $n_p$ such that

$$T = n_p\,\Delta t\,, \tag{3.1}$$

- time sampling points $t_1, \ldots, t_{n_p}$ of $[0, T]$, which are such that

$$t_k = t_1 + (k-1)\,\Delta t \quad , \quad k = 1, \ldots, n_p\,, \tag{3.2}$$

  in which

$$t_1 = 0 \quad , \quad t_{n_p} = (n_p - 1)\,\Delta t\,. \tag{3.3}$$

## 3.2 Time window, independent realizations, and frequency sampling

### 3.2.1 Time window

The criteria [97, 116] for choosing the time window $[0\,, T]$ are given below.

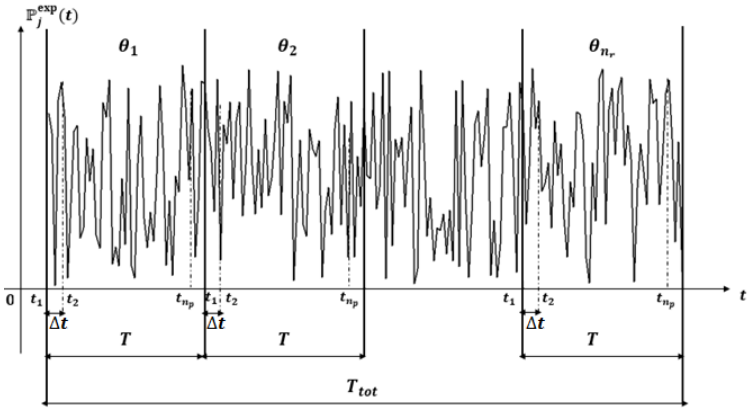


Figure 3.1: Schema illustrating the time window.

- $T$ is selected sufficiently large so that the associated frequency resolution $\Delta\nu = 1/T$ (Hz) is smaller than the half power bandwidth of the FRF at the fundamental resonance frequency $\nu_1$ of the structure. Moreover, $T$ must be much larger than the relaxation time $\tau_{\text{relax}}$ of the dynamic system, and is estimated by

$$\tau_{\text{relax}} = -\frac{1}{\omega_1\,\xi}\log\varepsilon$$

  in which $\omega_1 = 2\pi\nu_1$, $\xi = \min\{\xi_1, \ldots, \xi_N\}$, and $\varepsilon \ll 1$. For instance, for $\nu_1 = 0.5$ Hz, $\varepsilon = 1/100$, and $\xi = 0.01$, we obtain $\tau_{\text{relax}} = 146$ s. Then taking $T = 216$ s and $n_r = 100$, we obtain $T_{\text{tot}} = 21{,}600$ s, that means 6 hours.

- For fixed $T$, the number $n_r$ of independent realizations of $\{\mathbb{P}^{\text{exp}}(t), t \in [0, T]\}$ is such that

$$T_{\text{tot}} = n_r \times T\,. \tag{3.4}$$

  Usually, contiguous windows should not be taken. A time duration, longer than the correlation time, between two successive windows should be taken into account in order to ensure noncorrelation between successive windows [116]. When continuous windows are taken, there is a correlation between two successive windows and consequently, the speed of convergence of the spectral estimator constructed by the periodogram method is slightly degraded. In the context of these hypotheses, although the noncorrelation does not imply statistical independence (because the process is non-Gaussian), it will be assumed that each window provides an independent realization.

### 3.2.2 Independent realizations

The $n_r$ realizations of stochastic process $\{\mathbb{P}^{\text{exp}}(t), t \in [0,T]\}$, defined on probability space $(\Theta^{\text{exp}}, \mathcal{T}^{\text{exp}}, \mathscr{P}^{\text{exp}})$, with values in $\mathbb{R}^{m_{\text{exp}}}$, are denoted as

$$\{\mathbb{P}^{\text{exp}}(t;\theta_\ell), t \in [0,T]\} \quad , \quad \ell = 1, \ldots, n_r \,, \tag{3.5}$$

where $\theta_1, \ldots, \theta_{n_r} \in \Theta^{\text{exp}}$. Let $\{\mathbb{p}^{\text{exp}}(t), t \in [0, T_{\text{tot}}]\}$ be the experimental unsteady pressure vector carried out over the total duration $T_{\text{tot}}$. For $k = 1, \ldots, n_p$ and for $\ell = 1, \ldots, n_r$, the time sampling of the $n_r$ independent realizations of stochastic process $\{\mathbb{P}^{\text{exp}}(t), t \in [0,T]\}$ are given by

$$\mathbb{P}^{\text{exp}}(t_k;\theta_\ell) = \mathbb{p}^{\text{exp}}(t_k + (\ell-1)\,T) \,. \tag{3.6}$$

The time sampling values of the $n_r$ realizations of stochastic process $\mathbb{P}^{\text{exp}}$ are

$$\underbrace{\mathbb{P}^{\text{exp}}(t_1;\theta_1), \ldots, \mathbb{P}^{\text{exp}}(t_{n_p};\theta_1)}_{\text{realization } \theta_1}, \ldots\ldots, \underbrace{\mathbb{P}^{\text{exp}}(t_1;\theta_{n_r}), \ldots, \mathbb{P}^{\text{exp}}(t_{n_p};\theta_{n_r})}_{\text{realization } \theta_{n_r}} \,. \tag{3.7}$$

### 3.2.3 Frequency sampling

The frequency step is

$$\Delta\omega = 2\pi\Delta\nu = \frac{2\pi}{T} \,(\text{rad/s}) \,. \tag{3.8}$$

As the cutoff frequency is $\omega_c$, the frequency band for the signal processing is

$$[-\omega_c, \omega_c] \,(\text{rad/s}) \,. \tag{3.9}$$

Therefore, the frequency sampling points are

$$\omega_q = -\omega_c + (q - \frac{1}{2})\Delta\omega \quad , \quad q = 1, \ldots, n_p \,. \tag{3.10}$$

## 3.3 Estimation of the second-order quantities

The following classic estimates are used (see for instance [4, 68, 85, 92, 97, 110, 116]).

### 3.3.1 Mean value

Following Section 2.6, stochastic process $\{\mathbb{P}(t)\,, t \in [0,T]\}$ is the restriction to $[0,T]$ of the second-order stationary stochastic process $\{\mathbb{P}(t), t \in \mathbb{R}\}$, and consequently its mean function is a constant vector denoted by $\underline{\mathbf{p}} = E\{\mathbb{P}(t)\}$, for which

its estimate (also denoted by $\underline{\mathbf{p}}$) is given by

$$\underline{\mathbf{p}} \simeq \frac{1}{n_r} \sum_{\ell=1}^{n_r} \frac{1}{n_p} \sum_{k=1}^{n_p} \mathbb{P}^{\text{exp}}(t_k; \theta_\ell) \,. \tag{3.11}$$

Note that the classical proposed estimate of the mean value is coherent with periodogram method used for estimating matrix-valued power spectral density functions.

### 3.3.2 Realizations of the centered process

The centered process $\{\mathbf{P}^{\text{exp}}(t), t \in [0,T]\}$ is such that

$$\mathbf{P}^{\text{exp}}(t) = \mathbb{P}^{\text{exp}}(t) - \underline{\mathbf{p}} \quad , \quad \forall t \in [0\,, T] \,. \tag{3.12}$$

The time sampling values of the $n_r$ realizations of centered process $\{\mathbf{P}^{\text{exp}}(t), t \in [0,T]\}$ are directly deduced from Eq. (3.7),

$$\mathbf{P}^{\text{exp}}(t_k; \theta_\ell) = \mathbb{P}^{\text{exp}}(t_k; \theta_\ell) - \underline{\mathbf{p}} \quad , \quad k = 1, \ldots, n_p \quad ; \quad \ell = 1, \ldots, n_r \,. \tag{3.13}$$

### 3.3.3 Matrix-valued spectral density function

The centered second-order stochastic process $\{\mathbf{P}^{\text{exp}}(t)\,, t \in [0,T]\}$ is extended to a stationary stochastic process $\{\mathbf{P}^{\text{exp}}(t)\,, t \in \mathbb{R}\}$ on $\mathbb{R}$. The estimate of the matrix-valued spectral density function $\omega \mapsto [S_{\mathbf{P}^{\text{exp}}}(\omega)]$ with values in $\mathbb{M}_{m_{\text{exp}}}(\mathbb{C})$ of $\mathbf{P}^{\text{exp}}$ is constructed using the periodogram method,

$$[S_{\mathbf{P}^{\text{exp}}}(\omega_q)] \simeq \frac{1}{2\pi} \frac{1}{n_r} \sum_{\ell=1}^{n_r} \widehat{\mathbf{P}}^{\text{exp}}(\omega_q; \theta_\ell)\, \widehat{\mathbf{P}}^{\text{exp}}(\omega_q; \theta_\ell)^* \quad , \quad q = 1, \ldots, n_p \,, \tag{3.14}$$

$$\widehat{\mathbf{P}}^{\text{exp}}(\omega_q; \theta_\ell) = \sum_{k=1}^{n_p} \widetilde{\mathbf{P}}^{\text{exp}}(t_k; \theta_\ell)\, \exp\{-2i\pi \frac{(k-1)(q-1)}{n_p}\} \,, \tag{3.15}$$

$$\widetilde{\mathbf{P}}^{\text{exp}}(t_k; \theta_\ell) = \Delta t\, W_T(t_k)\, \mathbf{P}^{\text{exp}}(t_k; \theta_\ell)\, \exp\{-i(-\pi + \frac{\pi}{n_p})\,(k-1)\} \,. \tag{3.16}$$

In Eq. (3.16), $W_T$ is the Tukey-Hamming time window that is written as

$$W_T(t) = \frac{1}{\sqrt{T}} 1.5863\{0.54 - 0.46\, \cos(\frac{2\pi t}{T})\}\, \mathbb{1}_{[0,T]}(t) \,. \tag{3.17}$$

Eq. (3.15) shows that, for $\ell$ fixed in $\{1, \ldots, n_r\}$, the family $\{\widehat{\mathbf{P}}^{\text{exp}}(\omega_q; \theta_\ell), q = 1, \ldots, n_p\}$ of the complex vectors in $\mathbb{C}^{m_{\text{exp}}}$ is computed using the Fast Fourier Transform (FFT) (see Appendix C) of the family $\{\widetilde{\mathbf{P}}^{\text{exp}}(t_k; \theta_\ell), k = 1, \ldots, n_p\}$ of the real vectors in $\mathbb{R}^{m_{\text{exp}}}$ defined by Eq. (3.16).

## 3.4 Computation of the realizations $\mathbf{Q}(t)$ for $t$ in $[0\,,T]$

The developments presented in this section will be applied to $\mathbf{P}^{\text{exp}}$ and also to $\mathbf{P}$. In order to simplify the notations, this section is presented by using notation $\mathbf{P}$ (for the use with $\mathbf{P}^{\text{exp}}$, $\mathbf{P}$ must be substituted by $\mathbf{P}^{\text{exp}}$).

For all $t$ in $\mathbb{R}$, $\mathbf{Q}(t)$ is given by Eq. (2.58). For all $\ell$ in $1,\ldots,n_r$, we have to compute the realizations $\{\mathbf{Q}(t;\theta_\ell), t \in [0,T]\}$ at the sampling points $t_1,\ldots,t_{n_p}$ of $[0,T]$ and $\mathbf{Q}(T;\theta_\ell)$. Two approaches can be used.

- The first one is formulated in time domain and allows $\mathbf{Q}(T;\theta_\ell)$ to be computed (and not $\mathbf{Q}(t;\theta_\ell)$ for $t \in [0,T[$).
- The second one is formulated in frequency domain and allows $\mathbf{Q}(t;\theta_\ell)$ to be computed for all $t$ in $[0,T]$ and consequently, $\mathbf{Q}(T;\theta_\ell)$ to be computed.

Since we will need $\mathbf{Q}(t;\theta_\ell)$ for $t \in [0,T[$ and also $\mathbf{Q}(T;\theta_\ell)$, only the frequency domain formulation will be used.

### 3.4.1 Computing the realizations of $\mathbf{Q}(T)$ with the time domain formulation

As $T > \tau_{\text{relax}}$ (see Section 3.2.1), Eq. (2.58) can be, for $t \in [0,T]$, approximated by

$$\mathbf{Q}(t;\theta_\ell) \simeq \int_{t-T}^{t} [h_N(t-\tau)]\,[\phi_N^c]\,\mathbf{P}(\tau;\theta_\ell)d\tau\,, \tag{3.18}$$

and consequently, $\mathbf{Q}(T;\theta_\ell)$ is given by

$$\mathbf{Q}(T;\theta_\ell) \simeq \int_{0}^{T} [h_N(T-\tau)]\,[\phi_N^c]\,\mathbf{P}(\tau;\theta_\ell)d\tau\,, \tag{3.19}$$

for which the time sampling with time step $\Delta t$ yields

$$\mathbf{Q}(T;\theta_\ell) \simeq \Delta t \sum_{k=1}^{n_p} [h_N(T-t_k)]\,[\phi_N^c]\,\mathbf{P}(t_k;\theta_\ell)\,. \tag{3.20}$$

### 3.4.2 Computing the realizations of $\{\mathbf{Q}(t), t \in [0,T]\}$ with the frequency domain formulation

Let $\{\boldsymbol{\mathscr{P}}_N^c(t;\theta_\ell), t \in \mathbb{R}\}$ be the realization of the stochastic process $\{\boldsymbol{\mathscr{P}}_N^c(t), t \in \mathbb{R}\}$ such that

$$\boldsymbol{\mathscr{P}}_N^c(t) = [\phi_N^c]\,\mathbf{P}(t)\,. \tag{3.21}$$

Using Eqs. (2.58) and (3.21), the discrete Fourier transform $\{\widehat{\mathbf{Q}}(\omega_q;\theta_\ell), q=1,\ldots,n_p\}$ of the time sampling $\{\mathbf{Q}(t_k;\theta_\ell), k=1,\ldots,n_p\}$ of $\{\mathbf{Q}(t;\theta_\ell), t\in[0,T]\}$ is written as

$$\widehat{\mathbf{Q}}(\omega_q;\theta_\ell) = [\widehat{h}_N(\omega_q)]\,\widehat{\mathscr{P}}^c_N(\omega_q;\theta_\ell) \quad , \quad q=1,\ldots,n_p\,, \tag{3.22}$$

in which $[\widehat{h}_N(\omega_q)]$ is defined by Eq. (2.23) and where $\{\widehat{\mathscr{P}}^c_N(\omega_q;\theta_\ell), q=1,\ldots,n_p\}$ is computed by the fast Fourier transform,

$$\widehat{\mathscr{P}}^c_N(\omega_q;\theta_\ell) = \sum_{k=1}^{n_p} e^{-\frac{2i\pi}{n_p}(q-1)(k-1)}\widetilde{\mathscr{P}}^c_N(t_k;\theta_\ell)\,, \tag{3.23}$$

in which $\{\widetilde{\mathscr{P}}^c_N(t_k;\theta_\ell), k=1,\ldots,n_p\}$ is given by

$$\widetilde{\mathscr{P}}^c_N(t_k;\theta_\ell) = \Delta t\, e^{-i(-\pi+\frac{\pi}{n_p})(k-1)}\mathscr{P}^c_N(t_k;\theta_\ell)\,. \tag{3.24}$$

The time sampling $\{\mathbf{Q}(t_k;\theta_\ell), k=1,\ldots,n_p\}$ of $\{\mathbf{Q}(t;\theta_\ell), t\in[0\,,T]\}$ is given by

$$\mathbf{Q}(t_k;\theta_\ell) = \frac{\Delta\omega}{2} e^{+i(-\pi+\frac{\pi}{n_p})(k-1)}\widetilde{\mathbf{Q}}(t_k;\theta_\ell)\,, \tag{3.25}$$

in which $\{\widetilde{\mathbf{Q}}(t_k;\theta_\ell), k=1,\ldots,n_p\}$ is computed by the fast Fourier transform (inverse type)

$$\widetilde{\mathbf{Q}}(t_k;\theta_\ell) = \sum_{q=1}^{n_p} e^{+\frac{2i\pi}{n_p}(k-1)(q-1)}\widehat{\mathbf{Q}}(\omega_q;\theta_\ell)\,. \tag{3.26}$$

### 3.4.3 Computing of the realizations of $\mathbf{Q}(T)$ with the frequency domain formulation

Equation (3.25) allows for computing an approximation of the realization $\mathbf{Q}(T;\theta_\ell)$ by using the frequency domain formulation. It should be noted that $E\{\mathbf{Q}(T)\} \simeq \frac{1}{n_r}\sum_{\ell=1}^{n_r}\mathbf{Q}(T;\theta_\ell)$ is not zero in the numerical approximation framework because, for $k=1,\ldots,n_p$, $\frac{1}{n_r}\sum_{\ell=1}^{n_r}\mathbb{P}^{m_{\exp}}(t_k;\theta_\ell) = \underline{\mathbb{p}}(t_k)$ depends on $t_k$ and is different from $\underline{\mathbf{p}}$ computed using Eq. (3.11). But we have $\frac{1}{n_p}\sum_{k=1}^{n_p}\underline{\mathbb{p}}(t_k) = \underline{\mathbf{p}}$.

# Chapter 4

# Generator of realizations of the non-Gaussian stochastic process P

Since the number $n_r$ of realizations is assumed to be not sufficient for estimating the extreme value statistics, it is necessary to construct a generator for generating supplementary realizations of non-Gaussian stochastic process $\{\mathbf{P}(t), t \in [0,T]\}$ for which the available information is made up of the $n_r$ experimental measurements. For that, the following methodology is proposed, which consists (1) in performing a Karhunen-Loève (KL) statistical reduction of non-Gaussian process $\{\mathbf{P}(t), t \in [0,T]\}$, (2) in constructing polynomial chaos expansion (PCE) of the non-Gaussian random vector constituted by the coordinates of the KL statistical reduction, and (3) in estimating the coefficients of the PCE by solving a statistical inverse problem.

## 4.1 Statistical reduction of non-Gaussian stochastic process P

In this section, the KL statistical reduction [72, 82] of non-Gaussian stochastic process $\{\mathbf{P}(t), t \in [0,T]\}$ is presented. The KL statistical reduction $\{\mathbf{P}^{N_{\text{KL}}}(t), t \in [0,T]\}$ is given by the truncated KL expansion of stochastic process $\{\mathbf{P}(t), t \in [0,T]\}$,

$$\mathbf{P}^{N_{\text{KL}}}(t) = \sum_{j=1}^{N_{\text{KL}}} \sqrt{\mu_j}\, H_j\, \mathbf{b}^j(t) \quad , \quad t \in [0,T]\,,$$

in which $\mathbf{H} = (H_1, \ldots, H_{N_{\text{KL}}})$ is a second-order, centered, and non-Gaussian random vector (independent of time $t$) and where $N_{\text{KL}}$ is calculated such that $\mathbf{P}^{N_{\text{KL}}}$ be an approximation of $\mathbf{P}$ to $\varepsilon$ in a mean-square sense.

For given $t$ fixed in $[0\,,T]$, it is also useful to construct a reduced representation of random vector $\mathbf{P}(t)$, corresponding to its principal component analysis (PCA) [69],

$$\mathbf{P}^{N_{\text{PCA}}}(t) = \sum_{j=1}^{N_{\text{PCA}}} \sqrt{\Lambda_j}\, \Gamma_j(t)\, \mathbf{e}^j \,,$$

in which $\mathbf{\Gamma}(t) = (\Gamma_1(t), \ldots, \Gamma_{N_{\text{PCA}}}(t))$ is a centered non-Gaussian random vector, and where $N_{\text{PCA}}$ is calculated such that $\mathbf{P}^{N_{\text{PCA}}}(t)$ be an approximation of $\mathbf{P}(t)$ to $\varepsilon$ in a mean-square sense.

### 4.1.1 KL statistical reduction of non-Gaussian centered stochastic process $\{\mathbf{P}(t), t \in [0,T]\}$ with values in $\mathbb{R}^{m_{\text{exp}}}$

In accordance with the given explanations, the KL statistical reduction is based on the use of the truncated KL expansion of the second-order centered vector-valued stochastic process $\{\mathbf{P}(t)\,, t \in [0,T]\}$ whose covariance function is square integrable on $[0,T] \times [0,T]$ for which $T$ is finite.
The following items are presented:

- the continuous formulation of the KL statistical reduction;
- the time sampling of the continuous formulation;
- the algorithm for solving the eigenvalue problem related to time sampling of the continuous formulation;
- the generation of realizations for non-Gaussian random vector **H**.

#### 4.1.1.1 Continuous formulation of the KL statistical reduction

For the readability of this section, we summarize hereinafter the main mathematical properties for constructing the KL statistical reduction in the continuous formulation framework. Stochastic process $\mathbb{P}$ is such that

$$\mathbb{P}(t) = \underline{\mathbf{p}} + \mathbf{P}(t) \quad , \quad t \in [0,T]\,.$$

Since stochastic process $\{\mathbf{P}(t), t \in [0,T]\}$ is stationary, second-order, centered, and mean-square continuous, its covariance function (see Eq. (2.62)),

$$(t,t') \mapsto [C_{\mathbf{P}}(t-t')] = E\{\mathbf{P}(t)\mathbf{P}(t')^T\}$$

is continuous from $\mathbb{R} \times \mathbb{R}$ into $\mathbb{M}_{m_{\text{exp}}}(\mathbb{R})$. Consequently, $(t, t') \mapsto [C_{\mathbf{P}}(t - t')]$ is a bounded function on $[0, T] \times [0, T]$, which implies (see Eq. (2.65)),

$$\frac{1}{T^2} \int_0^T \int_0^T \|C_{\mathbf{P}}(t - t')\|_F^2 \, dt \, dt' < +\infty \,, \tag{4.1}$$

where $\|.\|_F$ is the Frobenius norm. Under these conditions [110], process $\{\mathbf{P}(t), t \in [0, T]\}$, admits the following KL expansion,

$$\mathbf{P}(t) = \sum_{j=1}^{+\infty} \sqrt{\mu_j} H_j \mathbf{b}^j(t) \quad , \quad t \in [0, T] \,, \tag{4.2}$$

in which $H_1, H_2, \ldots$ are non-Gaussian dependent real random variables, such that for all $j$ and $j'$ in $\mathbb{N}^*$,

$$E\{H_j\} = 0 \quad , \quad E\{H_j H_{j'}\} = \delta_{jj'} \,, \tag{4.3}$$

and where $\{\mu_j, \mathbf{b}^j(t)\}$ are the solutions of the eigenvalue problem,

$$\frac{1}{T} \int_0^T [C_{\mathbf{P}}(t - t')] \, \mathbf{b}^j(t') \, dt' = \mu_j \, \mathbf{b}^j(t) \quad , \quad \forall t \in [0, T] \,. \tag{4.4}$$

The eigenvalues constitute a decreasing ordered sequence such that

$$\mu_1 \geq \mu_2 \geq \ldots \geq 0 \,, \tag{4.5}$$

and the eigenvectors constitute a Hilbert basis of the space $\mathbf{L}^2([0, T], \mathbb{R}^{m_{\text{exp}}})$ of the square integrable functions on $[0, T]$ with values in $\mathbb{R}^{m_{\text{exp}}}$. Therefore, we have

$$< \mathbf{b}^j, \mathbf{b}^{j'} >_{\mathbf{L}^2} = \delta_{jj'} \,, \tag{4.6}$$

where $< ., . >_{\mathbf{L}^2}$ is the scalar product on $\mathbf{L}^2([0, T], \mathbb{R}^{m_{\text{exp}}})$ such that

$$< \mathbf{b}^j, \mathbf{b}^{j'} >_{\mathbf{L}^2} = \frac{1}{T} \int_0^T < \mathbf{b}^j(t), \mathbf{b}^{j'}(t) >_{\mathbb{R}^{m_{\text{exp}}}} \, dt \,. \tag{4.7}$$

The statistical reduction of order $N_{\text{KL}}$ of $\{\mathbf{P}(t), t \in [0, T]\}$ is written as,

$$\mathbf{P}^{N_{\text{KL}}}(t) = \sum_{j=1}^{N_{\text{KL}}} \sqrt{\mu_j} H_j \mathbf{b}^j(t) \quad , \quad t \in [0, T] \,, \tag{4.8}$$

and the reduction order $N_{\text{KL}}$ is computed such that

$$E\{\|\mathbf{P} - \mathbf{P}^{N_{\text{KL}}}\|_{\mathbf{L}^2}^2\} \leq \varepsilon^2 E\{\|\mathbf{P}\|_{\mathbf{L}^2}^2\} \,, \tag{4.9}$$

where $\|\mathbf{P}\|^2_{\mathbf{L}^2} =< \mathbf{P}, \mathbf{P} >_{\mathbf{L}^2} = \frac{1}{T}\int_0^T \|\mathbf{P}(t)\|^2_{\mathbb{R}^{m_{\exp}}} dt$ and where $\varepsilon > 0$ is chosen sufficiently small. Equation (4.9) leads us to introduce the error function,

$$\text{err}_{\text{KL}}(N_{\text{KL}}) = 1 - \frac{\sum_{j=1}^{N_{\text{KL}}} \mu_j}{E\{\|\mathbf{P}\|^2_{\mathbf{L}^2}\}}\,, \tag{4.10}$$

with

$$E\{\|\mathbf{P}\|^2_{\mathbf{L}^2}\} = \text{tr}[C_{\mathbf{P}}(0)]\,. \tag{4.11}$$

For all $j = 1, \ldots, N_{\text{KL}}$, random variable $H_j$ can be written as

$$H_j = \frac{1}{\sqrt{\mu_j}} < \mathbf{P}, \mathbf{b}^j >_{\mathbf{L}^2} = \frac{1}{\sqrt{\mu_j}} \frac{1}{T} \int_0^T < \mathbf{P}(t), \mathbf{b}^j(t) >_{\mathbb{R}^{m_{\exp}}} dt\,. \tag{4.12}$$

#### 4.1.1.2 Time sampling of the continuous formulation

There are several approaches for constructing a discretization of the eigenvalue problem defined by Eq. (4.4), such as the discretization of the weak formulation [28]. However, the framework adapted to the signal processing defined in Chapter 3 must be used, that is to say must be based on the time sampling $t_1, \ldots, t_{n_p}$ of $[0\,, T]$ with the constant time step $\Delta t = T/n_p$.

**Remark**. In order to simplify the notations, the same symbols are used for the time-sampled quantities.

The time sampling of Eq. (4.4) is written as,

$$\frac{1}{n_p} \sum_{k'=1}^{n_p} [C_{\mathbf{P}}(t_k - t_{k'})] \mathbf{b}^j(t_{k'}) = \mu_j \mathbf{b}^j(t_k) \quad , \quad k = 1, \ldots, n_p\,, \tag{4.13}$$

that can be rewritten as

$$\begin{bmatrix} [C_{11}] & \ldots & [C_{1n_p}] \\ \vdots & \ddots & \vdots \\ [C_{n_p 1}] & \ldots & [C_{n_p n_p}] \end{bmatrix} \begin{bmatrix} \mathbf{b}^j(t_1) \\ \vdots \\ \mathbf{b}^j(t_{n_p}) \end{bmatrix} = \mu_j \begin{bmatrix} \mathbf{b}^j(t_1) \\ \vdots \\ \mathbf{b}^j(t_{n_p}) \end{bmatrix}\,, \tag{4.14}$$

with

$$[C_{kk'}] = \frac{1}{n_p} [C_{\mathbf{P}}(t_k - t_{k'})] \in \mathbb{M}_{m_{\exp}}(\mathbb{R})\,. \tag{4.15}$$

Using a global notation, Eq. (4.14) can be rewritten as

$$[\mathscr{C}]\, \mathbb{b}^j = \mu_j \mathbb{b}^j \quad , \quad j = 1, \ldots, N_{\text{KL}}\,, \tag{4.16}$$

with $[\mathscr{C}] \in \mathbb{M}^{+0}_{m_{\text{exp}} \times n_p}(\mathbb{R})$ (with $\mathbb{M}^{+0}_n(\mathbb{R})$ the set of all the $(n \times n)$ positive symmetric real matrices) and where

$$\mathbb{b}^j = (\mathbf{b}^j(t_1), \ldots, \mathbf{b}^j(t_{n_p})) \in \mathbb{R}^{m_{\text{exp}} \times n_p} \quad , \quad j = 1, \ldots, N_{\text{KL}} \, . \tag{4.17}$$

Therefore, for $j$ and $j'$ in $\{1, \ldots, N_{\text{KL}}\}$, we have

$$\frac{1}{n_p} < \mathbb{b}^j, \mathbb{b}^{j'} >_{\mathbb{R}^{m_{\text{exp}} \times n_p}} = \delta_{jj'} \, . \tag{4.18}$$

Considering Eq. (4.8), the time-sampled statistical reduction of order $N_{\text{KL}}$ is written as,

$$\mathbf{P}^{N_{\text{KL}}}(t_k) = \sum_{j=1}^{N_{\text{KL}}} \sqrt{\mu_j} H_j \mathbf{b}^j(t_k) \quad , \quad k = 1, \ldots, n_p \, , \tag{4.19}$$

where $\mathbf{b}^j(t_1), \ldots, \mathbf{b}^j(t_{n_p})$ are the components of $\mathbb{b}^j$ defined by Eq. (4.17). The random vector $\mathbf{H} = (H_1, \ldots, H_{N_{\text{KL}}})$ with values in $\mathbb{R}^{N_{\text{KL}}}$ is second-order, non-Gaussian, with dependent components, and is such that

$$E\{\mathbf{H}\} = \mathbf{0} \quad ; \quad E\{\mathbf{H}\mathbf{H}^T\} = [I_{N_{\text{KL}}}] \, . \tag{4.20}$$

Each component $H_j$ is written as (see Eq. (4.12)),

$$H_j = \frac{1}{\sqrt{\mu_j}} \frac{1}{n_p} \sum_{k=1}^{n_p} < \mathbf{P}(t_k), \mathbf{b}^j(t_k) >_{\mathbb{R}^{m_{\text{exp}}}} \, . \tag{4.21}$$

#### 4.1.1.3 Algorithm for solving the eigenvalue problem related to time sampling of the continuous formulation

In order to construct the statistical reduction of order $N_{\text{KL}}$ defined by Eq. (4.19), the $N_{\text{KL}}$ largest positive eigenvalues $\mu_1 \geq \ldots \geq \mu_{N_{\text{KL}}} > 0$ of the eigenvalue problem defined by Eq. (4.16) must be computed. We recall that $N_{\text{KL}} < m_{\text{exp}} \times n_p$ is calculated for a fixed relative tolerance $\varepsilon$, by using the inequality $\text{err}_{\text{KL}}(N_{\text{KL}}) \leq \varepsilon$ (see Eq. (4.10)). The proposed method is based on [1, 45, 63]. It avoids the explicit construction of matrix $[\mathscr{C}]$.

**Algorithmic remarks.** The copmutation of the $N_{\text{KL}}$ largest eigenvalues $\mu_1 \geq \ldots \geq \mu_{N_{\text{KL}}}$ of matrix $[\mathscr{C}]$ requires, on the one hand the construction and the storage of matrix $[\mathscr{C}]$, and on the other hand the calculation of the largest eigenvalues and the associated eigenvectors using an iterative method such as the Krylov sequences [17] or the subspace iteration method [3]. For a high dimension problem, for instance $m_{\text{exp}} = 700$ and $n_p = 512$, we have $m_{\text{exp}} \times n_p = 358{,}400$. The

symmetric matrix $[\mathscr{C}]$ requires $(8 \times 358{,}400 \times 358{,}401/2)/10^9 = 514$ GB (Gega bytes) to be stocked. Therefore, a direct method induces difficulties and consequently, an algorithm based on the use of the SVD in "economy size" (existing in Matlab) also called "thin SVD" is proposed hereinafter, whose algorithm can be found in [50].

**Algorithm based on the "thin SVD".** It is recalled that $n_r$ realizations $\{\mathbf{P}(t;\theta_\ell), t \in [0,T]\}$ for $\ell = 1,\ldots,n_r$, of process $\{\mathbf{P}(t), t \in [0,T]\}$ sampled in $t_1,\ldots,t_{n_p}$ with the constant step $\Delta t = T/n_p$ are available. The following hypothesis (verified for the considered applications) is made

$$m_{\text{exp}} \times n_p > n_r \,. \tag{4.22}$$

For $\ell = 1,\ldots,n_r$, the vectors $\mathbb{P}^1,\ldots,\mathbb{P}^{n_r}$ are introduced such that

$$\mathbb{P}^\ell = (\mathbf{P}^\ell(t_1;\theta_\ell),\ldots,\mathbf{P}^\ell(t_{n_p};\theta_\ell)) \in \mathbb{R}^{m_{\text{exp}}\times n_p} \,. \tag{4.23}$$

Let $[w]$ be the rectangular matrix defined by

$$[w] = [\mathbb{P}^1 \ldots \mathbb{P}^{n_r}] \in \mathbb{M}_{m_{\text{exp}}\times n_p, n_r}(\mathbb{R}) \,. \tag{4.24}$$

The statistical estimation $[\widehat{\mathscr{C}}_{n_r}]$ of matrix $[\mathscr{C}]$, which is defined by Eqs. (4.14) and (4.16), can be written as,

$$[\widehat{\mathscr{C}}_{n_r}] = \frac{1}{n_p(n_r-1)} \sum_{\ell=1}^{n_r} \mathbb{P}^\ell (\mathbb{P}^\ell)^T \,, \tag{4.25}$$

and can be rewritten as,

$$[\widehat{\mathscr{C}}_{n_r}] = \frac{1}{n_r-1} (\frac{1}{\sqrt{n_p}}\,[w])\,(\frac{1}{\sqrt{n_p}}\,[w])^T \,. \tag{4.26}$$

It should be noted that the rank of matrix $[\widehat{\mathscr{C}}_{n_r}]$ is less or equal to $n_r$. Therefore, $N_{\text{KL}}$ is supposed to be such that

$$N_{\text{KL}} \leq n_r \,. \tag{4.27}$$

Let $[\mathbb{B}]$ be the $(m_{\text{exp}} \times n_p, n_r)$ real matrix whose columns are the eigenvectors $\mathbb{b}^1,\ldots,\mathbb{b}^{n_r}$ and let $[\mu]$ be the $(n_r \times n_r)$ diagonal matrix of the eigenvalues $\mu_1 \geq \ldots \geq \mu_{n_r}$,

$$[\mathbb{B}] = \frac{1}{\sqrt{n_p}}\,[\mathbb{b}^1 \ldots \mathbb{b}^{n_r}] \quad , \quad [\mu] = \begin{bmatrix} \mu_1 & & 0 \\ & \ddots & \\ 0 & & \mu_{n_r} \end{bmatrix} . \tag{4.28}$$

For $j = 1, \ldots, n_r$, Eqs. (4.16) and (4.18) can be rewritten, using the estimate $[\widehat{\mathscr{C}}_{n_r}]$ of $[\mathscr{C}]$, as

$$[\widehat{\mathscr{C}}_{n_r}]\,[\mathbb{B}] = [\mathbb{B}]\,[\mu]\,, \tag{4.29}$$

$$[\mathbb{B}]^T\,[\mathbb{B}] = [I_{n_r}]\,. \tag{4.30}$$

Then, it can easily be verified that the SVD of $[w] \in \mathbb{M}_{m_{\exp} \times n_p, n_r}(\mathbb{R})$ using the "thin SVD" algorithm, is written as

$$\frac{1}{\sqrt{n_p}}[w] = [\mathbb{B}][\Sigma][\mathbb{V}]^T\,, \tag{4.31}$$

in which matrix $[\mathbb{B}]$ is the solution of Eq. (4.29) under the constraint defined by Eq. (4.30), where $[\Sigma]$ is the $(n_r \times n_r)$ real diagonal matrix of the singular values, and where $[\mathbb{V}] \in \mathbb{M}_{n_r}(\mathbb{R})$ is such that $[\mathbb{V}]^T\,[\mathbb{V}] = [\mathbb{V}]\,[\mathbb{V}]^T = [I_{n_r}]$.
Considering Eqs. (4.26), (4.29), and (4.31), it can be deduced that

$$[\mu] = \frac{1}{n_r - 1}[\Sigma]^2\,. \tag{4.32}$$

Knowing $\mu_1 \geq \ldots \geq \mu_{n_r}$, and as $N_{\text{KL}} \leq n_r$, the error of the statistical reduction can be computed using Eq. (4.10) for $N_{\text{KL}} = 1, \ldots, n_r$.

#### 4.1.1.4 Generation of realizations for non-Gaussian random vector H

The notations of Section 4.1.1.3 are used, for which the $n_r$ time-sampled realizations of stochastic process **P** are represented by vectors $\mathbb{P}^\ell \in \mathbb{R}^{m_{\exp} \times n_p}$ for $\ell = 1, \ldots, n_r$. The $n_r$ corresponding realizations $\{\boldsymbol{\eta}^\ell\}_{\ell=1,\ldots,n_r}$ of random vector **H** are given by Eq.(4.21) in substituting **P** by its realizations. Consequently, for $j = 1, \ldots, N_{\text{KL}}$, we have

$$\eta_j^\ell = \frac{1}{\sqrt{\mu_j}}\frac{1}{n_p} < \mathbb{P}^\ell, \mathbb{b}^j >_{\mathbb{R}^{m_{\exp} \times n_p}}\,. \tag{4.33}$$

### 4.1.2 Reduction of centered non-Gaussian random vector $\mathbf{P}(t)$ at any fixed time $t$ using the principal component analysis

In this section, the PCA of random vector $\mathbf{P}(t)$ at any $t$ fixed in $[0, T]$ is constructed, which differs from the KL statistical reduction of stochastic process $\{\mathbf{P}(t), t \in [0\,, T]\}$ that is presented in Section 4.1.1. This reduction will be used for $t = T$, that is to say for the PCA of the random vector $\mathbf{P}(T)$ in Section 5.3. Let $[C_{\mathbf{P}}] \in \mathbb{M}_{m_{\exp}}(\mathbb{R})$ be the covariance matrix of centered second-order random

vector $\mathbf{P}(t)$, for $t$ fixed in $[0,T]$. As stochastic process $\mathbf{P}$ is stationary on $\mathbb{R}$, this covariance matrix that is defined by

$$[C_{\mathbf{P}}] = E\{\mathbf{P}(t)\mathbf{P}(t)^T\}\,, \tag{4.34}$$

is independent of $t$. Let $\mathbf{e}^1, \ldots, \mathbf{e}^{m_{\text{exp}}}$ be the orthonormal eigenvectors of $[C_{\mathbf{P}}]$ associated with the ordered eigenvalues

$$\Lambda_1 \geq \Lambda_2 \geq \ldots \geq \Lambda_{m_{\text{exp}}} \geq 0\,, \tag{4.35}$$

such that

$$[C_{\mathbf{P}}]\,\mathbf{e}^j = \Lambda_j\,\mathbf{e}^j \quad , \quad j = 1, \ldots, m_{m_{\text{exp}}}\,. \tag{4.36}$$

Let $N_{\text{PCA}} \leq m_{\text{exp}}$ be the reduction order. Let $[\mathbb{e}]$ be the rectangular matrix and $[\Lambda]$ be the diagonal matrix such that

$$[\mathbb{e}] = [\mathbf{e}^1 \ldots \mathbf{e}^{N_{\text{PCA}}}] \in \mathbb{M}_{m_{\text{exp}}, N_{\text{PCA}}}(\mathbb{R})\,, \tag{4.37}$$

$$[\mathbf{\Lambda}] = \begin{bmatrix} \Lambda_1 & & 0 \\ & \ddots & \\ 0 & & \Lambda_{N_{\text{PCA}}} \end{bmatrix}\,. \tag{4.38}$$

The orthonormality of vectors $\mathbf{e}^1, \ldots, \mathbf{e}^{N_{\text{PCA}}}$ yields

$$[\mathbb{e}]^T\,[\mathbb{e}] = [I_{N_{\text{PCA}}}]\,. \tag{4.39}$$

For all $t$ fixed in $[0,T]$, the statistical reduced representation of order $N_{\text{PCA}}$ is then written as,

$$\mathbf{P}^{N_{\text{PCA}}}(t) = [\mathbb{e}]\,[\mathbf{\Lambda}]^{1/2}\,\mathbf{\Gamma}(t)\,, \tag{4.40}$$

where $\mathbf{\Gamma}(t) = (\Gamma_1(t), \ldots, \Gamma_{N_{\text{PCA}}}(t))$ is the centered second-order non-Gaussian random vector such that

$$\mathbf{\Gamma}(t) = [\mathbf{\Lambda}]^{-1/2}\,[\mathbb{e}]^T\,\mathbf{P}(t)\,. \tag{4.41}$$

The reduction order $N_{\text{PCA}}$ is chosen such that

$$E\{\|\mathbf{P}(t) - \mathbf{P}^{N_{\text{PCA}}}(t)\|^2_{\mathbb{R}^{m_{\text{exp}}}}\} \leq \varepsilon^2\,E\{\|\mathbf{P}(t)\|^2_{\mathbb{R}^{m_{\text{exp}}}}\}\,, \tag{4.42}$$

where $\epsilon$ is the relative error tolerance. The value of $N_{\text{PCA}}$ is obtained by the analysis of the function $N_{\text{PCA}} \mapsto \text{err}_{\text{PCA}}(N_{\text{PCA}})$ such that

$$\text{err}_{\text{PCA}}(N_{\text{PCA}}) = 1 - \frac{\sum_{j=1}^{N_{\text{PCA}}} \Lambda_j}{\text{tr}[C_{\mathbf{P}}]}\,. \tag{4.43}$$

Using the notations introduced in Section 4.1.1, we define the vectors $\mathbf{p}_t^\ell$ such that,

$$\mathbf{p}_t^\ell = \mathbf{P}(t, \theta_\ell) \in \mathbb{R}^{m_{\text{exp}}} \quad , \quad \ell = 1, \ldots, n_r \, , \tag{4.44}$$

where $t$ is any time of the time sampling $t_1, \ldots, t_{n_p}$. Using these notations, the estimate $[\widehat{C}_{n_r}]$ of $[C_{\mathbf{P}}]$ is classically written as,

$$[\widehat{C}_{n_r}] = \frac{1}{n_r - 1} \sum_{\ell=1}^{n_r} \mathbf{p}_t^\ell \, \mathbf{p}_t^{\ell T} \, . \tag{4.45}$$

## 4.2 Polynomial chaos representation of non-Gaussian stochastic process P

The mehodology of the computation of the equivalent static forces, which is presented in Chapter 5, requires the estimation of non-Gaussian conditional probability density functions related to random variables $\mathbf{P}(T)$, $\mathbf{Q}(T)$, and $\mathbf{U}(T)$. These non-Gaussian conditional probability density functions cannot be given in an explicit form and consequently, will be estimated in a nonparametric probabilistic framework [13, 49, 61] using a large number of realizations. As it has been assumed that the number $n_r$ of experimental realizations is not sufficiently large for estimating extreme value statistics, it is necessary to construct a generator of realizations in order to be able to generate $\nu \gg n_r$ independent realizations of non-Gaussian stochastic process $\{\mathbf{P}(t), t \in [0, T]\}$. This generator will be obtained by using a PCE of non-Gaussian process $\{\mathbf{P}(t), t \in [0, T]\}$, whose construction is based on the PCE of the random coordinates of its truncated KL expansion presented in Section 4.1. The PCE of stochastic processes and fields has been initialized by Ghanem [47] based on the Wiener works. The methodology proposed by Ghanem has been used later to study several problems (see for instance [34, 37, 40, 79, 115]) and has been extended to the cases for which the chaos germ follows an arbitrary probability distribution [119, 117, 139], for which the coefficients of the PCE are random, for which the number of the PCE coefficients has to be reduced [11, 12, 128], for which the probability distribution is multimodal [113], and for which the probability distribution is on a manifold [120]. The identification method of the PCE coefficients from experimental data or from numerical simulations is presented in Section 4.3. It should be noted that there is no mathematical relation between the PCE of a non-Gaussian random vector and the orthogonal polynomial representation of its multidimensional probability density function. This last method was analyzed in detail in the 1980's by the scientific community and the works, which have been carried out, have shown that this type of approach posed some difficulties related to the convergence and to the preservation of algebraic properties such as positivity. Consequently, for the problem we

have to deal with, the PCE of non-Gaussian random vector $\mathbf{H} = (H_1, \ldots, H_{N_{\text{KL}}})$ that has been obtained from the truncated KL expansion of non-Gaussian stochastic process $\{\mathbf{P}(t), t \in [0,T]\}$ is used. The experimental identification of the deterministic $\mathbb{R}^{m_{\text{exp}}}$-valued coefficients of the PCE must be performed by using algorithms that must be efficient for large dimensions (see Section 4.3). Assuming the PCE of non-Gaussian $\mathbb{R}^{m_{\text{exp}}}$-valued stochastic process $\{\mathbf{P}(t), t \in [0,T]\}$ is constructed, we therefore dispose of a generator of independent realizations of $\{\mathbf{P}(t), t \in [0,T]\}$.

In this section, we present the construction of the PCE of non-Gaussian $\mathbb{R}^{m_{\text{exp}}}$-valued stochastic process $\{\mathbf{P}(t), t \in [0,T]\}$. As we have explained, the methodology and the algorithms devoted to the experimental identification of the PCE coefficients will be presented in Section 4.3.

### 4.2.1 Reminder on the KL statistical reduction of stochastic process $\{\mathbf{P}(t)\,, t \in [0,T]\}$

Assuming that the convergence analysis of the KL expansion of stochastic process $\{\mathbf{P}(t)\,, t \in [0,T]\}$ has already been done, the reduction-order value $N_{\text{KL}}$ that corresponds to a given tolerance of the error defined by Eq. (4.10), is known. It can then be written as,

$$\mathbf{P}(t) \simeq \mathbf{P}^{N_{\text{KL}}}(t) = \sum_{j=1}^{N_{\text{KL}}} \sqrt{\mu_j}\, H_j\, \mathbf{b}^j(t) \quad , \quad t \in [0,T]\,. \tag{4.46}$$

Let $\mathbf{H} = (H_1, \ldots, H_{N_{\text{KL}}})$ be the random vector with values in $\mathbb{R}^{N_{\text{KL}}}$. This vector is non-Gaussian, second-order,

$$E\{\|\mathbf{H}\|^2_{\mathbb{R}^{N_{\text{KL}}}}\} < +\infty\,, \tag{4.47}$$

centered and its covariance matrix is the identity matrix (see Eq. (4.20)),

$$E\{\mathbf{H}\} = \mathbf{0} \quad ; \quad E\{\mathbf{H}\,\mathbf{H}^T\} = [I_{N_{\text{KL}}}]\,. \tag{4.48}$$

### 4.2.2 Polynomial chaos expansion of non-Gaussian vector H

The random germ of the PCE of **H** is chosen as the normalized Gaussian vector and consequently, the orthogonal polynomials are the normalized multivariate Hermite polynomials. This choice is dictated by the fact that the Gaussian approximation is directly obtained by taking only the polynomials of degree zero and one, which would not be the case if non-Gaussian germ were taken.

**(i) Introduction of the Gaussian germ.** Let $\boldsymbol{\Xi} = (\Xi_1, \ldots, \Xi_{N_g})$ be the normalized Gaussian random vector defined on the probability space $(\Theta, \mathcal{T}, \mathscr{P})$ with values in $\mathbb{R}^{N_g}$, that is to say,

$$E\{\boldsymbol{\Xi}\} = \mathbf{0} \quad , \quad E\{\boldsymbol{\Xi}\,\boldsymbol{\Xi}^T\} = [I_{N_g}]\,. \tag{4.49}$$

The integer $N_g$ that defines the length of the Gaussian germ is such that

$$1 \leq N_g \leq N_{\text{KL}}\,, \tag{4.50}$$

and must be estimated using the identification procedure based on the experimental measurements of the unsteady pressure field (see Eq. (3.13) with Eqs. (3.7) and (3.11)).

**(ii) Introduction of the normalized multivariate Hermite polynomials.** Let $N_d \geq 1$ be a fixed integer corresponding to the maximum degree of the normalized multivariate Hermite polynomials,

$$\Psi_{\boldsymbol{\beta}}(\boldsymbol{\Xi}) = \psi_{\beta_1}(\Xi_1) \times \ldots \times \psi_{\beta_{N_g}}(\Xi_{N_g})\,, \tag{4.51}$$

where $\boldsymbol{\beta} = (\beta_1, \ldots, \beta_{N_g})$ is the multi-index of length $N_g$ such that

$$\beta_j \in \{0, 1, \ldots, N_d\} \quad , \quad j = 1, \ldots, N_g\,, \tag{4.52}$$

and where $\psi_{\beta_j}(\Xi_j)$ are the normalized Hermite polynomials such that

$$\psi_0(\Xi_j) = 1\,. \tag{4.53}$$

For all $\beta_j$ and $\beta'_j$, the orthonormality property writes,

$$E\{\psi_{\beta_j}(\Xi_j)\,\psi_{\beta'_j}(\Xi_j)\} = \int_{\mathbb{R}} \psi_{\beta_j}(\xi)\,\psi_{\beta'_j}(\xi)\,\frac{1}{\sqrt{2\pi}}\,e^{-\xi^2/2}\,d\xi = \delta_{\beta_j\beta'_j}\,. \tag{4.54}$$

The normalized Hermite polynomial of degree $n$ is written as $\psi_n(\xi) = H_n(\xi)/\sqrt{n!}$ with $H_n(\xi)$ the Hermite polynomial of degree $n$. These polynomials can be computed using the following recurrence relation,

$$H_{n+1}(\xi) = \xi\,H_n(\xi) - n\,H_{n-1}(\xi) \quad , \quad n \geq 1\,. \tag{4.55}$$

with $H_0(\xi) = 1$ and $H_1(\xi) = \xi$. Thus $H_2(\xi) = \xi^2 - 1$, etc. From Eqs. (4.51) and (4.54), it can be deduced the orthonormality property for the normalized multivariate Hermite polynomials,

$$E\{\Psi_{\boldsymbol{\beta}}(\boldsymbol{\Xi})\,\Psi_{\boldsymbol{\beta}'}(\boldsymbol{\Xi})\} = \int_{\mathbb{R}^{N_g}} \Psi_{\boldsymbol{\beta}}(\boldsymbol{\xi})\,\Psi_{\boldsymbol{\beta}'}(\boldsymbol{\xi})\,\frac{1}{(2\pi)^{N_g/2}}\,e^{-\frac{1}{2}\|\boldsymbol{\xi}\|^2_{\mathbb{R}^{N_g}}}\,d\boldsymbol{\xi} = \delta_{\boldsymbol{\beta}\boldsymbol{\beta}'}\,, \tag{4.56}$$

in which

$$\delta_{\boldsymbol{\beta}\boldsymbol{\beta}'} = \delta_{\beta_1\beta'_1} \times \ldots \times \delta_{\beta_{N_g}\beta'_{N_g}} \,. \tag{4.57}$$

Because the zero-degree multivariate polynomial $\Psi_{\mathbf{0}}(\boldsymbol{\Xi})$ is equal to 1, from Eq. (4.56), it can be deduced that, for all multi-index $\boldsymbol{\beta}$ not equal to $\mathbf{0}$,

$$E\{\Psi_{\boldsymbol{\beta}}(\boldsymbol{\Xi})\} = \mathbf{0} \,. \tag{4.58}$$

For fixed integer $N_d$ such that $1 \leq N_d \leq +\infty$ and for fixed $N_g$ such that $1 \leq N_g \leq N_{\text{KL}}$, we define the set $\mathcal{N}_{N_d,N_g}$ by

$$\mathcal{N}_{N_d,N_g} = \{\boldsymbol{\beta} = (\beta_1, \ldots, \beta_{N_g}) \in \mathbb{N}^{N_g} \,|\, 0 < \beta_1 + \ldots + \beta_{N_g} \leq N_d\} \,. \tag{4.59}$$

The number $K(N_d, N_g)$ of the elements of set $\mathcal{N}_{N_d,N_g}$, which depends on $N_d$ and $N_g$, is written as

$$K(N_d, N_g) = \frac{(N_g + N_d)!}{N_g!\, N_d!} - 1 \,. \tag{4.60}$$

This number does not include the zero-degree multivariate polynomial $\Psi_{\mathbf{0}}(\boldsymbol{\xi}) = 1$ for the multi-index $\mathbf{0} = (0, \ldots, 0)$.

**Remark**. The zero-degree multivariate polynomial is not included, because the non-Gaussian random vector $\mathbf{H}$ is centered (see Eq. (4.48)).

Let $\kappa$ be the integer belonging to the set $\{1, \ldots, K(N_d, N_g)\}$. We rewrite $\{\boldsymbol{\beta}^{(\kappa)}$, $\kappa = 1, \ldots, K(N_d, N_g)\}$, the set of the multi-indices $\boldsymbol{\beta}$ that belong to $\mathcal{N}_{N_d,N_g}$.

**(iii) Truncated Gaussian polynomial chaos expansion of non-Gaussian vector H.** The approximation $\mathbf{H}^{(N_d,N_g)}$ of second-order centered non-Gaussian random vector $\mathbf{H}$ with values in $\mathbb{R}^{N_{\text{KL}}}$, is written as

$$\mathbf{H}^{(N_d,N_g)} = \sum_{\kappa=1}^{K(N_d,N_g)} \mathbf{z}^{\kappa}\, \Psi_{\boldsymbol{\beta}^{(\kappa)}}(\boldsymbol{\Xi}) \,, \tag{4.61}$$

where $\mathbf{z}^1, \ldots, \mathbf{z}^{K(N_d,N_g)}$ are deterministic vectors in $\mathbb{R}^{N_{\text{KL}}}$ such that, for all $\kappa$ in $\{1, \ldots, K(N_d, N_g)\}$,

$$\mathbf{z}^{\kappa} = E\{\mathbf{H}\, \Psi_{\boldsymbol{\beta}^{(\kappa)}}(\boldsymbol{\Xi})\} \,. \tag{4.62}$$

Using Eqs. (4.56) and (4.58), it can be easily verified that

$$E\{\mathbf{H}^{(N_d,N_g)}\} = \mathbf{0} \,, \tag{4.63}$$

$$E\{\mathbf{H}^{(N_d,N_g)}\mathbf{H}^{(N_d,N_g)T}\} = \sum_{\kappa=1}^{K(N_d,N_g)} \mathbf{z}^{\kappa}\, (\mathbf{z}^{\kappa})^T \,. \tag{4.64}$$

Taking into account Eq. (4.48), from Eq. (4.64) it can be deduced that, for a fixed value of $N_g$,

$$\lim_{N_d \to +\infty} \sum_{\kappa=1}^{K(N_d,N_g)} \mathbf{z}^\kappa \, (\mathbf{z}^\kappa)^T = [I_{N_{\mathrm{KL}}}] \, . \tag{4.65}$$

**Remark**. For the identification of the vector-valued coefficients $\mathbf{z}^1, \ldots, \mathbf{z}^{K(N_d,N_g)}$ (see Section 4.3), Equation (4.65) is rewritten as

$$\sum_{\kappa=1}^{K(N_d,N_g)} \mathbf{z}^\kappa \, (\mathbf{z}^\kappa)^T = [I_{N_{\mathrm{KL}}}] \, , \tag{4.66}$$

and will be used as a constraint equation in the identification procedure.

**(iv) Convergence of the truncated polynomial chaos expansion of non-Gaussian vector H.** As **H** is a second-order random vector, it is known that

$$\lim_{N_d \to +\infty, N_g \to N_{\mathrm{KL}}} \mathbf{H}^{(N_d,N_g)} = \mathbf{H} \, , \tag{4.67}$$

in the space $\mathbf{L}^2(\Theta, \mathbb{R}^{N_{\mathrm{KL}}})$ of all the second-order random vectors defined on $(\Theta, \mathcal{T}, \mathscr{P})$, with values in $\mathbb{R}^{N_{\mathrm{KL}}}$. The considered norm of $\mathbf{L}^2(\Theta, \mathbb{R}^{N_{\mathrm{KL}}})$ is

$$\|\mathbf{H}\|_{\mathbf{L}^2(\Theta,\mathbb{R}^{N_{\mathrm{KL}}})} = \sqrt{E\{\|\mathbf{H}\|^2_{\mathbb{R}^{N_{\mathrm{KL}}}}\}} \, . \tag{4.68}$$

From Eq. (4.66), it can be seen that the convergence rate can be analyzed by studying the function $(N_d, N_g) \mapsto \|\mathbf{H}^{(N_d,N_g)}\|_{\mathbf{L}^2(\Theta,\mathbb{R}^{N_{\mathrm{KL}}})}$ such that

$$\|\mathbf{H}^{(N_d,N_g)}\|^2_{\mathbf{L}^2(\Theta,\mathbb{R}^{N_{\mathrm{KL}}})} = \sum_{\kappa=1}^{K(N_d,N_g)} \|\mathbf{z}^\kappa\|^2_{\mathbb{R}^{N_{\mathrm{KL}}}} \, . \tag{4.69}$$

Equations (4.48) and (4.67) yield

$$\lim_{N_d \to +\infty, N_g \to N_{\mathrm{KL}}} \|\mathbf{H}^{(N_d,N_g)}\|^2_{\mathbf{L}^2(\Theta,\mathbb{R}^{N_{\mathrm{KL}}})} = \mathrm{tr} E\{\mathbf{H}\,\mathbf{H}^T\} = N_{\mathrm{KL}} \, , \tag{4.70}$$

which gives, using Eq. (4.69),

$$\lim_{N_d \to +\infty, N_g \to N_{\mathrm{KL}}} \sum_{\kappa=1}^{K(N_d,N_g)} \|\mathbf{z}^\kappa\|^2_{\mathbb{R}^{N_{\mathrm{KL}}}} = N_{\mathrm{KL}} < +\infty \, . \tag{4.71}$$

**Remark 1**. As we will see in Section 4.3, using the convergence criterion related to Eq. (4.66), the experimental identification of the PCE of **H** requires the calculation of $N_d$, $N_g$, and $\mathbf{z}^1, \ldots, \mathbf{z}^{K(N_d,N_g)}$.

**Remark 2**. For all $1 \leq N_g \leq N_{\text{KL}}$, and for $N_d = 1$, it can be seen that, for all $\boldsymbol{\beta}$ fixed in $\mathcal{N}_{1,N_g}$ (therefore $0 < \beta_1 + \ldots + \beta_{N_g} = 1$), the centered random variable $\Psi_{\boldsymbol{\beta}}(\boldsymbol{\Xi})$ is Gaussian, and consequently, the centered random variable $\mathbf{H}^{(1,N_g)}$ defined by Eq. (4.61) is Gaussian. From Eq. (4.46), it can be deduced that $\{\mathbf{P}(t), t \in [0,T]\}$ is a Gaussian centered stochastic process. The non-Gaussian property of stochastic process $\{\mathbf{P}(t), t \in [0,T]\}$ is therefore taken into account by the representation defined by Eqs. (4.46) and (4.61), taking $N_d \geq 2$ in $\mathcal{N}_{N_d,N_g}$ that is defined by Eq. (4.59).

### 4.2.3 Truncated polynomial chaos expansion of non-Gaussian process $\{\mathbf{P}(t)\,, t \in [0,T]\}$

It is assumed that the identification procedure, which will be presented in Section 4.3, has been applied in order to calculate the values of $N_d$, $N_g$, and $\mathbf{z}^1, \ldots,$ $\mathbf{z}^{K(N_d,N_g)}$ for a given value of the error tolerance. Under these conditions, $N_d$ and $N_g$ being fixed to their optimal values, we have

$$\mathbf{H} \simeq \mathbf{H}^{(N_d,N_g)} = \sum_{\kappa=1}^{K(N_d,N_g)} \mathbf{z}^{\kappa}\, \Psi_{\boldsymbol{\beta}^{(\kappa)}}(\boldsymbol{\Xi})\,. \tag{4.72}$$

Using time sampling $t_1, \ldots, t_{n_p}$ of $[0,T]$ introduced in Chapter 3 and using Eq. (4.46), for all $k = 1, \ldots, n_p$, we have

$$\mathbf{P}(t_k) \simeq \mathbf{P}^{N_{\text{KL}}}(t_k) = \sum_{j=1}^{N_{\text{KL}}} \sqrt{\mu_j}\, H_j^{(N_d,N_g)}\, \mathbf{b}^j(t_k)\,, \tag{4.73}$$

in which $\mathbf{H}^{(N_d,N_g)} = (H_1^{(N_d,N_g)}, \ldots, H_{N_{\text{KL}}}^{(N_d,N_g)})$ is given by Eq. (4.72) and where, for all $j = 1, \ldots, N_{\text{KL}}$, the vectors $\mathbf{b}^j(t_1), \ldots, \mathbf{b}^j(t_{n_p})$ are computed using Eqs. (4.17), (4.28), and (4.31).

### 4.2.4 Generator of independent realizations of non-Gaussian stochastic process $\{\mathbf{P}(t), t \in [0,T]\}$

As explained before, the $n_r$ experimental realizations $\mathbf{P}(t_k;\theta_\ell)$ for $k = 1, \ldots, n_p$ and $\ell = 1, \ldots, n_r$ are assumed to be not sufficient for obtaining a reasonable convergence of the statistical estimators of the conditional probability density functions that will be constructed in Chapter 5. Consequently, $\nu \gg n_r$ independent realizations must be generated by Eq. (4.73) with Eq. (4.72). Let $\boldsymbol{\Xi}(\theta_1), \ldots, \boldsymbol{\Xi}(\theta_\nu)$ be independent realizations of the normalized Gaussian $\mathbb{R}^{N_g}$-valued random variable $\boldsymbol{\Xi}$. Therefore, the $\nu$ independent realizations of non-Gaussian random vectors

$\{\mathbf{P}(t_k), k = 1, \ldots, n_p\}$ are computed, for $k = 1, \ldots, n_p$, and $\ell = 1, \ldots, \nu$, by

$$\mathbf{P}(t_k; \theta_\ell) \simeq \sum_{j=1}^{N_{\text{KL}}} \sqrt{\mu_j}\, H_j^{(N_d,N_g)}(\theta_\ell)\, \mathbf{b}^j(t_k)\,, \tag{4.74}$$

in which $\mathbf{H}^{(N_d,N_g)}(\theta_\ell) = (H_1^{(N_d,N_g)}(\theta_\ell), \ldots, H_{N_{\text{KL}}}^{(N_d,N_g)}(\theta_\ell))$ is the $\ell$-th realization of $\mathbf{H}^{(N_d,N_g)}$ such that

$$\mathbf{H}^{(N_d,N_g)}(\theta_\ell) = \sum_{\kappa=1}^{K(N_d,N_g)} \mathbf{z}^\kappa\, \Psi_{\boldsymbol{\beta}^{(\kappa)}}(\Xi(\theta_\ell))\,. \tag{4.75}$$

## 4.3 Estimation of the coefficients of the polynomial chaos expansion of H

### 4.3.1 Brief review of methods

There exist several methods for identifing the coefficients $\mathbf{z}^\kappa$ of the PCE of **H** defined by Eq. (4.61), with the experimental realizations $\boldsymbol{\eta}^\ell = (\eta_1^\ell, \ldots, \eta_{N_{\text{KL}}}^\ell)$ that have been computed by using Eq. (4.33) for $\ell = 1, \ldots, n_r$. These methods belong to the class of the statistical inverse methods [66, 70, 123, 127, 138] that use the maximum likelihood principle [102, 123] and/or the Bayes method [15, 23, 124]. First works on the identification of the PCE coefficients of non-Gaussian stochastic processes and fields from experimental data have been proposed in [35]. Then some efficient methods have been proposed [46] for relatively small dimensions (see for instance [27, 86, 2, 12]). Then, more advanced approaches have been proposed for solving these statistical inverse problems for very large dimension [112, 95, 90, 115]. These methods require the construction of algebraic models that are informative [112, 54, 90, 115] to enrich available data that are mostly partial and limited, and also require the development of associated random generators.

In this work, the method proposed is deduced from the one initially developed in [112] and improved in [95]. This method uses a formulation based on the maximum likelihood for which the admissible set is a Stiefel manifold that corresponds to the constraint defined by Eq. (4.66). For solving the formulated optimization problem, it is necessary to use a random search algorithm for exploring the Stiefel manifold. Two algorithms are used, the first one has been proposed in [112] and is based on an exploitation, orthogonal direction by orthogonal direction, of the manifold, and the algorithm recently proposed in [118], which uses an appropriate

parameterization of the Stiefel manifold. In the case where the static acceleration method is used, $N_{\text{KL}}$ can be large (from $50$ to $100$ or even more). For such a case, it is possible to use additional methods with respect to the general method described before in order to reduce the numerical cost (see Sections 4.3.3 and 4.3.5).

**Remark**. The estimation of coefficients $\mathbf{z}^\kappa, \kappa = 1, \ldots, K(N_d, N_g)$ of the PCE defined by Eq. (4.61) cannot be done using Eq. (4.62) because the experimental realizations $\{\boldsymbol{\eta}^\ell, \ell = 1, \ldots, n_r\}$ of $\mathbf{H}$ are independent of the random vector $\boldsymbol{\Xi}$ and consequently Eq. (4.62) gives $\mathbf{z}^\kappa = \mathbf{0}$. That is the reason why the maximum likelihood is used.

### 4.3.2 Estimation of the coefficients in the general framework

For fixed $N_d$ and $N_g$, and for $\kappa = 1, \ldots, K(N_d, N_g)$, the estimate $\mathbf{z}^{\kappa,\text{opt}}$ of coefficients $\mathbf{z}^\kappa$ of non-Gaussian random vector $\mathbf{H}^{(N_d,N_g)}$ defined by Eq. (4.61) is performed using the maximum likelihood principle. In this section, $K(N_d, N_g)$ is simply denoted by $K$. Taking into account Eq. (4.66), the admissible set $\mathscr{C}_{\text{ad}}$ is defined as the subset of $(\mathbb{R}^{N_{\text{KL}}})^K$, such that

$$\mathscr{C}_{\text{ad}} = \{(\mathbf{z}^1, \ldots, \mathbf{z}^K) \in (\mathbb{R}^{N_{\text{KL}}})^K \; ; \; \sum_{\kappa=1}^{K} \mathbf{z}^\kappa \, (\mathbf{z}^\kappa)^T = [I_{N_{\text{KL}}}]\} \, . \tag{4.76}$$

Therefore, the maximum likelihood principle yields the following optimization problem

$$(\mathbf{z}^{1,\text{opt}}, \ldots, \mathbf{z}^{K,\text{opt}}) = \arg\{\max_{(\mathbf{z}^1,\ldots,\mathbf{z}^K)\in\mathscr{C}_{\text{ad}}} \mathscr{L}(\mathbf{z}^1, \ldots, \mathbf{z}^K)\} \, , \tag{4.77}$$

where $\mathscr{L}(\mathbf{z}^1, \ldots, \mathbf{z}^K)$ is the $\log_{10}$ likelihood function that is written as

$$\mathscr{L}(\mathbf{z}^1, \ldots, \mathbf{z}^K) = \sum_{\ell=1}^{n_r} \log_{10} p_{\mathbf{H}^{(N_d,N_g)}}(\boldsymbol{\eta}^\ell; \mathbf{z}^1, \ldots, \mathbf{z}^K) \, , \tag{4.78}$$

where $\{\boldsymbol{\eta}^\ell\}_{\ell=1,\ldots,n_r}$ are given by Eq. (4.33), and where $\boldsymbol{\eta} \mapsto p_{\mathbf{H}^{(N_d,N_g)}}(\boldsymbol{\eta}; \mathbf{z}^1, \ldots, \mathbf{z}^K)$ is the probability density function on $\mathbb{R}^{N_{\text{KL}}}$ of random vector $\mathbf{H}^{(N_d,N_g)}$ defined by Eq. (4.61). For all $\mathbf{z}^1, \ldots, \mathbf{z}^K$ fixed in $\mathbb{R}^{N_{\text{KL}}}$, the value $p_{\mathbf{H}^{(N_d,N_g)}}(\boldsymbol{\eta}^\ell; \mathbf{z}^1, \ldots, \mathbf{z}^K)$ of $p_{\mathbf{H}^{(N_d,N_g)}}(\boldsymbol{\eta}; \mathbf{z}^1, \ldots, \mathbf{z}^K)$ at $\boldsymbol{\eta} = \boldsymbol{\eta}^\ell$ is estimated using the Gaussian kernel estimation method on the nonparametric statistics for which $\nu$ realizations $\{\widetilde{\boldsymbol{\eta}}^{\ell'}, \ell' = 1, \ldots, \nu\}$ of $\mathbf{H}^{(N_d,N_g)}$ are calculated by

$$\widetilde{\boldsymbol{\eta}}^{\ell'} = \sum_{\kappa=1}^{K} \mathbf{z}^\kappa \Psi_{\boldsymbol{\beta}^{(\kappa)}}(\boldsymbol{\Xi}(\theta'_{\ell'})) \, , \tag{4.79}$$

in which $\boldsymbol{\Xi}(\theta'_1), \ldots, \boldsymbol{\Xi}(\theta'_\nu)$ are $\nu$ independent realizations of $\boldsymbol{\Xi}$.

### 4.3.3 Partition of H in a group of independent random vectors

It could be interesting to analyze if the non-Gaussian dependent components $H_1, \ldots, H_{N_{\text{KL}}}$ of random vector $\mathbf{H}$ can be written as

$$\mathbf{H} = (\mathbf{H}^1, \ldots, \mathbf{H}^{n_{\text{ind}}}) \,, \tag{4.80}$$

in which $\mathbf{H}^1, \ldots, \mathbf{H}^{n_{\text{ind}}}$ are independent random vectors of dimension smaller than $N_{\text{KL}}$. For all $\gamma = 1, \ldots n_{\text{ind}}$, the random vector $\mathbf{H}^\gamma = (H_1^\gamma, \ldots, H_{n_\gamma}^\gamma)$ is with values in $\mathbb{R}^{n_\gamma}$, such that

$$\sum_{\gamma=1}^{n_{\text{ind}}} n_\gamma = N_{\text{KL}} \,. \tag{4.81}$$

If such a partition can be constructed with $n_{\text{ind}} > 1$, then the PCE of $\mathbf{H}$ that is defined by Eq. (4.61), for which there is $K(N_d, N_g)$ coefficients $\mathbf{z}^\kappa$ with values in $\mathbb{R}^{N_{\text{KL}}}$, can be replaced by $n_{\text{ind}}$ PCE such that, for $\gamma = 1, \ldots, n_{\text{ind}}$,

$$\mathbf{H}^\gamma = \sum_{\kappa=1}^{K^\gamma(N_d^\gamma, N_g^\gamma)} \mathbf{z}_\gamma^\kappa \Psi_{\boldsymbol{\beta}_\gamma^{(\kappa)}}(\boldsymbol{\Xi}^\gamma) \,, \tag{4.82}$$

in which $\boldsymbol{\Xi}^1, \ldots, \boldsymbol{\Xi}^{n_{\text{ind}}}$ are independent normalized Gaussian vectors with unknown dimensions $N_g^1, \ldots, N_g^{n_{\text{ind}}}$ respectively, which have to be identified under the following constraints

$$\sum_{\gamma=1}^{n_{\text{ind}}} N_g^\gamma = N_g \quad , \quad N_g^\gamma \leq n_\gamma \ , \ \gamma = 1, \ldots, n_{\text{ind}} \,. \tag{4.83}$$

It can be verified that $N_g = \sum_{\gamma=1}^{n_{\text{ind}}} N_g^\gamma \leq \sum_{\gamma=1}^{n_{\text{ind}}} n_\gamma = N_{\text{KL}}$, which shows that $N_g$ is effectively smaller or equal to $N_{\text{KL}}$. Under these conditions, for each $\gamma$, the number of coefficients to be estimated is smaller than the number $n_r$ of experimental realizations for identifying the coefficients of $\mathbf{H}^\gamma$. The convergence speed of the maximum likelihood approach (see Section 4.3.2) is then faster. The methodology and the algorithm for constructing such a partition can be found in [114] for large dimension problems for which a set of few realizations is available and for which the classical statistic methods, such as "data clustering" method [67], are not efficient.

### 4.3.4 Analyzing the independence of the components of H

For a given application, if the method presented in Section 4.3.3 gives $n_{\text{ind}} = N_{\text{KL}}$, so all the components of $\mathbf{H}$ are non-Gaussian and independent. If stochastic process $\mathbf{P}$ were Gaussian (which is not the case), the random vector $\mathbf{H}$ would then

be Gaussian and taking into account Eq. (4.20), the components of **H** would also be independent. For the case considered in this work, **H** is non-Gaussian and the components of **H** are uncorrelated and then are dependent. These remarks show that it is licit to construct a first approximation for the estimation of the coefficients $\mathbf{z}^\kappa$ of the PCE given by Eq. (4.61) assuming the independence of the components of **H**. With these estimation hypotheses, we can control its efficiency by applying the convergence criterion defined in Section 4.2.2 (iv).

### 4.3.5 Method proposed as a first approximation for estimating the coefficients of the polynomial chaos expansion of H

#### 4.3.5.1 Formulation

This method is based on the explanations given in Section 4.3.3 and is formulated as follows
**(i)**- The components $H_1, \ldots, H_{N_{\text{KL}}}$ of non-Gaussian random vector **H**, which are centered and uncorrelated, are assumed to be independent in a first approximation.
**(ii)**- Hypothesis **(i)** implies that, for $j = 1, \ldots, N_{\text{KL}}$, each component $H_j$ of **H** admits a PCE that is written as

$$H_j^{(N_d)} = \sum_{\kappa=1}^{N_d} z_j^\kappa \psi_\kappa(\Xi_j)\,, \tag{4.84}$$

- in which $\Xi_1, \ldots, \Xi_{N_d}$ are independent random variables such that for each $j$, the real-valued random variable $\Xi_j$ is Gaussian, centered, with a variance equal to 1.

- in which $\psi_1, \ldots, \psi_{N_d}$ are the normalized Hermite polynomials such that, for all $\kappa$ and $\kappa'$ in $\{1, \ldots, N_d\}$,

$$\psi_0(\Xi_j) = 1\ ,\ E\{\psi_\kappa(\Xi_j)\} = 0\ ,\ E\{\psi_\kappa(\Xi_j)\,\psi_{\kappa'}(\Xi_j)\} = \delta_{\kappa\kappa'}\,. \tag{4.85}$$

  Consequently, for all $j$ and $j'$ in $\{1, \ldots, N_{\text{KL}}\}$ with $j \neq j'$ and for $\kappa$ and $\kappa'$ in $\{1, \ldots, N_d\}$, it can be deduced that

$$E\{\psi_\kappa(\Xi_j)\,\psi_{\kappa'}(\Xi_{j'})\} = 0\,. \tag{4.86}$$

- where for all $j = 1, \ldots, N_{\text{KL}}$, the real coefficients to be estimated are $z_j^1, \ldots, z_j^{N_d}$. It is supposed that the degree $N_d$ is independent of $j$, which is not restrictive, the convergence being globally analyzed for **H** where $N_d$ is increasing.

**(iii)**- In accordance to Section 4.2.2 (iii), Eqs. (4.63) and (4.64) will be verified for the approximation

$$\mathbf{H}^{(N_d)} = (H_1^{(N_d)}, \ldots, H_{N_{\text{KL}}}^{(N_d)}) \,. \tag{4.87}$$

Taking into account Eqs. (4.84) and (4.85), we have

$$E\{H_j^{(N_d)}\} = 0 \,. \tag{4.88}$$

On the other hand, $[E\{\mathbf{H}^{(N_d)}\,\mathbf{H}^{(N_d)T}\}]_{jj'} = E\{H_j^{(N_d)}\,H_{j'}^{(N_d)}\}$ and taking into account Eqs. (4.84) to (4.86) yield

$$E\{H_j^{(N_d)}\,H_{j'}^{(N_d)}\} = \delta_{jj'} \sum_{\kappa=1}^{N_d} (z_j^\kappa)^2 \,. \tag{4.89}$$

Consequently, we have

$$E\{\mathbf{H}^{(N_d)}\} = 0 \quad , \quad E\{\mathbf{H}^{(N_d)}\mathbf{H}^{(N_d)T}\} = [I_{N_{\text{KL}}}] \,, \tag{4.90}$$

which correspond to Eqs. (4.63) and (4.64), and where the constraint defined by Eq. (4.65) is replaced by the $N_{\text{KL}}$ scalar constraints,

$$\sum_{\kappa=1}^{N_d} (z_j^\kappa)^2 = 1 \quad , \quad j = 1, \ldots, N_{\text{KL}} \,. \tag{4.91}$$

#### 4.3.5.2 Estimation of the coefficients

Taking into account the formulation presented in Section 4.3.5.1, the identification of the PCE coefficients defined by Eq. (4.84), using the maximum likelihood principle presented in Section 4.3.2, is rewritten as follows. For all $j$ fixed in $\{1, \ldots, N_{\text{KL}}\}$, let $\mathscr{C}_{\text{ad}}^j$ be the subset of $\mathbb{R}^{N_d}$ such that

$$\mathscr{C}_{\text{ad}}^j = \{\mathbf{z}^j = (z_j^1, \ldots, z_j^{N_d}) \in \mathbb{R}^{N_d} \;;\; \|\mathbf{z}^j\|^2 = \sum_{\kappa=1}^{N_d} (z_j^\kappa)^2 = 1\} \,. \tag{4.92}$$

The optimal value $\mathbf{z}^{j,\text{opt}}$ in $\mathscr{C}_{\text{ad}}^j$ of $\mathbf{z}^j = (z_j^1, \ldots, z_j^{N_d})$, calculated by the maximum likelihood, is given by

$$\mathbf{z}^{j,\text{opt}} = \arg\{ \max_{\mathbf{z}^{j,\text{opt}} \in \mathscr{C}_{\text{ad}}^j} \mathscr{L}^j(\mathbf{z}^j)\} \,, \tag{4.93}$$

where $\mathscr{L}^j(\mathbf{z}^j)$ is $\log_{10}$ likelihood function that is written as,

$$\mathscr{L}^j(\mathbf{z}^j) = \sum_{\ell=1}^{n_r} \log_{10}\, p_{H_j^{(N_d)}}(\eta_j^\ell; \mathbf{z}^j) \,, \tag{4.94}$$

where $\{\eta_j^\ell\}_{\ell=1,\ldots,n_r}$ are the realizations of the component $j$ of $\boldsymbol{\eta}^\ell$ given by Eq. (4.33) and where $\eta_j \mapsto p_{H_j^{(N_d)}}(\eta_j;\mathbf{z}^j)$ is the probability density function in $\mathbb{R}$ of the random variable $H_j^{(N_d)}$ defined by Eq. (4.84). The value $p_{H_j^{(N_d)}}(\eta_j^\ell;\mathbf{z}^j)$ is calculated using the Gaussian kernel estimation method for which $\nu$ realizations $\{\widetilde{\eta}_j^{\ell'}, \ell' = 1,\ldots,\nu\}$ of $H_j^{(N_d)}$ are computed by

$$\widetilde{\eta}_j^{\ell'} = \sum_{\kappa=1}^{N_d} z_j^\kappa \Psi_\kappa(\Xi_j(\theta'_{\ell'}))\,. \tag{4.95}$$

in which $\Xi_j(\theta'_1),\ldots,\Xi_j(\theta'_\nu)$ are $\nu$ independent realizations of $\Xi_j$. It should be noted that the random variables $\Xi_1,\ldots,\Xi_{N_{\text{KL}}}$ are assumed here to be independent.

#### 4.3.5.3 Convergence analysis with respect to $N_d$ and calculation of the optimal value $N_d^{\text{opt}}$

**(i) Error function for the convergence analysis.** For all $j$ fixed in $\{1,\ldots,N_{\text{KL}}\}$, the truncated PCE of $H_j^{(N_d)}$ defined by Eq. (4.84) depends on $N_d$ (taken independent of $j$), which is unknown and which must be estimated using a convergence analysis of the sequence $\{H_j^{(N_d)}\}_{N_d}$ towards $H_j$ when $N_d$ goes to $+\infty$. The error function is defined by

$$\text{err}_j(N_d) = \frac{\int_{\mathbb{R}} |p_{H_j^{(N_d)}}(\eta_j;\mathbf{z}^{j,\text{opt}}) - p_{H_j}(\eta_j)|\, d\,\eta_j}{\int_{\mathbb{R}} p_{H_j}(\eta_j)\, d\,\eta_j}\,. \tag{4.96}$$

For the numerical implementation of Eq. (4.96), the probability density functions of $H_j^{(N_d)}$ and $H_j$ are calculated using the Gaussian kernel estimation method. The probability density function of $H_j^{(N_d)}$ is estimated with the realizations $\{\widetilde{\eta}_j^{\ell'}\}_{\ell'=1,\ldots,\nu}$ defined by

$$\widetilde{\eta}_j^{\ell'} = \sum_{\kappa=1}^{N_d} z_j^{\kappa,\text{opt}} \Psi_\kappa(\Xi_j(\theta'_{\ell'}))\,. \tag{4.97}$$

The probability density function of $H_j$ is estimated with the realizations $\{\eta_j^\ell\}_{\ell=1,\ldots,n_r}$. The total error is defined by

$$\text{err}(N_d) = \frac{1}{N_{\text{KL}}} \sum_{j=1}^{N_{\text{KL}}} \text{err}_j(N_d)\,. \tag{4.98}$$

**(ii) Calculation of the optimal value $N_d^{\text{opt}}$.** The optimal value $N_d^{\text{opt}}$ of $N_d$ is calculated using the formulation proposed in [95, 115], which is written as,

$$N_d^{\text{opt}} = \arg\{\min_{N_d \geq 1} \text{err}(N_d)\}. \tag{4.99}$$

#### 4.3.5.4 Numerical aspects for solving the optimization problem

For each $j$ fixed in $\{1, \ldots, N_{\text{KL}}\}$, the optimization problem defined by Eqs. (4.93) and (4.94) is solved by a random search algorithm in the admissible set $\mathscr{C}_{\text{ad}}^j$. The following parameterization of $\mathscr{C}_{\text{ad}}^j$ in the neighborhood of the point $\underline{\mathbf{z}}^j$ is then introduced,

$$\underline{\mathbf{z}}^j = (1, 0, \ldots, 0) \in \mathscr{C}_{\text{ad}}^j \subset \mathbb{R}^{N_d} . \tag{4.100}$$

The only non-zero components of $\underline{\mathbf{z}}^j$ is the first component $\underline{z}_j^1 = 1$. The choice of this point $\underline{\mathbf{z}}^j$ is justified by the fact that the admissible set $\mathscr{C}_{\text{ad}}^j$ must be explored around the Gaussian case. Since $\Psi_1(\Xi_j) = \Xi_j$, Eq. (4.84) shows that $H_j^{(N_d)}$ is a Gaussian random variable when $z_j^1 = 1$ and $z_j^\kappa = 0$ for $\kappa = 2, \ldots, N_d$. These values define the point $\underline{\mathbf{z}}^j$ given by Eq. (4.100).

**(i) Random search algorithm.** This algorithm is deduced from the one presented in [118] based on the use of a parameterization of the Stiefel manifold.

**(ii) Deterministic algorithm.** Using the point $\underline{\mathbf{z}}^j$ defined by Eq. (4.100) as an initial point, the maximum of the cost function defined by Eq. (4.94) is searched under the constraint defined by Eq. (4.92). The optimization algorithm can be chosen as the "interior points" algorithm [14] with the nonlinear constraint defined by Eq. (4.92), that is to say $\sum_{\kappa=1}^{N_d} (z_j^\kappa)^2 = 1$. Gradient and Hessian of the cost function (the log likelihood function) are computed numerically by the finite difference methods.

# Chapter 5

# Estimation of the equivalent static forces

In this chapter, we present a probabilistic approach for estimating the equivalent static forces that allow for reproducing the extreme value statistics of the stochastic dynamical responses in structures submitted to unsteady pressure fields induced by wind, when these equivalent static forces are statically applied to structures. For estimating the equivalent static forces induced by wind dynamic effects on structures, methods have widely been developed since the 70's (see [105, 24, 75, 73]) and have given rise to numerous works and applications [18, 19, 21, 42, 60, 62, 76, 98, 130, 145, 146, 144], and more recently to works that can be found in [9, 52, 81, 125, 140, 8, 94]. These works introduce different levels of approximations on the modal coordinates and the computation of their correlations, on the probability laws and the extreme value statistics of the observation, and on the observations chosen for computing the equivalent static forces. These works are generally based on the following hypotheses:

- the joint probability law of the equivalent forces and of the observations at a given time is Gaussian.

- the conditional probability density function of the equivalent forces, conditioned by the observation, is derived from a Gaussian assumption and is computed for an observation that is equal to the statistical mean of its extreme values, which is calculated by using the gust loading factor for a Gaussian process. Envelop methods are then used for estimating the equivalent static loads.

- the linear dynamics of the structure is taken into account using a classical reduced-order modal model.

- the approaches used are of the analytical type, which is made possible given the assumptions introduced.

Recently, correction terms have been introduced to take into account the non-Gaussianity of the unsteady pressure field in order to compute the extreme value statistics, using the orthogonal polynomial expansion method of the probability density function (a method that had already been used in 1978 for analyzing the wind effects on structures (see for instance [108]) have been revisited [10].
In this work, the probabilistic approach presented is based on methods already proposed in the literature and previously referenced, but it is developed to overcome the assumptions described above and thus fundamentally differs on the following points that are developed hereinafter.

- Stochastic process $\{\mathbf{P}(t)\,, t \in [0,T]\}$ is non-Gaussian and this non-Gaussianity is taken into account by computing the conditional probability density functions of $\mathbb{R}^N$-valued random vector $\mathbf{Q}(T)$ conditioned by the fact that $\mathbb{R}^{m_u}$-valued random vector $\mathbb{U}(T)$ must belong to domain $\mathscr{D} \subset \mathbb{R}^{m_u}$. If a maximum observation is searched, this domain contains the mean value $\underline{\mathbf{U}}_{\max} = (\underline{U}_{\max,1}, \ldots, \underline{U}_{\max,m_u})$ such that, for $j$ in $\{1, \ldots, m_u\}$, $\underline{U}_{\max,j}$ is the mean value of $\mathbb{U}_{\max,j} = \max_{t\in[0,T]} \mathbb{U}_j(t)$. Similarly, if a minimum observation is searched, this domain contains $\underline{\mathbf{U}}_{\min} = (\underline{U}_{\min,1}, \ldots, \underline{U}_{\min,m_u})$ such that, for $j$ in $\{1, \ldots, m_u\}$, $\underline{U}_{\min,j}$ is the statistical mean of $\mathbb{U}_{\min,j} = \min_{t\in[0,T]} \mathbb{U}_j(t)$.

- Equivalent static force is defined by the maximum likelihood principle taking into account the non-Gaussianity and the statistical dependence of the random components. No envelop method is used.

- Non-Gaussian aspect is taken into account by the use of the polynomial chaos expansion for which the coefficients are identified with the experimental measurements, and not by computing corrective terms based on a truncated orthogonal polynomial expansion of the non-Gaussian multidimensional probability density function.

- Reduced-order model of the structure includes a quasi-static term for accelerating the convergence with respect to dimension $N$ of the reduced-order model.

- Taking into account the introduced hypotheses, the proposed approach is essentially numerical, the analytical computations, which are possible for the Gaussian case, can no longer be carried out.

- A given observation can be a vector and the conditioning event is, as we have just pointed out before, $\mathbb{U}(T) \in \mathscr{D} \subset \mathbb{R}^{m_u}$. For each given couple

$\{\mathbb{U}^i(T), \mathscr{D}_i\}$ of observation, in which $i \in \{1, \ldots, m_{\mathbb{f}}\}$ with $m_{\mathbb{f}}$ the number of observations, the equivalent static force $\mathbb{f}^{e,s,i}$ with values in $\mathbb{R}^m$ is estimated by using the method presented in this chapter. The set of equivalent static forces can be defined by an algebraically free family of vectors (principal equivalent static forces or principal static loads), denoted by $\mathbb{e}^1, \ldots, \mathbb{e}^{m_{\mathbb{e}}}$ with $\mathbb{e}^i \in \mathbb{R}^m$ and $m_{\mathbb{e}} \leq m_{\mathbb{f}}$. Under these conditions, each equivalent static force $\mathbb{f}^{e,s,i}$ can be written as

$$\mathbb{f}^{e,s,i} = \sum_{i'=1}^{m_{\mathbb{e}}} f^i_{i'}\, \mathbb{e}^{i'} \,. \tag{5.1}$$

- The proposed approach will be developed for two cases
  - the dynamic reduced-order model is used without taking into account the quasi-static acceleration term,
  - and the dynamic reduced-order model is used taking into account this term.

## 5.1 Centering of domain $\mathscr{D}$

Domain $\mathscr{D} \subset \mathbb{R}^{m_u}$ introduced in Section 2.3.2, which is associated with observation $\mathbb{U}(t)$ is transformed into a domain $\mathscr{D}^c \subset \mathbb{R}^{m_u}$ of the centered observation, denoted by $\mathbf{U}(t)$, which is such that

$$\mathbb{U}(t) = \underline{\mathbf{u}} + \mathbf{U}(t) \,, \tag{5.2}$$

in which $\underline{\mathbf{u}}$ is the vector in $\mathbb{R}^{m_u}$, which is computed by Eq. (2.45). Domain $\mathscr{D}^c \subset \mathbb{R}^{m_u}$ is defined by

$$\mathscr{D}^c = \{\mathbf{u} \in \mathbb{R}^{m_u} \,|\, \mathbb{u} = \underline{\mathbf{u}} + \mathbf{u} \in \mathscr{D}\} \,. \tag{5.3}$$

Under these conditions, for all $t$ in $[0, T]$, the probability of the event $\{\mathbb{U}(T) \in \mathscr{D}\}$ is equal to the probability of the event $\{\mathbf{U}(T) \in \mathscr{D}^c\}$

$$\text{Proba}\{\mathbb{U}(T) \in \mathscr{D}\} = \text{Proba}\{\mathbf{U}(T) \in \mathscr{D}^c\} \,. \tag{5.4}$$

## 5.2 Estimation of the equivalent static force for a given observation without taking into account the quasi-static acceleration term in the reduced-order model

For a given observation, as the equivalent static force is estimated without taking into account the quasi-static acceleration term, the reduced-order model only depends on $\mathbb{R}^N$-valued random vector $\mathbf{Q}(T)$ of the generalized coordinates. Taking into account Eq. (2.47), the equivalent static force, denoted by $\mathbb{f}^{e,s} \in \mathbb{R}^m$, associated with observation $\mathbb{U}(t)$ defined by Eq. (2.42), is written as

$$\mathbb{f}^{e,s} = \underline{\mathbf{f}} + \mathbf{f}^{e,s}\,, \tag{5.5}$$

where $\underline{\mathbf{f}}$ is the $\mathbb{R}^m$-vector defined by Eq. (2.36). Without the static acceleration term, $[\mathscr{S}_N^c] = [0]$ must be taken in Eq. (2.28), and under these conditions, Eq. (2.49) is written as $\mathbf{F}^e(t) = [\mathcal{F}_N^{\mathbf{Q}}]\mathbf{Q}(t)$. In this case, the part $\mathbf{f}^{e,s} \in \mathbb{R}^m$ of the equivalent static force $\mathbb{f}^{e,s}$ is defined by

$$\mathbf{f}^{e,s} = [\mathcal{F}_N^{\mathbf{Q}}]\,\mathbf{q}^{\text{MV}} \tag{5.6}$$

where $\mathbf{q}^{\text{MV}}$ is the vector in $\mathbb{R}^N$, such that

$$\mathbf{q}^{\text{MV}} = \arg\{\max_{\mathbf{q}\in\mathbb{R}^N} p_{\mathbf{Q}(T)\,|\,\mathbf{U}(T)}(\mathbf{q}\,|\,\mathbf{U}(T)\in\mathscr{D}^c)\}\,, \tag{5.7}$$

in which $p_{\mathbf{Q}(T)\,|\,\mathbf{U}(T)}(\mathbf{q}\,|\,\mathbf{U}(T)\in\mathscr{D}^c)$ is the conditional probability density function of random vector $\mathbf{Q}(T)$ conditioned by non-Gaussian random vector $\mathbf{U}(T)$ given in domain $\mathscr{D}^c \subset \mathbb{R}_{m_u}$, and where $\mathbf{U}(T)$ is the non-Gaussian $\mathbb{R}^{m_u}$-valued random variable, which is written, taking into account Eq. (2.43) for $t = T$ with $[\mathscr{U}_N^{oc}] = [0]$, as

$$\mathbf{U}(T) = [\phi_N^o]\,\mathbf{Q}(T)\,. \tag{5.8}$$

As stochastic processes $\{\mathbf{Q}(t),\, t\in[0,T]\}$ and $\{\mathbf{U}(t), t\in[0,T]\}$ are the restriction to $[0,T]$ of stationary stochastic processes $\{\mathbf{Q}(t), t\in\mathbb{R}\}$ and $\{\mathbf{U}(t), t\in\mathbb{R}\}$, the conditional probability density function $p_{\mathbf{Q}(T)\,|\,\mathbf{U}(T)}$, which appears in the optimization problem defined by Eq. (5.7), is independent of $T$, and is written as

$$p_{\mathbf{Q}(T)\,|\,\mathbf{U}(T)}(\mathbf{q}\,|\,\mathbf{U}(T)\in\mathscr{D}^c) = \frac{\int_{\mathscr{D}^c} p_{\mathbf{Q}(T),\mathbf{U}(T)}(\mathbf{q},\mathbf{u})d\mathbf{u}}{\int_{\mathscr{D}^c} p_{\mathbf{U}(T)}(\mathbf{u})\,d\mathbf{u}}\,, \tag{5.9}$$

where $p_{\mathbf{U}(T)}$ is the probability density function on $\mathbb{R}^{m_u}$ of non-Gaussian random vector $\mathbf{U}(T)$ such that

$$p_{\mathbf{U}(T)}(\mathbf{u}) = \int_{\mathbb{R}^N} p_{\mathbf{Q}(T),\mathbf{U}(T)}(\mathbf{q},\mathbf{u})d\mathbf{q}\,, \tag{5.10}$$

and where $p_{\mathbf{Q}(T),\mathbf{U}(T)}(\mathbf{q},\mathbf{u})$ is the joint probability density function on $\mathbb{R}^N \times \mathbb{R}^{m_u}$ of the dependent non-Gaussian random variables $\mathbf{Q}(T)$ with values in $\mathbb{R}^N$ and $\mathbf{U}(T)$ with values in $\mathbb{R}^{m_u}$. As the denominator of the right-hand side of Eq. (5.9) is a constant, the optimization problem defined by Eq. (5.7) can be replaced by the following one,

$$\mathbf{q}^{\text{MV}} = \arg\{\max_{\mathbf{q}\in\mathbb{R}^N} \int_{\mathscr{D}^c} p_{\mathbf{Q}(T),\mathbf{U}(T)}(\mathbf{q},\mathbf{u})\, d\mathbf{u}\}\,. \tag{5.11}$$

In order to accelerate the convergence of the optimization problem defined by Eq. (5.11) while considering only a reasonable number $\nu$ of realizations, we superimpose the constraint on the vector $\mathbf{U}(T)$ by introducing the following admissible set for the values of $\mathbf{Q}(T)$,

$$\mathscr{C}_{\mathbf{q}} = \{\mathbf{q}\in\mathbb{R}^N; \mathbf{u}\in\mathscr{D}^c\}\,. \tag{5.12}$$

Consequently, in Eq. (5.11), the maximization on $\mathbf{q}\in\mathbb{R}^N$ is replaced by the maximization on $\mathbf{q}\in\mathscr{C}_{\mathbf{q}}$. Using Eq. (2.43) and without taking into account the quasi-static acceleration term, centered observation $\mathbf{U}$ at time $T$ is written as,

$$\mathbf{U}(T) = [\phi^o_N]\,\mathbf{Q}(T)\,. \tag{5.13}$$

Let $[B]$ be the matrix in $\mathbb{M}_{m_u,N}(\mathbb{R})$ such that

$$[B] = [\phi^o_N]\,. \tag{5.14}$$

The constraint $\mathbf{u}\in\mathscr{D}^c$ introduced by Eq. (5.12) is expressed in term of $\mathbf{q}$ as follows

$$[\mathbb{A}]\,\mathbf{q} \le \mathbb{d}\,, \tag{5.15}$$

in which $[\mathbb{A}]\in\mathbb{M}_{2\times m_u,N}(\mathbb{R})$ and $\mathbb{d}\in\mathbb{R}^{2\times m_u}$ are such that

$$[\mathbb{A}] = \begin{bmatrix} -[B] \\ [B] \end{bmatrix} \quad , \quad \mathbb{d} = \begin{bmatrix} -\mathscr{D}^c_{\text{inf}} \\ \mathscr{D}^c_{\text{sup}} \end{bmatrix}\,, \tag{5.16}$$

where $\mathscr{D}^c_{\text{inf}}$ and $\mathscr{D}^c_{\text{sup}}$ are the lower and the upper bounds of domain $\mathscr{D}^c$ (see Section 5.4.4 (iii-2) and Appendix A).

## 5.3 Estimation of the equivalent static forces for a given observation taking into account the static acceleration term in the reduced-order model

As explained in Section 5.2, the equivalent static force $\mathbb{f}^{e,s}\in\mathbb{R}^m$, associated with observation $\mathbb{U}$, is always given by Eq. (5.5), but now $\mathbf{f}^{e,s}$ is modified. With the

static acceleration term and for $t = T$, Eq. (2.49) is rewritten as,

$$\mathbf{F}^e(T) = [\mathscr{F}_N^c]\,\mathbf{P}(T) + [\mathcal{F}_N^{\mathbf{Q}}]\mathbf{Q}(T)\,. \tag{5.17}$$

This expression induces potential difficulties for computing the centered part $\mathbf{f}^{e,s}$ of the equivalent static force $\mathbb{f}^{e,s}$, because of the presence of $\mathbf{P}(t)$, which is with values in $\mathbb{R}^{m_{\text{exp}}}$ where $m_{\text{exp}}$ can be large (for instance of the order of $700$ for a wind tunnel test). We then propose below a method that allows for partially eliminating these difficulties.

### 5.3.1 Estimation of the equivalent static force

The method consists in constructing $\mathbf{f}^{e,s}$ such that,

$$\mathbf{f}^{e,s} = [\mathscr{F}_N^c]\,\mathbf{p}^{\text{MV}} + [\mathcal{F}_N^{\mathbf{Q}}]\,\mathbf{q}^{\text{MV}}\,, \tag{5.18}$$

where the vector $\mathbf{p}^{\text{MV}} \in \mathbb{R}^{m_{\text{exp}}}$ and $\mathbf{q}^{\text{MV}} \in \mathbb{R}^N$ are computed by solving the optimization problem

$$(\mathbf{p}^{\text{MV}}, \mathbf{q}^{\text{MV}}) = \arg\{\max_{(\mathbf{p},\mathbf{q})\in\mathbb{R}^{m_{\text{exp}}}\times\mathbb{R}^N} \int_{\mathscr{D}^c} p_{\mathbf{P}(T),\mathbf{Q}(T),\mathbf{U}(T)}(\mathbf{p},\mathbf{q},\mathbf{u})\,d\mathbf{u}\}\,, \tag{5.19}$$

in which $p_{\mathbf{P}(T),\mathbf{Q}(T),\mathbf{U}(T)}(\mathbf{p},\mathbf{q},\mathbf{u})$ is the joint probability density function on $\mathbb{R}^{m_{\text{exp}}} \times \mathbb{R}^N \times \mathbb{R}^{m_u}$ of dependent random vectors $\mathbf{P}(T)$, $\mathbf{Q}(T)$, and $\mathbf{U}(T)$, and where $\mathbf{U}(T)$ is the non-Gaussian $\mathbb{R}^{m_u}$-valued random variable, which is written, taking into account Eq. (2.43) for $t = T$

$$\mathbf{U}(T) = [\mathscr{U}_N^{oc}]\,\mathbf{P}(T) + [\phi_N^o]\,\mathbf{Q}(T)\,. \tag{5.20}$$

### 5.3.2 Reformulation by introducing a statistical reduction of random vector $\mathbf{P}(T)$

As the dimension $m_{\text{exp}}$ of random vector $\mathbf{P}(T)$ can be large enough and as $\mathbf{P}(T)$ does not have the same magnitude order as $\mathbf{Q}(T)$ and $\mathbf{U}(T)$, the construction of the joint probability density function $p_{\mathbf{P}(T),\mathbf{Q}(T),\mathbf{U}(T)}(\mathbf{p},\mathbf{q},\mathbf{u})$ can induce numerical difficulties and in addition, can induce significant numerical costs for solving the optimization problem defined by Eq. (5.19).

#### 5.3.2.1 Statistical reduction of random vector $\mathbf{P}(T)$

A principal component analysis of random vector $\mathbf{P}(T)$ is introduced, which allows for normalizing and possibly, statistically reducing dimension. We then have

$$\mathbf{P}(T) \simeq \underline{\mathbf{p}}_T + \sum_{j=1}^{N_{\text{PCA}}} \sqrt{\Lambda_j}\,H_j\,\mathbf{a}^j\,, \tag{5.21}$$

in which $N_{\text{PCA}}$ is the reduction order that is estimated by the method presented hereinafter and such that $N_{\text{PCA}} \leq m_{\text{exp}}$. The vectors $\mathbf{a}^1, \ldots, \mathbf{a}^{N_{\text{PCA}}}$ are the eigenvectors associated with the $N_{\text{PCA}}$ largest eigenvalues $\Lambda_1 \geq \Lambda_2 \geq \ldots \geq \Lambda_{N_{\text{PCA}}}$ of the covariance matrix $[C_{\mathbf{P}(T)}]$ of $\mathbf{P}(T)$, which is estimated with the set $\{\mathbf{p}^\ell = \mathbf{P}(T;\theta_\ell), \ell = 1, \ldots, \nu\}$ of realizations, which is also used for estimating the constant empirical mean $\underline{\mathbf{p}}_T$. The normalization of the eigenvectors $\mathbf{a}^j$ is chosen so that $< \mathbf{a}^j, \mathbf{a}^k >= \delta_{jk}$. The random coordinates $H_j$ are given by,

$$H_j = \frac{1}{\sqrt{\Lambda_j}} < (\mathbf{P}(T) - \underline{\mathbf{p}}_T), \mathbf{a}^j > \quad , \quad j = 1, \ldots, N_{\text{PCA}} \, . \tag{5.22}$$

Let $\mathbf{H} = (H_1, \ldots, H_{N_{\text{PCA}}})$ be the $\mathbb{R}^{N_{\text{PCA}}}$-valued random variable. The $\nu$ realizations $\mathbf{H}(\theta_\ell)$ of $\mathbf{H}$ for $\ell = 1, \ldots, N_{\text{PCA}}$ are then computed by

$$H_j(\theta_\ell) = \frac{1}{\sqrt{\Lambda_j}} < (\mathbf{p}^\ell - \underline{\mathbf{p}}_T), \mathbf{a}^j > \quad , \quad j = 1, \ldots, N_{\text{PCA}} \, . \tag{5.23}$$

**Remark**. In order to not overburden the notations, we have kept the notations of Chapter 4 concerning $N_{\text{PCA}}$, $\Lambda_j$, and $H_j$, although the quantities are different. Theoretically, $\mathbf{P}(T)$ is a centered random vector ($E\{\mathbf{P}(T)\} = 0$). Practically, as $n_r$ can be not sufficiently large, the estimate $\underline{\mathbf{p}}$ of $E\{\mathbf{P}(T)\}$ can be not close to $0$. Consequently, in order not to modify the realizations of $\mathbf{P}(T)$ using the representation defined by Eq. (5.21), $\underline{\mathbf{p}}_T$ is kept (not set to zero).

The centered realizations $\mathbf{p}_c^\ell$ of $\mathbf{P}(T)$ are defined (in the empirical mean sense) by

$$\mathbf{p}_c^\ell = \mathbf{p}^\ell - \underline{\mathbf{p}}_T \quad , \quad \ell = 1, \ldots, \nu \, , \tag{5.24}$$

where

$$\underline{\mathbf{p}}_T = \frac{1}{\nu} \sum_{\ell=1}^{\nu} \mathbf{p}^\ell \, . \tag{5.25}$$

The estimate $[\widehat{C}_\nu] \in \mathbb{M}_{m_{\text{exp}}}(\mathbb{R})$ of the covariance matrix of $\mathbf{P}_c = \mathbf{P}(T) - \underline{\mathbf{p}}_T$ is calculated by

$$[\widehat{C}_\nu] = \frac{1}{\nu - 1} \sum_{\ell=1}^{\nu} \mathbf{p}_c^\ell \, (\mathbf{p}_c^\ell)^T \, . \tag{5.26}$$

Let $[w]$ be the matrix in $\mathbb{M}_{m_{\text{exp}},\nu}(\mathbb{R})$ such that

$$[w] = [\mathbf{p}_c^1 \ldots \mathbf{p}_c^\nu] \, , \tag{5.27}$$

which allows Eq. (5.26) to be rewritten as,

$$[\widehat{C}_\nu] = \frac{1}{\nu - 1} [w] \, [w]^T \, . \tag{5.28}$$

Two cases are considered:

**(i)** $m_{\text{exp}} \leq \nu$**.** The eigenvalue problem of the positive symmetric matrix $[\widehat{C}_\nu]$ is written as

$$[\widehat{C}_\nu]\,[a] = [\Lambda]\,[a]\,, \tag{5.29}$$

with $[\Lambda]_{ij} = \Lambda_j \delta_{ij}$ such that $\Lambda_1 \geq \ldots \geq \Lambda_{m_{\text{exp}}}$ and where the matrix $[a] \in \mathbb{M}_{m_{\text{exp}}}(\mathbb{R})$ of eigenvectors is such that

$$[a]^T\,[a] = [I_{m_{\text{exp}}}]\,. \tag{5.30}$$

Matrix $[\widehat{C}_\nu]$ can then be rewritten as,

$$[\widehat{C}_\nu] = \sum_{j=1}^{m_{\text{exp}}} \Lambda_j\, \mathbf{a}^j\, \mathbf{a}^{jT}\,. \tag{5.31}$$

**(ii)** $m_{\text{exp}} > \nu$**.** Using the "thin SVD" [50], matrix $[w]$ can be written as

$$[w] = [a]\,[\Sigma]\,[\mathbb{V}]\,, \tag{5.32}$$

in which $[a] \in \mathbb{M}_{m_{\text{exp}},\nu}(\mathbb{R})$ is such that $[a]^T\,[a] = [I_\nu]$, where $[\mathbb{V}] \in \mathbb{M}_\nu(\mathbb{R})$ is such that $[\mathbb{V}]^T[\mathbb{V}] = [\mathbb{V}]\,[\mathbb{V}]^T = [I_\nu]$, and where $[\Sigma]$ is the diagonal $(\nu \times \nu)$ real matrix such that

$$[\Lambda] = \frac{1}{\nu - 1}[\Sigma]^2\,, \tag{5.33}$$

in which $[\Lambda]$ is the diagonal $(\nu \times \nu)$ real matrix with $\Lambda_1 \geq \Lambda_2 \geq \ldots \Lambda_\nu \geq 0$.

**Estimation of the error induced by the PCA for cases (i) and (ii).** In both cases, the reduction order $N_{\text{PCA}}$ is computed so that the error is smaller than a given $\varepsilon$ that is chosen sufficiently small,

$$\text{err}_{\text{PCA}}(N_{\text{PCA}}) = 1 - \frac{\sum_{j=1}^{N_{\text{PCA}}} \Lambda_j}{\sum_{j=1}^{m_{\max}} \Lambda_j} < \varepsilon\,, \tag{5.34}$$

in which $m_{\max} = m_{\text{exp}}$ for case (i) and $m_{\max} = \nu$ for case (ii).

#### 5.3.2.2 Computation of the equivalent static force

If the PCA of $\mathbf{P}(T)$ leads us to a value of $N_{\text{PCA}}$ that is much smaller than $m_{\text{exp}}$, then $N_{\text{PCA}} \ll m_{\text{exp}}$. Consequently, there is an advantage to change the representation and to reformulate the computation of the static equivalent force by the following method. Vector $\mathbf{f}^{e,s} \in \mathbb{R}^m$ is estimated by

$$\mathbf{f}^{e,s} = [\mathscr{F}_N^c]\,\mathbf{p}^{\text{MV}} + [\mathcal{F}_N^{\mathbf{Q}}]\,\mathbf{q}^{\text{MV}}\,, \tag{5.35}$$

in which $\mathbf{p}^{\text{MV}}$ is given by

$$\mathbf{p}^{\text{MV}} \simeq \underline{\mathbf{p}}_T + \sum_{j=1}^{N_{\text{PCA}}} \sqrt{\Lambda_j}\, \eta_j^{\text{MV}}\, \mathbf{a}^j \,. \tag{5.36}$$

The vector $\boldsymbol{\eta}^{\text{MV}} = (\eta_1^{\text{MV}}, \ldots, \eta_{N_{\text{PCA}}}^{\text{MV}})$ in $\mathbb{R}^{N_{\text{PCA}}}$ and the vector $\mathbf{q}^{\text{MV}} \in \mathbb{R}^N$ are estimated as the solution of the following optimization problem

$$(\boldsymbol{\eta}^{\text{MV}}, \mathbf{q}^{\text{MV}}) = \arg\{ \max_{(\boldsymbol{\eta},\mathbf{q}) \in \mathbb{R}^{N_{\text{PCA}}} \times \mathbb{R}^N} \int_{\mathscr{D}^c} p_{\mathbf{H},\mathbf{Q}(T),\mathbf{U}(T)}(\boldsymbol{\eta}, \mathbf{q}, \mathbf{u})\, d\mathbf{u} \} \,, \tag{5.37}$$

in which $p_{\mathbf{H},\mathbf{Q}(T),\mathbf{U}(T)}(\boldsymbol{\eta}, \mathbf{q}, \mathbf{u})$ is the joint probability density function on $\mathbb{R}^{N_{\text{PCA}}} \times \mathbb{R}^N \times \mathbb{R}^{m_u}$ of random vectors $\mathbf{H}$, $\mathbf{Q}(T)$, and $\mathbf{U}(T)$.

In order to accelerate the convergence of the optimization problem defined by Eq. (5.37) while considering only a reasonable number $\nu$ of realizations, as previously, we superimpose a constraint on vector $\mathbf{U}(T)$ by introducing the following admissible set for the values of $(\mathbf{H}, \mathbf{Q}(T))$,

$$\mathscr{C}_{\boldsymbol{\eta}\mathbf{q}} = \{(\boldsymbol{\eta}, \mathbf{q}) \in \mathbb{R}^{N_{\text{PCA}}} \times \mathbb{R}^N ; \mathbf{u} \in \mathscr{D}^c\} \,. \tag{5.38}$$

Then, in Eq. (5.37), the maximization on $(\boldsymbol{\eta}, \mathbf{q}) \in \mathbb{R}^{N_{\text{PCA}}} \times \mathbb{R}^N$ is replaced by the maximization on $(\boldsymbol{\eta}, \mathbf{q}) \in \mathscr{C}_{\boldsymbol{\eta}\mathbf{q}}$. Using Eq. (2.43), the centered observation $\mathbf{U}$ at time $T$ is written as,

$$\mathbf{U}(T) = [\mathscr{U}_N^{oc}]\, \mathbf{P}(T) + [\phi_N^o]\, \mathbf{Q}(T) \,. \tag{5.39}$$

The statistical reduction of $\mathbf{P}(T)$ introduced in Section 5.3.2.1 is used (see Eq. (5.21)),

$$\mathbf{P}(T) \simeq \underline{\mathbf{p}}_T + \sum_{j=1}^{N_{\text{PCA}}} \sqrt{\Lambda_j}\, H_j\, \mathbf{a}^j \,. \tag{5.40}$$

Random vector $\mathbf{U}(T)$ can be rewritten in the following form

$$\mathbf{U}(T) = \mathbf{u}_T^{oc} + [v_N^{oc}]\, \mathbf{H} + [\phi_N^o]\, \mathbf{Q}(T) \,, \tag{5.41}$$

in which $\mathbf{u}_T^{oc} \in \mathbb{R}^{m_u}$ is such that

$$\mathbf{u}_T^{oc} = [\mathscr{U}_N^{oc}]\, \underline{\mathbf{p}}_T \,, \tag{5.42}$$

and where the matrix $[v_N^{oc}] \in \mathbb{M}_{m_u, N_{\text{PCA}}}(\mathbb{R})$ is such that, for $i = 1, \ldots, m_u$ and $j = 1, \ldots, N_{\text{PCA}}$,

$$[v_N^{oc}]_{ij} = \sum_{k=1}^{m_{\text{exp}}} \sqrt{\Lambda_j}\, [\mathscr{U}_N^{oc}]_{ik}\, a_k^j \,. \tag{5.43}$$

Matrix $[v_N^{oc}]$ can be rewritten in the following form,

$$[v_N^{oc}] = [\mathscr{U}_N^{oc}]\,[\widetilde{a}]\,, \tag{5.44}$$

with

$$[\widetilde{a}]_{kj} = a_k^j\,\sqrt{\Lambda_j}\,. \tag{5.45}$$

Let $\mathbf{u}$ be the vector such that

$$\mathbf{u} = \mathbf{u}_T^{oc} + [v_N^{oc}]\,\boldsymbol{\eta} + [\phi_N^o]\,\mathbf{q}\,, \tag{5.46}$$

and let $[B]$ be the matrix in $\mathbb{M}_{m_u,N_{\text{PCA}}+N}(\mathbb{R})$ such that

$$[B] = [[v_N^{oc}] \quad [\phi_N^o]]\,. \tag{5.47}$$

Therefore, the constraint $\mathbf{u} \in \mathscr{D}^c$, introduced in Eq. (5.38), is expressed in term of $(\boldsymbol{\eta}, \mathbf{q})$ as follows

$$[\mathbb{A}] \begin{bmatrix} \boldsymbol{\eta} \\ \mathbf{q} \end{bmatrix} \leq \mathbb{d}\,, \tag{5.48}$$

in which $[\mathbb{A}] \in \mathbb{M}_{2\times m_u,N_{\text{PCA}}+N}(\mathbb{R})$ and $\mathbb{d} \in \mathbb{R}^{2\times m_u}$ are defined by

$$[\mathbb{A}] = \begin{bmatrix} -[B] \\ [B] \end{bmatrix} \quad , \quad \mathbb{d} = \begin{bmatrix} \mathbf{u}_T^{oc} - \mathscr{D}_{\text{inf}}^c \\ \mathscr{D}_{\text{sup}}^c - \mathbf{u}_T^{oc} \end{bmatrix}\,, \tag{5.49}$$

where $\mathscr{D}_{\text{inf}}^c$ and $\mathscr{D}_{\text{sup}}^c$ are the lower and the upper bounds of domain $\mathscr{D}^c$ (see Section 5.4.4 (iii-2) and Appendix A).

## 5.4 Numerical method for solving the optimization problem for the two cases

Depending on the chosen case, the optimization problem defined by Eq. (5.11) for the case without quasi-static term or by Eq. (5.37) for the case with quasi-static term has to be solved. These two optimization problems are of the same type, they are non-convex and require the estimation of the non-Gaussian joint probability density function on a set that can be of large dimension, particularly for Eq. (5.37).

### 5.4.1 Proposed approach for solving the non-convex optimization problem

The optimization algorithm used is the "active set" without constraint [48] for which the gradient and the Hessian can easily be analytically computed. The construction of the initial point denoted by $\mathbf{q}^0 \in \mathbb{R}^N$ for the problem defined by Eq. (5.11), or the initial point denoted by $(\boldsymbol{\eta}^0, \mathbf{q}^0) \in \mathbb{R}^{N_{\text{PCA}}} \times \mathbb{R}^N$ for the problem defined by Eq. (5.37), is given in details in Appendix D.

### 5.4.2 Construction of a vector basis for the equivalent static forces

The equivalent static forces are assumed to be estimated for $m_{\mathbb{f}}$ couples of observations $\{\mathbb{U}^i(T), \mathscr{D}_i\}$ with $i = 1, \ldots, m_{\mathbb{f}}$. For each couple $\{\mathbb{U}^i(T), \mathscr{D}_i\}$, the equivalent static force $\mathbb{f}^{e,s,i} \in \mathbb{R}^m$ is estimated using the method previously presented. The objective is the construction of a vector basis $\mathbb{e}^1, \ldots, \mathbb{e}^{m_{\mathbb{e}}}$ with $\mathbb{e}^i \in \mathbb{R}^m$ and $m_{\mathbb{e}} < m_{\mathbb{f}}$ of the vector subspace $\mathcal{R}_m$ of $\mathbb{R}^m$, spanned by all the equivalent static forces $\{\mathbb{f}^{e,s,i}, i = 1, \ldots, m_{\mathbb{f}}\}$. Each equivalent static force $\mathbb{f}^{e,s,i}$, which belongs to $\mathcal{R}_m \subset \mathbb{R}^m$, is written as,

$$\mathbb{f}^{e,s,i} = \sum_{i''=1}^{m_{\mathbb{e}}} f^i_{i''}\, \mathbb{e}^{i''} \,. \tag{5.50}$$

The construction of the vector basis $\{\mathbb{e}^1, \ldots, \mathbb{e}^{m_{\mathbb{e}}}\}$ is classically performed using the singular value decomposition of the matrix $[\mathbb{f}^{e,s}]$ defined by

$$[\mathbb{f}^{e,s}] = [\,\mathbb{f}^{e,s,1} \ldots \mathbb{f}^{e,s,m_{\mathbb{f}}}] \in \mathbb{M}_{m,m_{\mathbb{f}}}(\mathbb{R}) \,. \tag{5.51}$$

The dimension $m_{\mathbb{e}}$ is less than or equal to $m_{\mathbb{f}}$ and is defined by the rank of matrix $[\mathbb{f}^{e,s}]$,

$$m_{\mathbb{e}} = \text{rank}\,[\mathbb{f}^{e,s}] \,, \tag{5.52}$$

It should be noted that if $m_{\mathbb{e}} = m_{\mathbb{f}}$, then the family $\{\mathbb{f}^{e,s,i}, i = 1, \ldots, m_{\mathbb{f}}\}$ is algebraically free and this family is called the system of the principal equivalent static forces. However, this vector basis is not orthonormal. The SVD is used for orthonormalizing it as for the case for which $m_{\mathbb{e}} < m_{\mathbb{f}}$. Let us now assume that

$$m_{\mathbb{e}} \leq m_{\mathbb{f}} \,. \tag{5.53}$$

Let $[\mathbb{e}]$ be the matrix defined by

$$[\mathbb{e}] = [\mathbb{e}^1 \ldots \mathbb{e}^{m_{\mathbb{e}}}] \in \mathbb{M}_{m,m_{\mathbb{e}}}(\mathbb{R}) \,. \tag{5.54}$$

By keeping only the $m_{\mathbb{e}}$ strictly positive singular values, the SVD of matrix $[\mathbb{f}^{e,s}]$ is written as,

$$[\mathbb{f}^{e,s}] = [\mathbb{e}]\,[\Sigma]\,[\mathbb{d}]^T \,, \tag{5.55}$$

in which $[\Sigma]$ is the $(m_{\mathbb{e}} \times m_{\mathbb{e}})$ positive-definite diagonal matrix, where $[\mathbb{e}] \in \mathbb{M}_{m,m_{\mathbb{e}}}(\mathbb{R})$ and $[\mathbb{d}] \in \mathbb{M}_{m_{\mathbb{f}},m_{\mathbb{e}}}(\mathbb{R})$ are the matrices such that

$$[\mathbb{e}]^T\,[\mathbb{e}] = [I_{m_{\mathbb{e}}}] \quad , \quad [\mathbb{d}]^T\,[\mathbb{d}] = [I_{m_{\mathbb{e}}}] \,. \tag{5.56}$$

Let $[f]$ be the matrix in $\mathbb{M}_{m_{\mathbb{e}},m_{\mathbb{f}}}(\mathbb{R})$ such that

$$[f]_{i''i} = f^i_{i''} \quad , \quad i = 1, \ldots, m_{\mathbb{f}} \quad , \quad i'' = 1, \ldots, m_{\mathbb{e}} \,, \tag{5.57}$$

in which $f_{i''}^{i}$ are the coefficients introduced in Eq. (5.57). It can then be verified that

$$[f] = [\Sigma]\,[\mathbb{d}]^T\,. \tag{5.58}$$

In these conditions:

- the system of the principal equivalent static forces is represented by the $m_{\mathbb{e}}$ orthonormal vectors corresponding to the columns of matrix $[\mathbb{e}]$.
- the matrix $[f]$ of the coefficients on the vector basis $[\mathbb{e}]$ allows for generating the equivalent static forces represented by matrix $[\mathbb{f}^{e,s}]$ such that

$$[\mathbb{f}^{e,s}] = [\mathbb{e}]\,[f]\,. \tag{5.59}$$

**Remark**. If $m_{\mathbb{f}} < m$, the SVD must be carried out with the "thin SVD" algorithm (see for instance [50]), which corresponds, for instance, to the "economy size" option in Matlab. The number of nonzero singular values with respect to the numerical zero gives the value of $m_{\mathbb{e}}$.

### 5.4.3 Estimation of the joint probability density function by the non-parametric statistics

For the cases without the static acceleration term (Section 5.2) or with the static acceleration term (Section 5.3), Eqs. (5.11) and (5.37) show that it is necessary to estimate the joint probability density function $p_{\mathbf{Q}(T),\mathbf{U}(T)}(\mathbf{q},\mathbf{u})$ or $p_{\mathbf{H},\mathbf{Q}(T),\mathbf{U}(T)}(\boldsymbol{\eta},\mathbf{q},\mathbf{u})$ from $\nu$ independent realizations $\mathbf{Q}(T;\theta_\ell)$, $\mathbf{U}(T;\theta_\ell)$, and $\mathbf{H}(\theta_\ell)$ for $\ell = 1,\ldots,\nu$, of centered dependent non-Gaussian random vectors $\mathbf{Q}(T)$, $\mathbf{U}(T)$, and $\mathbf{H}$.
The problem is therefore the following. Let $\mathbf{V} = (V_1,\ldots,V_n)$ be the $\mathbb{R}^n$-valued random variable defined on $(\Theta,\mathcal{T},\mathscr{P})$ with the probability distribution $P_{\mathbf{V}}(d\mathbf{v}) = p_{\mathbf{V}}(\mathbf{v})\,d\mathbf{v}$, for which $\nu$ independent realizations

$$\mathbf{v}^1 = \mathbf{V}(\theta_1),\ldots,\mathbf{v}^\nu = \mathbf{V}(\theta_\nu)\,, \tag{5.60}$$

are available such that $\theta_1,\ldots,\theta_\nu$ are in $\Theta$. For $\mathbf{v}$ fixed in $\mathbb{R}^n$, we want to estimate the value $\widehat{p}_{\mathbf{V}}(\mathbf{v})$ at point $\mathbf{v}$ of the PDF $p_{\mathbf{V}}$ using the Gaussian kernel estimation method in the nonparametric statistic framework. For $j = 1,\ldots,n$, let $\widehat{m}_j$ and $\widehat{\sigma}_j^2$ be the estimates of the mean and the variance of the real-valued second-order centered random variable $V_j$, which are classically written as,

$$\widehat{m}_j = \frac{1}{\nu}\sum_{\ell=1}^{\nu} v_j^\ell \quad , \quad \widehat{\sigma}_j^2 = \frac{1}{\nu-1}\sum_{\ell=1}^{\nu}(v_j^\ell - \widehat{m}_j)^2\,, \tag{5.61}$$

with $\mathbf{v}^\ell = (v_1^\ell, \ldots, v_n^\ell)$. Using the modification [113] of the classical estimate given by the Gaussian kernel estimation methode [13], the estimate $\widehat{p}_{\mathbf{V}}(\mathbf{v})$ of $p_{\mathbf{V}}(\mathbf{v})$ is written as

$$\widehat{p}_{\mathbf{V}}(\mathbf{v}) = c_n \, \rho_{\mathbf{V}}(\mathbf{v}) \,, \tag{5.62}$$

with $\rho_{\mathbf{V}}(\mathbf{v})$ the function defined by

$$\rho_{\mathbf{V}}(\mathbf{v}) = \frac{1}{\nu} \sum_{\ell=1}^{\nu} \exp \left\{ -\frac{1}{2\widehat{s}_n^2} \sum_{j=1}^{n} \frac{1}{\widehat{\sigma}_j^2} (\frac{\widehat{s}_n}{s_n} v_j^\ell - v_j)^2 \right\} \,, \tag{5.63}$$

with $s_n$ and $\widehat{s}_n$ the positive parameters defined by

$$s_n = \left\{ \frac{4}{\nu(2+n)} \right\}^{1/(n+4)} \quad , \quad \widehat{s}_n = \frac{s_n}{\sqrt{s_n^2 + \frac{\nu-1}{\nu}}} \,, \tag{5.64}$$

where $s_n$ is the Silverman multidimensional optimal bandwidth. Finally, $c_n$ is the normalization constant, which is written as

$$c_n = \frac{1}{(\sqrt{2\pi}\, \widehat{s}_n)^n \, \widehat{\sigma}_1 \times \ldots \times \widehat{\sigma}_n} \,. \tag{5.65}$$

### 5.4.4 Estimation of the cost functions for the optimization problems

For solving the optimization problems formulated in Sections 5.2 and 5.3, we use the estimates of the probability density functions presented in Section 5.4.3. These optimization problems (see Eqs. (5.11) and (5.37)) require the estimation of the cost functions $\mathbb{J}_1(\mathbf{q})$ and $\mathbb{J}_2(\boldsymbol{\eta}, \mathbf{q})$, with $\mathbf{q}$ in $\mathbb{R}^N$ and $\boldsymbol{\eta}$ in $\mathbb{R}^{N_{\text{PCA}}}$, which are defined by

$$\mathbb{J}_1(\mathbf{q}) = \int_{\mathscr{D}^c} p_{\mathbf{Q}(T),\mathbf{U}(T)}(\mathbf{q}, \mathbf{u}) \, d\mathbf{u} \,, \tag{5.66}$$

$$\mathbb{J}_2(\boldsymbol{\eta}, \mathbf{q}) = \int_{\mathscr{D}^c} p_{\mathbf{H},\mathbf{Q}(T),\mathbf{U}(T)}(\boldsymbol{\eta}, \mathbf{q}, \mathbf{u}) \, d\mathbf{u} \,. \tag{5.67}$$

Let us assume that $\nu$ independent realizations

$$\mathbf{q}^\ell = \mathbf{Q}(T; \theta_\ell) \,, \, \mathbf{u}^\ell = \mathbf{U}(T; \theta_\ell) \,, \, \boldsymbol{\eta}^\ell = \mathbf{H}(\theta_\ell) \quad , \quad \ell = 1, \ldots, \nu \,, \tag{5.68}$$

have been generated for $\theta_1, \ldots, \theta_\nu$ in $\Theta$.

**(i) Expression of $\mathbb{J}_1(\mathbf{q})$.** Using Eqs. (5.62) to (5.65), $\mathbb{J}_1(\mathbf{q})$ can be rewritten as,

$$\mathbb{J}_1(\mathbf{q}) = c_{1,n,m_u} \times \frac{1}{\nu} \sum_{\ell=1}^{\nu} I_\ell \times J_\ell(\mathbf{q}) \,, \tag{5.69}$$

in which

$$n = N + m_u \,, \tag{5.70}$$

where $c_{1,n,m_u}$ is a normalized constant that can easily be computed but that will not be used. For all $\mathbf{q}$ in $\mathbb{R}^N$ and for all $\ell = 1, \ldots, \nu$, the positive-valued functions $J_\ell(\mathbf{q})$ are defined by

$$J_\ell(\mathbf{q}) = \exp\left\{ -\frac{1}{2\widehat{s}_n^2} \sum_{\alpha=1}^{N} \frac{1}{\widehat{\sigma}_\alpha^2} (\frac{\widehat{s}_n}{s_n} q_\alpha^\ell - q_\alpha)^2 \right\} . \tag{5.71}$$

For all $\ell = 1, \ldots, \nu$, the real numbers $I_\ell$ are positive and defined by

$$I_\ell = \int_{\mathscr{D}^c} \widetilde{c}_{m_u} \exp\left\{ -\frac{1}{2\widehat{s}_n^2} \sum_{j=1}^{m_u} \frac{1}{\widetilde{\sigma}_j^2} (\frac{\widehat{s}_n}{s_n} u_j^\ell - u_j)^2 \right\} du_1 \ldots du_{m_u} \,, \tag{5.72}$$

in which

$$\widetilde{c}_{m_u} = \frac{1}{(\sqrt{2\pi}\,\widehat{s}_n)^{m_u}\, \widetilde{\sigma}_1 \times \ldots \times \widetilde{\sigma}_{m_u}} \,. \tag{5.73}$$

In these equations, $s_n$ and $\widehat{s}_n$ are defined by Eq. (5.64). For $\alpha = 1, \ldots, N$ and for $j = 1, \ldots, m_u$, the empirical variances $\widehat{\sigma}_\alpha^2$ and $\widetilde{\sigma}_j^2$ are calculated by

$$\widehat{\sigma}_\alpha^2 = \frac{1}{\nu - 1} \sum_{\ell=1}^{\nu} (q_\alpha^\ell - \widehat{m}_\alpha)^2 \quad , \quad \widetilde{\sigma}_j^2 = \frac{1}{\nu - 1} \sum_{\ell=1}^{\nu} (u_j^\ell - \widetilde{m}_j)^2 \,. \tag{5.74}$$

with

$$\widehat{m}_\alpha = \frac{1}{\nu} \sum_{\ell=1}^{\nu} q_\alpha^\ell \quad , \quad \widetilde{m}_j = \frac{1}{\nu} \sum_{\ell=1}^{\nu} u_j^\ell \,. \tag{5.75}$$

**(ii) Expression of $\mathbb{J}_2(\boldsymbol{\eta}, \mathbf{q})$.** Using Eqs. (5.62) to (5.65), $\mathbb{J}_2(\boldsymbol{\eta}, \mathbf{q})$ can be rewritten as,

$$\mathbb{J}_2(\boldsymbol{\eta}, \mathbf{q}) = c_{2,n,m_u} \times \frac{1}{\nu} \sum_{\ell=1}^{\nu} I_\ell \times J_\ell(\mathbf{q}) \times K_\ell(\boldsymbol{\eta}) \,, \tag{5.76}$$

in which

$$n = N_{\text{PCA}} + N + m_u \,, \tag{5.77}$$

where $c_{2,n,m_u}$ is a normalized constant that can easily be computed but that will not be used, and where $J_\ell(\mathbf{q})$ and $I_\ell$ are defined by Eqs. (5.71) and (5.72). For all $\boldsymbol{\eta}$ in $\mathbb{R}^{N_{\text{PCA}}}$ and for all $\ell = 1, \ldots, \nu$, the positive-valued functions $K_\ell(\boldsymbol{\eta})$ are defined by

$$K_\ell(\boldsymbol{\eta}) = \exp\left\{ -\frac{1}{2\widehat{s}_n^2} \sum_{j=1}^{N_{\text{PCA}}} \frac{1}{\sigma_j^2} (\frac{\widehat{s}_n}{s_n} \eta_j^\ell - \eta_j)^2 \right\} . \tag{5.78}$$

For all $j$ fixed in $\{1, \ldots, N_{\text{PCA}}\}$, the empirical variance $\sigma_j^2$ of $H_j$ is defined by

$$\sigma_j^2 = \frac{1}{\nu - 1} \sum_{\ell=1}^{\nu} (\eta_j^\ell - m_j)^2 , \tag{5.79}$$

in which

$$m_j = \frac{1}{\nu} \sum_{\ell=1}^{\nu} \eta_j^\ell , \tag{5.80}$$

and is such that $\sigma_j = 1$, taking into account the PCA of $\mathbf{H}$ that has been performed in Section 5.3.2.1.

**(iii) Computation of $I_\ell$ for $\ell = 1, \ldots, \nu$.** For $\ell$ fixed in $(1, \ldots, \nu)$, the positive number $I_\ell$ defined by Eq. (5.72) cannot usually be computed by a numerical quadrature. Two cases are considered.

**(iii-1) Domain $\mathscr{D}^c$ is non separable.** The integral on $\mathscr{D}^c$ is then estimated using the Monte Carlo method and for that, Eq. (5.72) is rewritten as

$$I_\ell = E\{ \mathbb{1}_{\mathscr{D}^c}([\sigma_{\boldsymbol{\mathcal{U}}}]\, \boldsymbol{\mathcal{G}} + \mathbf{m}_{\boldsymbol{\mathcal{U}}}^\ell) \} , \tag{5.81}$$

in which $\mathbb{1}_{\mathscr{D}^c}(\mathbf{u}) = 1$ if $\mathbf{u} \in \mathscr{D}^c$ and $= 0$ if $\mathbf{u} \notin \mathscr{D}^c$, and where $\boldsymbol{\mathcal{G}}$ is the Gaussian centered $\mathbb{R}^{m_u}$-valued random variable whose covariance matrix is the identity matrix. The matrix $[\sigma_{\boldsymbol{\mathcal{U}}}]$ is an $(m_u \times m_u)$ diagonal matrix that is written as

$$[\sigma_{\boldsymbol{\mathcal{U}}}]_{jj'} = \delta_{jj'}\, \widehat{s}_n\, \widetilde{\sigma}_j . \tag{5.82}$$

For $\ell$ fixed in $(1, \ldots, \nu)$, the vector $\mathbf{m}_{\boldsymbol{\mathcal{U}}}^\ell$ is in $\mathbb{R}^{m_u}$ and is written as

$$\mathbf{m}_{\boldsymbol{\mathcal{U}}}^\ell = (\frac{\widehat{s}_n}{s_n}\, u_1^\ell, \ldots, \frac{\widehat{s}_n}{s_n}\, u_{m_u}^\ell) . \tag{5.83}$$

**(iii-2) Domain $\mathscr{D}^c$ is separable.** Domain $\mathscr{D}^c$ can be written as

$$\mathscr{D}^c = \Pi_{j=1}^{m_u} \mathscr{D}_j^c \quad , \quad \mathscr{D}_j^c = (\mathscr{D}_{\inf,j}^c, \mathscr{D}_{\sup,j}^c)\,, \tag{5.84}$$

and

$$\mathscr{D}_{\inf}^c = (\mathscr{D}_{\inf,1}^c, \ldots, \mathscr{D}_{\inf,m_u}^c) \quad , \quad \mathscr{D}_{\sup}^c = (\mathscr{D}_{\sup,1}^c, \ldots, \mathscr{D}_{\sup,m_u}^c) \tag{5.85}$$

where the real bounds of $\mathscr{D}_j^c$ (which can be infinity) are such that $\mathscr{D}_{\inf,j}^c < \mathscr{D}_{\sup,j}^c$ and the method for estimating these bounds is presented in Appendix A. The computation of $I_\ell$ is explicit and is developed in Appendix E.

## 5.5 Comments about the software that has been developed

A general software written in Matlab language has been developed for computing the static equivalent forces. The algorithms of all the methods presented in this thesis have been implemented.
The inputs of this software are made up of:

- the parameters devoted to the general data, to the type of analyses performed, to the signal processing, and to the outputs concerning prints and plots.
- the realizations of the unsteady pressures that are measured in a wind tunnel or that are simulated.
- the finite element model of the structure.
- the controlability matrix and the observability matrices for the structure.

# Chapter 6

# Application to a simple structure and experimental validation

The aim of this chapter is to present a validation of the proposed theory on a simple structure on which experimental measurements have been carried out. Moreover, analysis of convergence and robustness of the approach are presented, as well as a study of the influence of the non-Gaussianity level.

## 6.1 Application description

This application is devoted to the Maine-Montparnasse Tower in Paris for which measurements have been carried out [16, 77]. In the framework of the model predictions with measurements, the structure is assumed to have a linear elastic behavior. To calculate the response of this structure subjected to wind loads, the computational model used is a finite element model of beam type. Since the atmospheric turbulence energy is concentrated in a frequency band smaller than 3 Hz, only the first two vibration modes of the structure have to be taken into account for computing the dynamical response. However, in order to ensure a good convergence of the reduced-order model based on the use of only these first two modes, quasi-static acceleration terms are taken into account. In this chapter:

- Finite element model of the structure is introduced and observations are defined.

- For the experimental validation, a Gaussian model for the longitudinal velocity field $\mathbb{V}(z,t) = \underline{v}(z) + V(z,t)$ for $z \in [z_{\inf}, z_{\sup}] \subset \mathbb{R}^+$ and for $t \in \mathbb{R}$ is chosen (as in [77]). The realizations of stochastic field $\{V(z,t)\}_{(z,t)}$ are then constructed using the algorithm proposed in [103, 96].

- Three models are introduced for generating the pressure field applied to the structure. Each one is expressed using the velocity field $\mathbb{V}(z,t) = \underline{v}(z) + V(z,t)$:
  - Model 1: The pressure field is an affine function of $V$ and consequently, is a Gaussian field. This model is used for the comparisons related to the non-gaussianity analysis, but is not used for the experimental validation.
  - Model 2: The pressure field is a quadratic function of $V$ and therefore, is non-Gaussian. The non-gaussianity is relatively small for the experimental value of the reference mean wind velocity $\underline{V}_R$ for which the measurements on the Maine-Montparnasse Tower were made. This model is used for its experimental validation.
  - Model 3: The pressure field is a nonlinear empirical function of $V$, specially introduced to analyze the non-Gaussian effects and consequently, is not used for the experimental validation.
- The method that has been presented in this work is applied to compute the equivalent static forces.

## 6.2 Computational model

### 6.2.1 Finite element model of the structure and observations

#### 6.2.1.1 Finite element model of the structure

An orthonormal reference frame $oxyz$ is considered, whose the origin is located at the base of the Tower (at the foundations level), such that $x$-axis is perpendicular to the largest tower parallel faces, $y$-axis is perpendicular to the smallest parallel faces, and $z$-axis is vertical. We are interested in the bending of the Tower in the plane $xoz$ (see figure 6.1). The structure is modeled by a 2D linear Timoshenko beam with variable bending inertia in $xoz$-bending mode. This 2D beam is discretized into 20 Timoshenko beam finite elements with two nodes (21 nodes over the whole structure), with 3 degrees of freedom per node (63 DOFs over the whole structure): displacement along $ox$, displacement along $oz$, and rotation around $oy$. The width $L$ of the largest parallel faces subjected to wind effects is $61.8$ m, and does not depend on $z$. The $i$-th FE has node $i$ as the origin node and node $i+1$ as the end node. Node $21$ that is the end node of the $20$-th FE corresponds to the beam length that is $H = 221.34$ m. The flexibility of the foundation (raft) is taken into account by an elastic connection for the rotation around $y$-axis of node $1$. Data related to this model are described in Section H.1 of Appendix H.

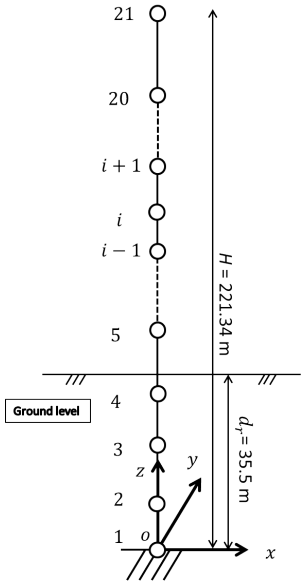


Figure 6.1: FE model of the Maine-Montparnasse Tower.

#### 6.2.1.2 Observations

The observations of the structure, which are used for computing the static equivalent forces, are the following:

- Observation 1: shear force $\mathbb{U}^1$ in the section located at the origin of the 1-st FE (node 1).
- Observation 2: bending moment $\mathbb{U}^2$ in the section located at the origin of the 1-st FE (node 1).
- Observation 3: shear force $\mathbb{U}^3$ in the section located at the origin of the 13-th FE (node 13).
- Observation 4: bending moment $\mathbb{U}^4$ in the section located at the origin of the 13-th FE (node 13).

For $i = 1, 2, 3, 4$, $\mathbb{U}^i = \underline{u}^i + U^i$ where $\underline{u}^i$ is the mean value. The mean value of the shear force for observation 1 and the mean value of the bending moment for observation 2 (induced by the mean pressure) are simultaneously maximum. The bending moment for observation 4 is maximum when the beam deformation corresponds to the deformation of the second elastic mode.

### 6.2.2 Stochastic model of the longitudinal wind velocity

At point $z$ and at time $t$, the longitudinal wind velocity $\mathbb{V}(z,t)$ is written as

$$\mathbb{V}(z,t) = \underline{v}(z) + V(z,t)\,, \tag{6.1}$$

where $\underline{v}(z)$ is the wind mean profile, which depends on $z$, and $V(z,t)$ is the fluctuations part at point $z$ and at time $t$.

#### 6.2.2.1 Mean wind profile [7, 25, 38, 107]

The model of the mean wind profile $\underline{v}(z)$ is written as

$$\begin{aligned} \underline{v}(z) &= \underline{V}_R\, k_r\, \log(\frac{z-d_r}{z_0}) \quad , \quad z \geq z_0 + d_r\,, \\ \underline{v}(z) &= 0 \qquad\qquad\qquad\quad , \quad z < z_0 + d_r\,, \end{aligned} \tag{6.2}$$

where

- $\underline{V}_R$ is the reference mean wind velocity
- $z_0$ is the roughness length
- $k_r$ is the terrain factor depending on the roughness length $z_0$
- $d_r$ is the displacement height for wind generation.

The numerical values of the wind mean profile parameters are given in Section H.2.1 of Appendix H.

#### 6.2.2.2 Random field $\{V(z,t)\}_{(z,t)}$

Over a period of about 10 minutes, the statistical fluctuations $\{V(z,t)\}_{(z,t)}$ of the longitudinal velocity field is locally time stationary and is modeled by a stochastic field indexed by $t$ that is extended to $\mathbb{R}$. Random field $\{V(z,t), z \in [z_0 + d_r, H], t \in \mathbb{R}\}$ is a second-order, centered, time stationary stochastic process that is assumed to be Gaussian. The cross-spectral density function $S_V(z,z',\omega)$ is defined in Section H.2.2 and the power spectral density function $S_V(z,\omega)$ is defined in Section H.2.3 of Appendix H.

#### 6.2.2.3 Generator of realizations of random field $\{V(z,t)\}_{(z,t)}$

Let $z_1, \ldots, z_{m_{\text{exp}}}$ be the altitudes of the $m_{\text{exp}} = 17$ points in which the pressure is generated such that, for $j = 1, \ldots, m_{\text{exp}}$, $z_j$ is the altitude of node $j + 4$. Let $\{\mathbf{V}(t), t \in \mathbb{R}\}$ be the Gaussian stationary $\mathbb{R}^{m_{\text{exp}}}$-valued stochastic process indexed by $\mathbb{R}$ such that

$$\mathbf{V}(t) = (V_1(t), \ldots, V_{m_{\text{exp}}}(t)) \quad , \quad V_j(t) = V(z_j, t) \quad , \quad j = 1, \ldots, m_{\text{exp}} \,. \tag{6.3}$$

Using the generator of realizations defined in Appendix F for a Gaussian stationary process, $n_r = 100$ independent realizations $\{\mathbf{V}(t, \theta^\ell), t \in [0, T]\}$ for $\ell \in \{1, \ldots, n_r\}$ of $\{\mathbf{V}(t), t \in \mathbb{R}\}$ are calculated, in which $T$ is defined in Chapter 3.

#### 6.2.2.4 Matrix-valued spectral density function of V

Let $[S_{\mathbf{V}}(\omega)]$ be the matrix-valued spectral density function of the stationary stochastic process $\{\mathbf{V}(t), t \in \mathbb{R}\}$, such that

$$[R_{\mathbf{V}}(\tau)] = E\{\mathbf{V}(t+\tau)\,\mathbf{V}(t)^T\} = \int_{\mathbb{R}} e^{i\omega\tau}[S_{\mathbf{V}}(\omega)]d\omega \,. \tag{6.4}$$

Figure 6.2 shows the graph of the function $f \mapsto \|[S_{\mathbf{V}}(2\pi f)]\|_F$ and the graph of the corresponding function $f \mapsto \|[\widehat{S}_{\mathbf{V}}(2\pi f)]\|_F$ estimated using the periodogram method with $n_r$ realizations (see Section 3.3.3 in which $\mathbf{P}^{\text{exp}}$ must be replaced by $\mathbf{V}$). This figure shows that the two curves are superimposed, which validates the digital signal processing used for which the signal processing parameters are given in Section H.3 of Appendix H.

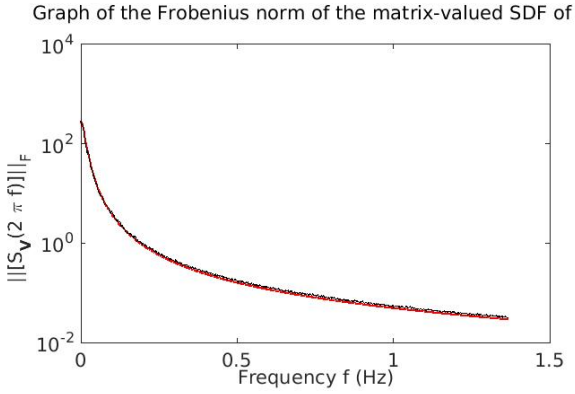


Figure 6.2: Graphs of the Frobenius norm of the matrix-valued spectral density function of $\{\mathbf{V}(t)\}_t$: Graph of $f \mapsto \|[S_{\mathbf{V}}(2\pi f)]\|_F$ (red thick regular solid line) and graph of $f \mapsto \|[\widehat{S}_{\mathbf{V}}(2\pi f)]\|_F$ (black thin irregular solid line).

### 6.2.3 Random pressure field model

According to Section 6.1, three models of the pressure field are considered.

- Model 1: the pressure $\mathbb{P}(z,t)$ is written as

$$\mathbb{P}(z,t) = \frac{1}{2}\rho\,\underline{v}(z)^2 + \rho\,\underline{v}(z)\,V(z,t)\,, \tag{6.5}$$

  and is thus a Gaussian field.

- Model 2: the pressure $\mathbb{P}(z,t)$, which corresponds to the dynamic pressure, is written as

$$\mathbb{P}(z,t) = \frac{1}{2}\rho(\underline{v}(z) + V(z,t))^2\,, \tag{6.6}$$

  is weakly non-Gaussian for the value $\underline{V}_R = 17$ m/s retained for the experimental comparison.

- Model 3: the pressure $\mathbb{P}(z,t)$ is empirically constructed as

$$\mathbb{P}(z,t) = \frac{1}{2}\rho\,\underline{v}(z)^2 \times (1 + 2\,\frac{V(z,t)}{\underline{v}(z)}\exp\{4\,\frac{V(z,t)}{\underline{v}(z)}\})\,, \tag{6.7}$$

  which is a strongly non-Gaussian field for the value $\underline{V}_R = 17$ m/s.

In these equations, $\rho$ is the air density (kg/m$^3$). For $j = 1,\ldots,m_{\text{exp}}$, let $\mathbb{P}_j(t) = \mathbb{P}(z_j,t)$. The $\mathbb{R}^{m_{\text{exp}}}$-valued process $\mathbb{P}(t) = (\mathbb{P}_1(t),\ldots,\mathbb{P}_{m_{\text{exp}}}(t))$ is written as $\mathbb{P}(t) = \underline{\mathbf{p}} + \mathbf{P}(t)$ (see Eq. (2.34)) in which $\mathbf{P}(t) = (P_1(t),\ldots,P_{m_{\text{exp}}}(t))$. For each one of these three models, the graphs of the power spectral density (PSD) functions $f \mapsto S_{P_1}(2\pi f)$ and $f \mapsto S_{P_{17}}(2\pi f)$ of the components $P_1(t)$ and $P_{17}(t)$ of stochastic process $\mathbf{P}$ (corresponding to nodes 5 and 21), are shown in Figures 6.3, 6.4, and 6.5.

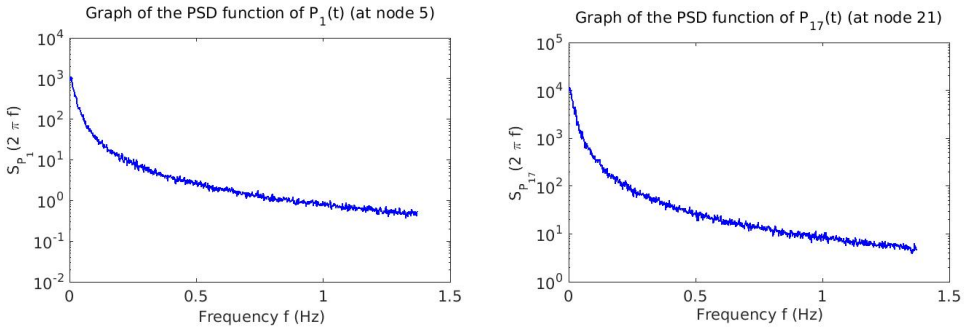


Figure 6.3: Model 1: Graph of the PSD function $f \mapsto S_{P_1}(2\pi f)$ of $P_1(t)$ at node 5 (left) and graph of the PSD function $f \mapsto S_{P_{17}}(2\pi f)$ of $P_{17}(t)$ at node 21 (right). Horizontal axis in Hz and vertical axis in N$^2$ m$^{-4}$ s.

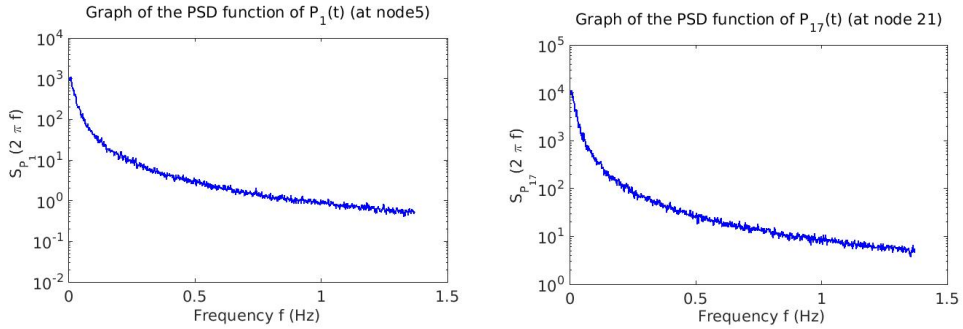


Figure 6.4: Model 2: Graph of the PSD function $f \mapsto S_{P_1}(2\pi f)$ of $P_1(t)$ at node 5 (left) and graph of the PSD function $f \mapsto S_{P_{17}}(2\pi f)$ of $P_{17}(t)$ at node 21 (right). Horizontal axis in Hz and vertical axis in $\mathrm{N}^2\ \mathrm{m}^{-4}$ s.

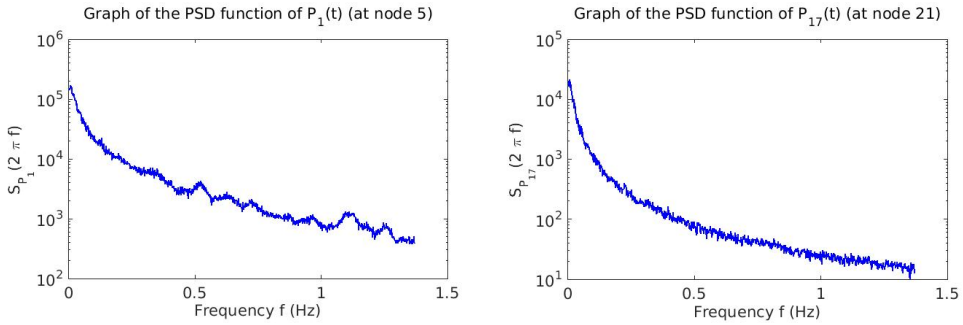


Figure 6.5: Model 3: Graph of the PSD function $f \mapsto S_{P_1}(2\pi f)$ of $P_1(t)$ at node 5 (left) and graph of the PSD function $f \mapsto S_{P_{17}}(2\pi f)$ of $P_{17}(t)$ at node 21 (right). Horizontal axis in Hz and vertical axis in $\mathrm{N}^2\ \mathrm{m}^{-4}$ s.

## 6.3 Experimental measurements

The measurements that made by the CEBTP (see [16, 77]) on the Tower are the following.

- The total static flexibility at node $21$ ($z = 221.34$ m) along $x$-axis is equal to $0.2625$ mm/Tf (this means that if a force of $1$ tonne-force ($9{,}810$ Newton) is applied at node $21$ along $x$-axis, then the total displacement along this axis is $0.2625$ mm). This information has been used for updating the stiffness model of the structure, in particular the value of the elasticity constant for the rotation of the elastic connection at node $1$.

- The experimental eigenfrequency of the first mode is $f_1^{\exp} = 0.20$ Hz.
- The experimental eigenfrequency of the second mode is $f_2^{\exp} = 0.92$ Hz.
- The experimental damping rate of the first two modes are $\xi_1^{\exp} = \xi_2^{\exp} = 0.00832$.
- For the measured value $\underline{V}_R = 17$ m/s of the reference mean wind velocity, the time responses have been measured for several sequences of $800$ s concerning the relative displacement along $x$-axis at the top of the Tower (the relative displacement with respect to the frame linked to the raft). These measurements are used in Section 6.5 for the model experimental validation.

## 6.4 Construction of the reduced-order model with the quasi-static acceleration term

Using the method presented in Section 2.4.2 (ii), the reduced-order model of order $N$ in taking into account the quasi-static acceleration term is constructed. The eigenfrequencies of the first two modes computed with the updated model are $f_1 = 0.20$ Hz and $f_2 = 0.93$ Hz. These frequencies match with the experimental feigenfrequencies given in Section 6.3. The graph of function $N \mapsto \|\widehat{\mathbb{h}}_N^{c,\mathrm{acc}}\|_{\mathbf{L}^2(\mathscr{B})}$, defined by Eq. (2.32) is plotted in Figure 6.6 (left), for $N = 1, \ldots, 10$. This figure shows that the convergence of the reduced-order model is reached for $N = 2$ (the first two bending modes) that was expected. For $N = 2$, Figure 6.6 (right) displays the graph of function $f \mapsto \|\widehat{\mathbb{h}}_N^{c,\mathrm{acc}}(2\pi f)\|_M^2$ defined by Eq. (2.33).

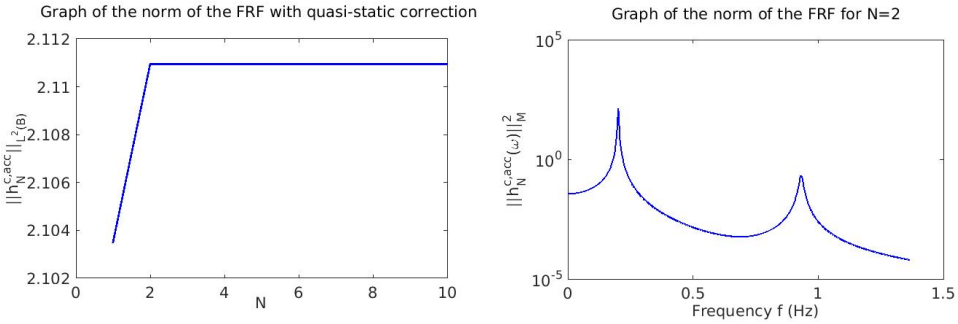


Figure 6.6: Graph of function $N \mapsto \|\widehat{\mathbb{h}}_N^{c,\mathrm{acc}}\|_{\mathbf{L}^2(\mathscr{B})}$ (left) and, for $N = 2$, graph of function $f \mapsto \|\widehat{\mathbb{h}}_N^{c,\mathrm{acc}}(2\pi f)\|_M^2$ (right).

## 6.5 Experimental validation of the model

### 6.5.1 Objective of the validation

Let $\mathbb{U}_d^1(t) = Y_{62}(t) - Y_3(t) \times H$ be the relative displacement at node 21 (top of the Tower) with respect to the frame linked to the raft that is in rotation around $y$-axis, in which $Y_{62}(t)$ is the displacement at node 21 and $Y_3(t)$ is the rotation at node 1. This relative displacement is written as $\mathbb{U}_d^1(t) = \underline{u}_d^1 + U_d^1(t)$ in which $\underline{u}_d^1$ is the mean value. Model 2 is used, that is to say, pressure field $\mathbb{P}$ is weakly non-Gaussian. The objective is validation of the computational model for the extreme value statistics of $\mathbb{U}_d^1$ (see Section 6.3).

### 6.5.2 Statistical reduction of the non-Gaussian centered process $\{\mathbf{P}(t), t \in [0,T]\}$

Using the method presented in Section 4.1, the KL statistical reduction of pressure field $\{\mathbf{P}(t), t \in [0,T]\}$ is performed with $n_r = 100$. Figure 6.7 (left) shows the square root of the eigenvalues $\mu_j$ for $j = 1, \ldots, N_{\text{KL}}$ of the eigenvalue problem defined by Eq. (4.13). Error function $N_{\text{KL}} \mapsto \text{err}_{\text{KL}}(N_{\text{KL}})$ defined by Eq. (4.10) is plotted in Figure 6.7 (right). For an error $\text{err}_{\text{KL}} = 10^{-3}$, we obtain $N_{\text{KL}} = 100$.

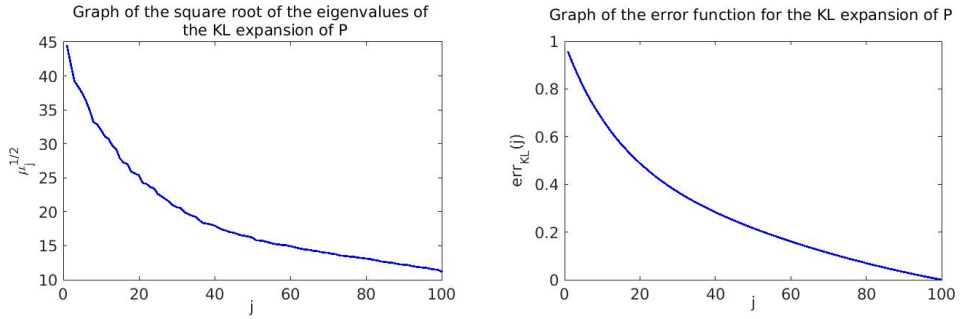


Figure 6.7: Graph of $j \mapsto \sqrt{\mu_j}$ for $j = 1, \ldots, N_{\text{KL}}$ (left) and graph of $N_{\text{KL}} \mapsto \text{err}_{\text{KL}}(N_{\text{KL}})$ related to the KL statistical reduction of $\{\mathbf{P}(t), t \in [0,T]\}$ (right).

Therefore, $n_r$ realizations of random vector $\mathbf{H}$ with values in $\mathbb{R}^{N_{\text{KL}}}$, for which its components are defined by Eq. (4.21), are deduced from the $n_r$ generated realizations of $\{\mathbf{P}(t), t \in [0,T]\}$.

### 6.5.3 Polynomial chaos expansion of non-Gaussian random vector H

Using the methodology presented in Sections 4.2 and 4.3, the PCE of non-Gaussian random vector $\mathbf{H}$ is constructed. Figure 6.8 presents error function $N_d \mapsto \text{err}(N_d)$ defined by Eq. (4.98) with Eq. (4.96). The convergence is reached for the degree $N_d = 4$. The coefficients of the PCE of $\mathbf{H}$ are estimated according to the method and the hypotheses presented in Section 4.3.5. The generator of independent realizations of non-Gaussian process $\{\mathbf{P}(t), t \in [0, T]\}$, defined in Section 4.2.4, is used for generating $\nu = 1{,}000$ realizations.

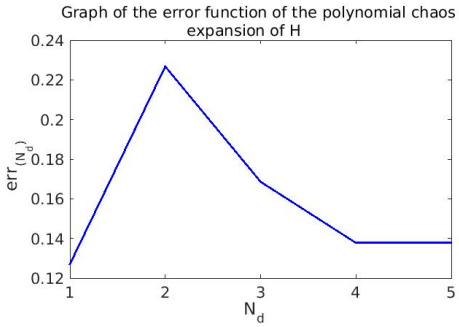


Figure 6.8: Graph of error function $N_d \mapsto \text{err}(N_d)$ of the PCE of $\mathbf{H}$.

### 6.5.4 Power spectral density function of process $\mathbf{U}_d^1$

Figure 6.9 shows the PSD function $f \mapsto S_{U_d^1}(2\pi f)$ of centered observation $U_d^1(t)$ estimated with $\nu = 1{,}000$. This figure shows that there is a non negligible quasi-static contribution in the frequency band $[0, 0.12]$ Hz.

### 6.5.5 Probability density function, extreme values statistics of $\mathbb{U}_d^1$, and experimental comparison

As the mean value $\underline{u}_d^1$ is positive, then the worst case corresponds to the maximum case (and not to the minimum case). Let $U_{d,\max}^1 = \max_{t\in[0,T]} U_d^1(t)$ be the maximum of $U_d^1(t)$ on $[0, T]$ and let $\mathbb{U}_{d,\max}^1 = \max_{t\in[0,T]} \mathbb{U}_d^1(t)$ be the maximum of $\mathbb{U}_d^1(t)$ on $[0, T]$. We consider the following extreme value statistics (mean value and standard deviation):

- $\underline{U}_{d,\max}^1 = E\{U_{d,\max}^1\}$ and $\sigma_{U_{d,\max}^1} = E\{(U_{d,\max}^1 - \underline{U}_{d,\max}^1)^2\}$,
- $\underline{\mathbb{U}}_{d,\max}^1 = E\{\mathbb{U}_{d,\max}^1\}$ and $\sigma_{\mathbb{U}_{d,\max}^1} = E\{(\mathbb{U}_{d,\max}^1 - \underline{\mathbb{U}}_{d,\max}^1)^2\} = \sigma_{U_{d,\max}^1}$.

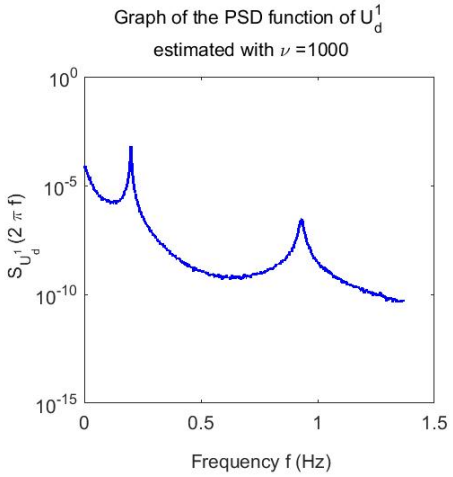


Figure 6.9: Graph of PSD function $f \mapsto S_{U_d^1}(2\pi f)$ of observation $U_d^1$ estimated with $\nu = 1{,}000$ realizations. Horizontal axis in Hz and vertical axis in $\mathrm{m}^2$ s.

Let $g_d^+$ be the gust loading factor defined in Section G.1 of Appendix G, and let $g_{d,\mathrm{gauss}}^1$ be the gust loading factor defined in Section G.2 of Appendix G for the Gaussian approximation. The extreme value statistics of $\mathbb{U}_d^1$ are given in Table 6.1.

| Observation | $\underline{u}_d^1$ | $\underline{U}_{d,\max}^1$ | $\sigma_{U_{d,\max}^1}$ | $\underline{\mathbb{U}}_{d,\max}^1$ |
|---|---|---|---|---|
| $\mathbb{U}_d^1 \times 10^{-2}$ (m) | 2.199 | 2.424 | 0.446 | 4.623 |

Table 6.1: Extreme value statistics of $U_d^1$.

**Experimental comparison.** From Table 6.1,it can be deduced that $\underline{\mathbb{U}}_{d,\max}^1/\underline{u}_d^1 = (4.623\times10^{-2})/(2.199\times10^{-2}) = 2.11$, which matches with the experimental measurements (see [16, 77]) that belong to the interval $[1.9\,, 2.06]$. It should be noted that gust loading factor $g_d^+ = 2.866$ obtain with the proposed stochastic model is different from $g_{d,\mathrm{gauss}}^1 = 3.274$ that is obtained with a Gaussian approximation.

Figure 6.10 shows the probability density function of each one of the random variables $U_d^1$, $U_{d,\max}^1 = \max_{t\in[0,T]} U_d^1(t)$, and $U_{d,\min}^1 = \min_{t\in[0,T]} U_d^1(t)$, which are estimated with $\nu = 1{,}000$ realizations.

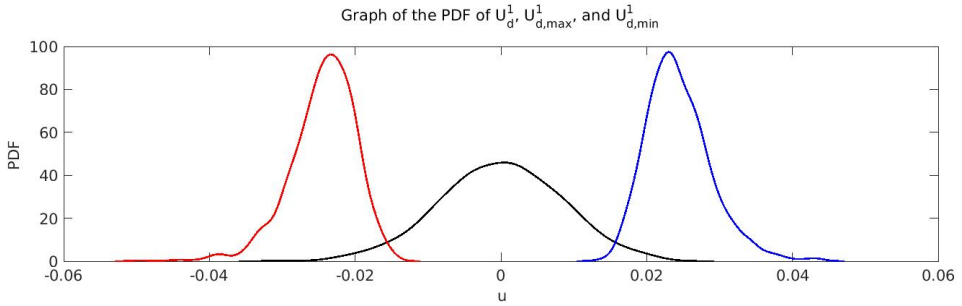


Figure 6.10: Graph of $u \mapsto p_{U_d^1}(u)$ of $U_d^1$ (black line, central curve), $u \mapsto p_{U_{d,\max}^1}(u)$ of $U_{d,\max}^1$ (blue line, right curve), and $u \mapsto p_{U_{d,\min}^1}(u)$ of $U_{d,\min}^1$ (red line, left curve). Horizontal axis in m.

## 6.6 Validation of the proposed method for the computation of the equivalent static forces and convergence analysis with respect to the number of realizations

### 6.6.1 Framework of the equivalent static forces computation

For the validation of method that allows the equivalent static forces to be computed and for the convergence analysis with respect to the number of realizations, the following framework is chosen.

- Model 2 of the pressure field is used, that is to say, the pressure field $\mathbb{P}(t)$ is weakly non-Gaussian for the value $\underline{V}_R = 17$ m/s of the reference mean wind velocity.
- The reduced-order model is constructed taking into account the quasi-static acceleration term.
- The observations for which the equivalent static forces are computed are $\mathbb{U}^2$ and $\mathbb{U}^4$.
- The domain $\mathscr{D}$ associated with $\mathbb{U}^2$ or $\mathbb{U}^4$ is separable.
- For $j = 2$ or $j = 4$, the lower and the upper bounds, $\mathscr{D}_{\text{inf},j}^c$ and $\mathscr{D}_{\text{sup},j}^c$, are directly defined by using the mean of the extreme values (see Section A.2 in Appendix A).

### 6.6.2 Estimation of the equivalent static forces with the proposed method

The equivalent static forces are computed by the method presented in Chapter 5. For each observation, the couple $(\boldsymbol{\eta}^{\mathrm{MV}}, \mathbf{q}^{\mathrm{MV}})$ is obtained as the solution of the optimization problem defined by Eq. (5.37). This couple allows for computing the corresponding centered equivalent static force $\mathbf{f}^{e,s}$ using Eq. (5.35).
In this section, we present the graphs related to the equivalent static forces $\mathbb{f}^{2,e,s}$ and $\mathbb{f}^{4,e,s}$ computed with observations $\mathbb{U}^2$ and $\mathbb{U}^4$. The components of the equivalent static forces along $z$-axis are zero. Figures 6.11 and 6.12 show the equivalent forces along $x$-axis and the moment around $y$-axis.

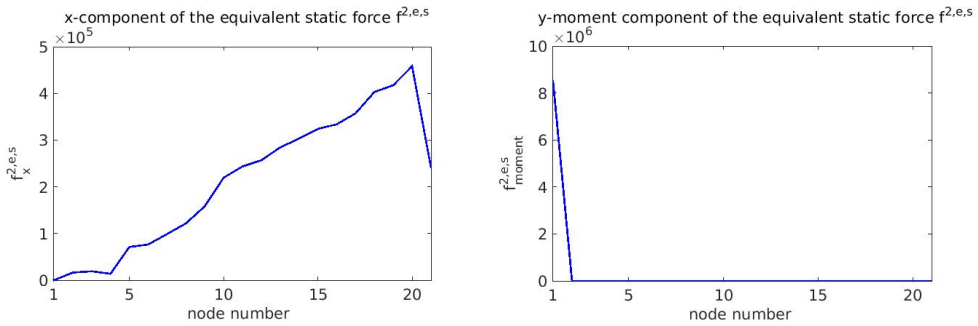


Figure 6.11: Graphs of $x$-component (left) and $y$-moment component (right) of the equivalent static force associated with observation $\mathbb{U}^2$ at each node of the FE mesh. Vertical axis (left) in N and (right) in N m.

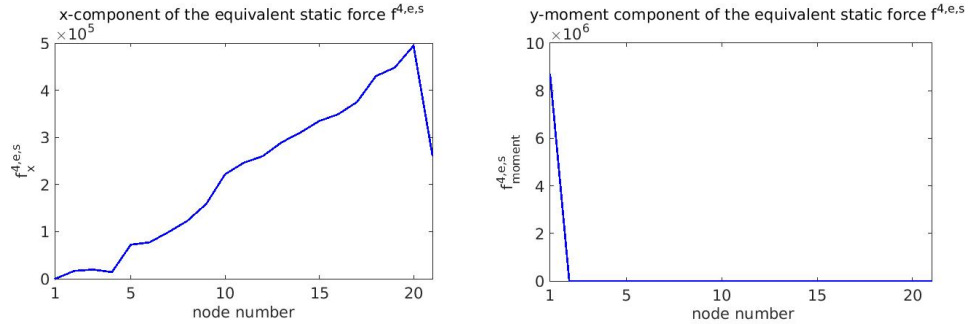


Figure 6.12: Graphs of $x$-component (left) and $y$-moment component (right) of the equivalent static force associated with observation $\mathbb{U}^4$ at each node of the FE mesh. Vertical axis (left) in N and (right) in N m.

It should be noted that the moment at node 1 (see Figures 6.11 (right) and 6.12 (right))

corresponds to the reaction of the elastic connection for the rotation around $y$-axis. It will be noted that the exterior moments are zero for the other DOFs. Figures 6.11 (left) and 6.12 (left) show that the amplitude of $x$-component of the equivalent forces at node 21 is smaller than the amplitude at node 20. This is due to the fact that the wind effects surface associated with node 21 has an area ($427.6$ m$^2$) that is smaller than the area ($813.9$ m$^2$) associated with node 20.

### 6.6.3 Validation of the predicted equivalent static forces

In order to validate the proposed approach related to the prediction of the equivalent static forces, for each observation $\mathbb{U}$, the equivalent static observation $\mathfrak{u}^{e,s}$ is recomputed from the predicted equivalent static force associated with $\mathbb{U}$, by solving the static problem

$$\mathfrak{u}^{e,s} = [A_o]\, \mathbf{y}^{e,s} \,,$$

where $\mathbf{y}^{e,s}$ is the equivalent static displacement computed by

$$[K]\, \mathbf{y}^{e,s} = \mathfrak{f}^{e,s} \,.$$

For observations $\mathbb{U}^2$ and $\mathbb{U}^4$, the mean values $\underline{u}^2$ and $\underline{u}^4$ are negative. Therefore, for these observations, the worst case corresponds to a minimum. For $i = 2$ or $i = 4$, let $\mathfrak{u}^{i,e,s}$ be the equivalent static observation $\mathfrak{u}^{e,s}$ associated with $\mathbb{U}^i$, which is such that $\mathfrak{u}^{i,e,s} = \underline{u}^i + u^{i,e,s}$. Let $\underline{\mathbb{U}}^i_{\min} = E\{\mathbb{U}^i_{\min}\}$ with $\mathbb{U}^i_{min} = \min_{t\in[0,\,T]} \mathbb{U}^i$. Let $\mathscr{D}^i_{\sup}$ be the upper bound of the domain associated with $\mathbb{U}^i$. The numerical values obtained for these variables are given in Table 6.2.

| Observation | $\underline{u}^i$ | $\underline{\mathbb{U}}^i_{\min}$ | $\mathfrak{u}^{i,e,s}$ | $\mathscr{D}^i_{\sup}$ |
|---|---|---|---|---|
| $\mathfrak{u}^{2,e,s} \times 10^8$ (N.m) | $-3.153$ | $-6.503$ | $-6.503$ | $-6.503$ |
| $\mathfrak{u}^{4,e,s} \times 10^8$ (N.m) | $-0.739$ | $-1.611$ | $-1.611$ | $-1.611$ |

Table 6.2: Numerical values of the variables related to $\mathfrak{u}^{2,e,s}$ and $\mathfrak{u}^{4,e,s}$.

The results presented in Table 6.2 validate the method proposed because $\mathfrak{u}^{i,e,s}$ is equal to $\underline{\mathbb{U}}^i_{\min}$ for $i = 1$ and $i = 4$. It should be noted the the optimizer finds as optimal value the mean value $\underline{\mathbb{U}}^i_{\min}$ because the input upper bound is $\mathscr{D}^i_{\sup} = \underline{\mathbb{U}}^i_{\min}$ and the probability density function for which the maximum likelihood is searched, presents its maximum for a value slightly higher than $\mathscr{D}^i_{\sup}$, due to the dissymmetry of the non-Gaussian probability density function.

### 6.6.4 Principal equivalent static forces

Using the method presented in Section 5.4.2, an algebraic basis of the equivalent static forces is constructed (principal equivalent static forces). The dimension of the algebraic basis $\{\mathfrak{e}^1, \ldots, \mathfrak{e}^{m_\mathfrak{e}}\}$ is such that $m_\mathfrak{e} \leq m_\mathfrak{f} = 4$.

### 6.6.5 Analysis of the convergence with respect to the number $\nu$ of realizations

In order to analyze the convergence of the stochastic model with respect to the number $\nu$ of realizations, four cases are considered, which correspond to $\nu = n_r = 100$ (the number of realizations used for the experimental validation) and to $\nu$ equal to 1,000, to 10,000, and to 100,000. For $i = 2$ and $i = 4$, Figures 6.13 and 6.14 show the probability density functions of $U^i$, $U^i_{\max} = \max_{t\in[0,T]} U^i(t)$, and $U^i_{\min} = \min_{t\in[0,T]} U^i(t)$ for the four values of $\nu$. Figures 6.15 and 6.16 show the convergence graphs for the means of the extreme values $\underline{U}^i_{\max}$ and $\underline{U}^i_{\min}$ as a function of $\nu$.

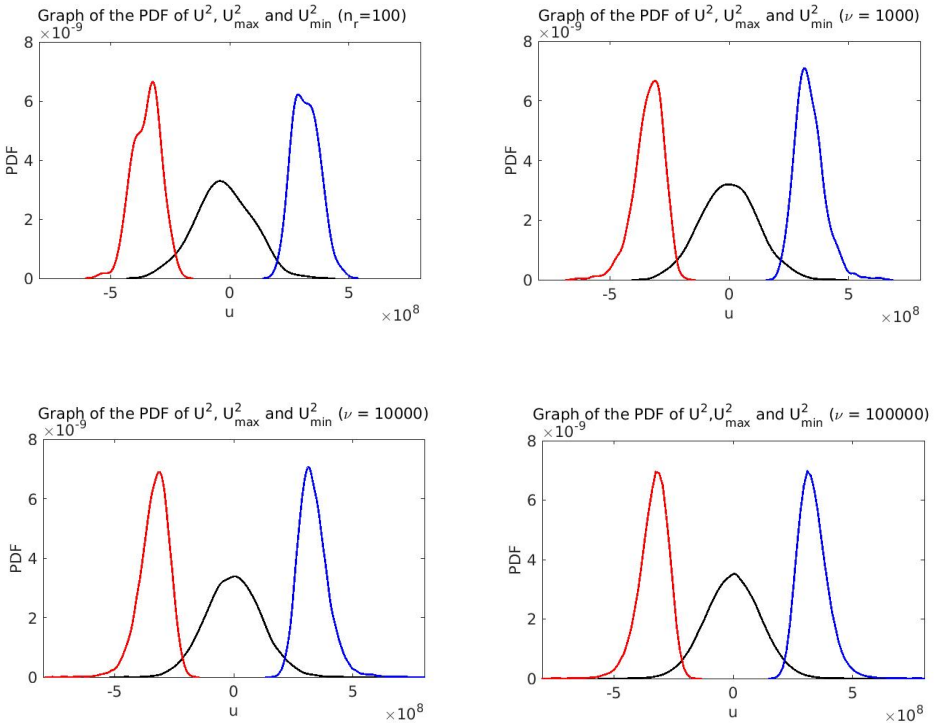


Figure 6.13: Graphs of the PDF of $U^2$ (black line, central curve), $U^2_{\max}$ (blue line, right curve) and $U^2_{\min}$ (red line, left curve) for $\nu = n_r = 100$ (upper left), $\nu = 1{,}000$ (upper right), $\nu = 10{,}000$ (lower left) and $\nu = 100{,}000$ (lower right). Horizontal axis in N m.

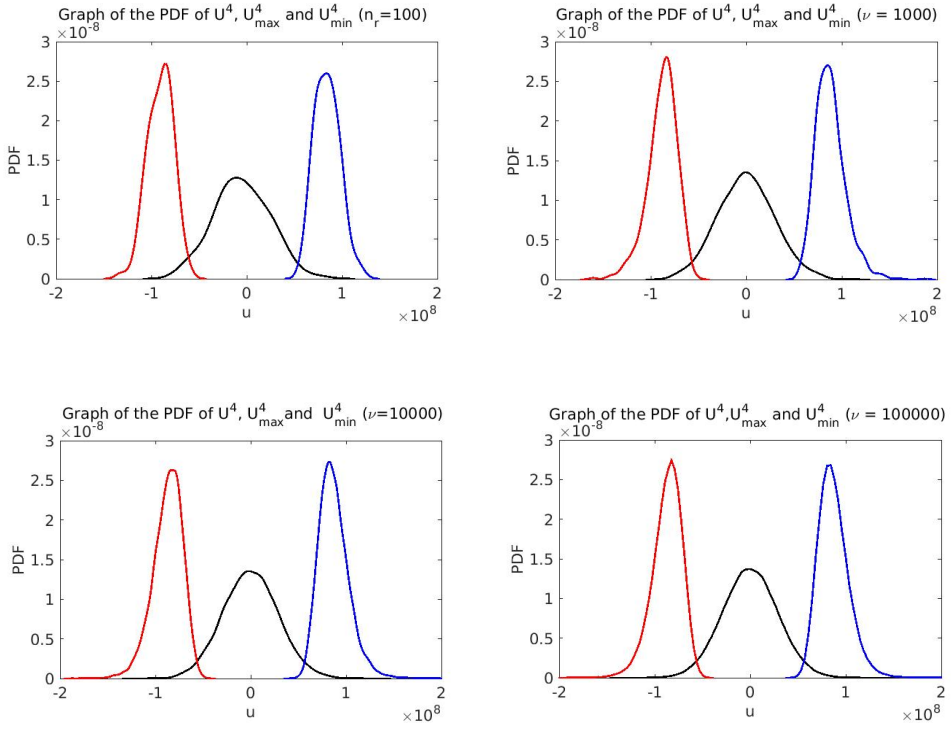


Figure 6.14: Graphs of the PDF of $U^4$ (black line, central curve), $U^4_{\max}$ (blue line, right curve) and $U^4_{\min}$ (red line, left curve) for $\nu = n_r = 100$ (upper left), $\nu = 1{,}000$ (upper right), $\nu = 10{,}000$ (lower left) and $\nu = 100{,}000$ (lower right). Horizontal axis in N m.

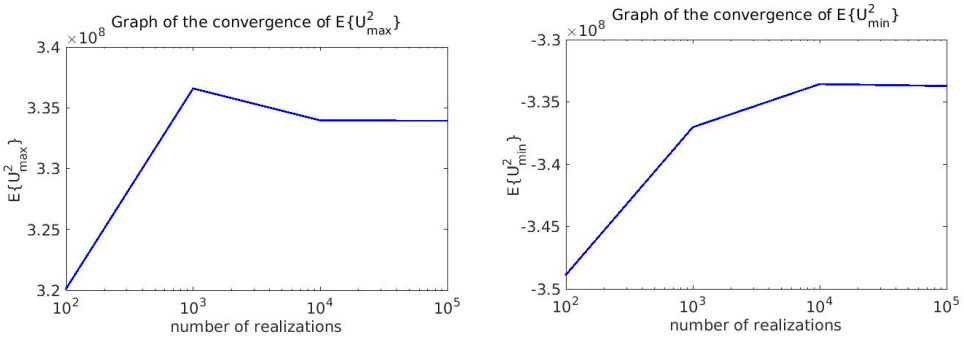


Figure 6.15: Graph of the convergence of $\underline{U}^2_{\max} = E\{U^2_{\max}\}$ (left) and of $\underline{U}^2_{\min} = E\{U^2_{\min}\}$ (right) as a function of $\nu$. Vertical axis in N m.

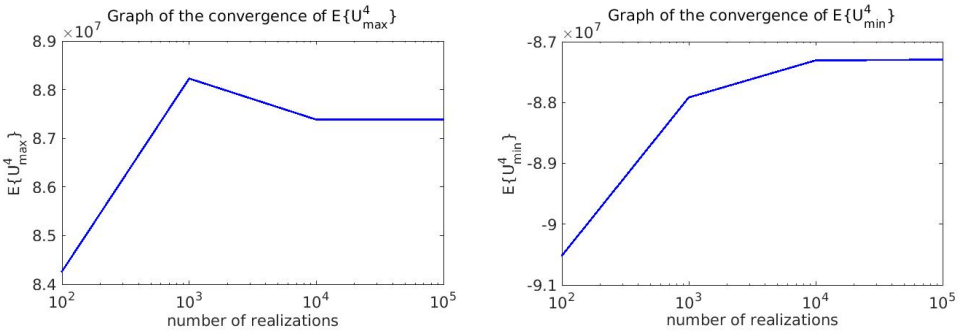


Figure 6.16: Graph of the convergence of $\underline{U}^4_{\max} = E\{U^4_{\max}\}$ (left) and of $\underline{U}^2_{\min} = E\{U^4_{\min}\}$ (right) as a function of $\nu$. Vertical axis in N m.

These figures show that the convergence is reached for $\nu = 1{,}000$. This signifies that to correctly estimate the extreme values and the probability density functions, $\nu = 1{,}000$ generated realizations are sufficient.

## 6.7 Analysis of the non-Gaussianity

For $\nu = 1{,}000$, the non-Gaussianity is performed by analyzing the gust loading factors as a function of the three models of the pressure field. The results are given in Table 6.3:

| Observation | Model 1 | | Model 2 | | | Model 3 | | |
|---|---|---|---|---|---|---|---|---|
| | $g_{\text{gauss}}$ | $g^+ \simeq g^-$ | $g_{\text{gauss}}$ | $g^+$ | $g^-$ | $g_{\text{gauss}}$ | $g^+$ | $g^-$ |
| $\mathbb{U}^1$ | 3.20 | 2.928 | 3.321 | 2.814 | 2.832 | 3.391 | 2.953 | 3.080 |
| $\mathbb{U}^2$ | 3.264 | 2.941 | 3.264 | 2.812 | 2.830 | 3.283 | 2.617 | 2.672 |
| $\mathbb{U}^3$ | 3.273 | 2.961 | 3.273 | 2.864 | 2.879 | 3.001 | 2.732 | 2.763 |
| $\mathbb{U}^4$ | 3.316 | 3.034 | 3.317 | 2.932 | 2.938 | 3.389 | 2.809 | 2.841 |

Table 6.3: Gust loading factors of $\mathbb{U}^i$ for $i = 1, 2, 3, 4$.

For the three models of the pressure field, Table 6.3 presents the gust loading factor $g_{\text{gauss}}$, computed with the Gaussian hypothesis (see Section G.2 of Appendix G), and the gust loading factors $g^+$ and $g^-$ computed with the non-Gaussian approach (see Section G.1 in Appendix G). The analysis of these results show that, even though model 1 is Gaussian, the values of $g_{\text{gauss}}$ are different from the values of $g^+ \simeq g^-$. This difference comes from the fact that the probability distribution of the extreme values defined in Section G.2 of Appendix G is an asymptotic expression based on a Poisonian distribution hypothesis of the point process of

upcrossings by high levels (level goes to infinity) (see [77] pp. 136). This expression gives an overestimation of the gust loading factor with respect to the statistical estimation of the extreme value statistics constructed from the realizations. These differences also remain for models 2 and 3 that are non-Gaussian. It should also be noted that the gust loading factors are not the same for all the observations (what was expected because the responses simultaneously depend on the quasi-static response and on the dynamic response).

# Chapter 7

# Application to a stadium structure with wind tunnel pressure measurements

The objective of this chapter is to present the estimation of the equivalent static forces on the Nice stadium in France, which is a very complex structure, for which the unsteady pressure measurements have been carried out in the boundary layer wind tunnel at CSTB in Nantes [135] and for which the finite element of the roof structure has been provided by CSTB.

## 7.1 Description of the roof structure in terms of dynamical properties

The structure is the roof of the Allianz Riviera stadium in Nice for which unsteady pressure measurements have been performed in a boundary layer wind tunnel [135]. For the wind velocity that is considered, the structure has a linear elastic behavior. The responses of this structure subjected to the wind loads are predicted by using the finite element model from CSTB. The cutoff frequency of the pressure measurements performed in the wind tunnel is $1.38$ Hz. Consequently, the reduced-order model is constructed by using all the eigenmodes whose eigenfrequencies belong to the frequency band of analysis, $[0\,,1.38]$ Hz. Therefore, the first $12$ modes of the structure, which belong to the frequency band $[0\,,1.38]$ Hz are kept. The eigenfrequencies of the first $12$ modes are, in Hz, $1.107$, $1.118$, $1.129$, $1.133$, $1.148$, $1.186$, $1.191$, $1.240$, $1.248$, $1.264$, $1.349$, and $1.360$. The $13$-th eigenfrequency is $1.416$ Hz that is outside the frequency band of analysis. However, for such a complex three-dimensional structure without any slender character, a reduced-order model that would be constructed by using only

these 12 modes would not be converged at all. This is the reason why the quasi-static acceleration terms are absolutely necessary and are taken into account in the reduced-order model. If such quasi-static acceleration terms were not taken into account, several thousands modes should be introduced for constructing the reduced-order model because there are numerous beam local modes in the roof structure. In this chapter,

- the finite element model of the structure is introduced and a set of observations are defined;
- the unsteady pressure field applied to the structure is measured in boundary layer wind tunnel;
- the method presented in the previous chapters is applied to compute the equivalent static forces associated with the set of observations.

## 7.2 Finite element model of the structure and set of observations

### 7.2.1 Finite element model of the structure

The finite element model of the Allianz Riviera stadium roof has been provided by CSTB. This FE model is given in an orthonormal reference frame $oxyz$, and corresponds to the discretization of the roof structure by using finite elements of truss and beam types, with two nodes by element. There are $3{,}656$ nodes in the FE model, with $6$ degrees of freedom per node ($3$ displacements and $3$ rotations), which yields $21{,}936$ DOFs. Figure 7.1 shows the finite element model of the roof structure.

### 7.2.2 Observations

The structure zone chosen to observe the response of the roof structure is the light blue part shown in Figure 7.1. The calculation of the equivalent static forces is performed by using $m_{\mathbb{f}} = 181$ selected observations that are internal forces in truss and beam elements. In order to limit the number of figures that will be used for presenting the results, only four observations, numbered $144$, $145$, $146$, and $147$, among the $181$ observations, have been selected. These four observations correspond to normal forces in truss elements, and consequently, each one is scalar (then $m_{u^i} = 1$) and is written $\mathbb{U}^i = \underline{u}^i + U^i$ in which $\underline{u}^i$ is the mean value. Figure 7.2 shows the geometry of the roof structure in the observed zone.

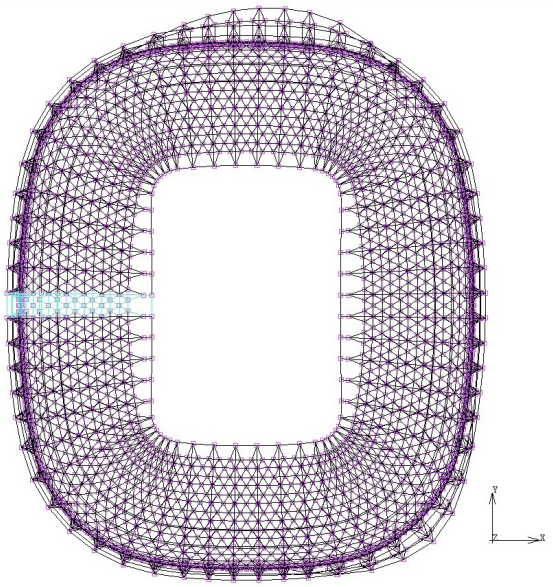

Figure 7.1: Finite element model of the roof structure (from CSTB).

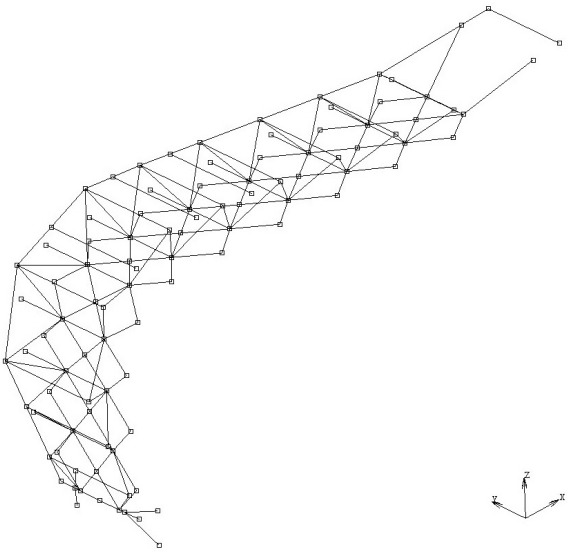

Figure 7.2: FE model of the roof structure in the structure zone chosen to observe the response.

The displacements observed in this zone are $x$- and $z$-displacements of node $1{,}415$ (see Figure 7.3 (left)), and node $3{,}571$ (see Figure 7.3 (right)).

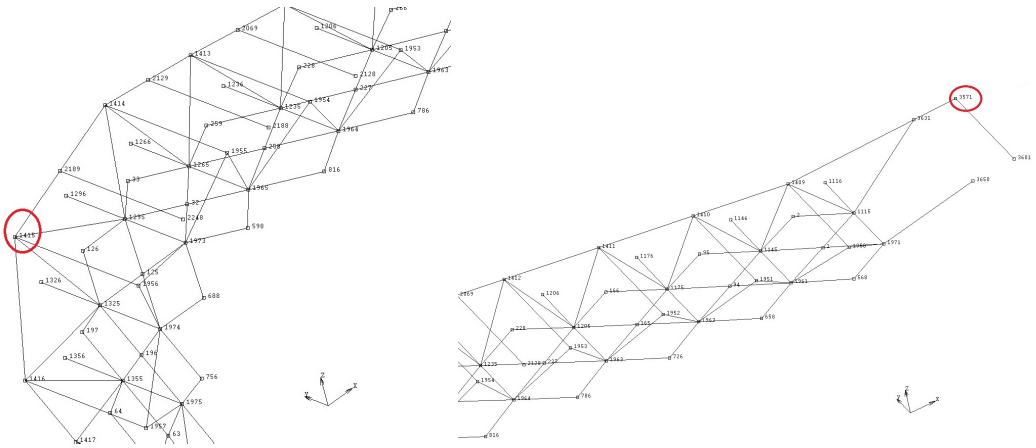

Figure 7.3: Location of node $1{,}415$ (left) and location of node $3{,}571$ (right) spotted by red circles.

## 7.3 Boundary layer wind tunnel measurements

The wind tunnel tests have been carried out by CSTB [135]. For each incident wind direction analyzed in the wind tunnel, the unsteady pressure field applied to the roof structure has been measured with $720$ pressure taps, from which $m_{\text{exp}} = 348$ differential unsteady pressures $\mathbb{P}_1^{\text{exp}}(t), \ldots, \mathbb{P}_{m_{\text{exp}}}^{\text{exp}}(t)$ between the interior and exterior locations of the roof are defined as well as the associated controlability matrix $[A_c]$. We introduce the experimental unsteady pressure vector $\mathbb{P}^{\text{exp}}(t) = (\mathbb{P}_1^{\text{exp}}(t), \ldots, \mathbb{P}_{m_{\text{exp}}}^{\text{exp}}(t))$. Only incidence $76^o$ is presented in order to limit the number of figures. The total duration, at scale $1$, of the boundary layer wind tunnel measurements is $T_{\text{tot}} \simeq 8{,}900$ s. The parameters of signal processing for the experiments are defined hereinafter.

- Cutoff frequency, $\nu_c = 1.38$ Hz.
- Sampling frequency, $\nu_e = 2.76$ Hz.
- Sampling time step, $\Delta t = 0.36$ s.
- Duration of the time window, $T = 371$ s.
- Number of independent experimental realizations, $n_r = 24$.

- Number of time steps in the time window, $n_p = 1{,}024$.

Figure 7.4 displays the model of the stadium roof in the boundary layer wind tunnel.

Figure 7.4: Model of the roof of the Allianz Riviera stadium in the boundary layer wind tunnel at CSTB in Nantes [135].

As explain in Section 3.3, we introduce the experimental centered unsteady pressure $\mathbf{P}^{\text{exp}}(t) = \mathbb{P}^{\text{exp}}(t) - \underline{\mathbf{p}}$ in which $\underline{\mathbf{p}}$ is defined by Eq. (3.11). As explain in Chapters 3 and 4, the $\mathbb{R}^{m_{\text{exp}}}$-valued stochastic process $\{\mathbf{P}(t), t \in [0\,, T]\}$ is constructed by generating $\nu > n_r$ additional realizations with the PCE that is identified with the $n_r$ experimental measurements $\{\mathbf{P}^{\text{exp}}(t;\theta_\ell), t \in [0\,, T]\}$. In order to simplify the notations, $\mathbf{P}^{\text{exp}}(t)$ is simply rewritten as $\mathbf{P}(t)$. For $j$ equal to 140, 141, 144, 146, 152, and 155, that correspond to pressure taps located in the observed zone, the graphs of the PSD functions of the experimental centered unsteady pressure $P_j$ is thus denoted by $f \mapsto S_{P_j}(2\pi f)$ and are shown in Figure 7.5. A brief analysis has been carried out to optimize the choice of the number of time steps in the time window. When $n_p$ varies from 256 to 2,048, the number of experimental realizations $n_r$ goes from 96 to 12. The compromise that has been found for choosing $n_r$ and $n_p$ has been based on the following criteria. The number of experimental realizations $n_r$ must be chosen in order to correctly estimate the coefficients of the PCE of $\{\mathbf{P}(t), t \in [0\,, T]\}$. The number of time steps $n_p$ in the time window must be chosen in order that the duration $T$ be large enough for obtaining a sufficiently stationary signal on $T$ and also for obtaining a good frequency resolution. The value $n_p = 1{,}024$ has therefore been retained, which gives $n_r = 24$. From the point of view of signal processing concerning stationarity and statistical estimates

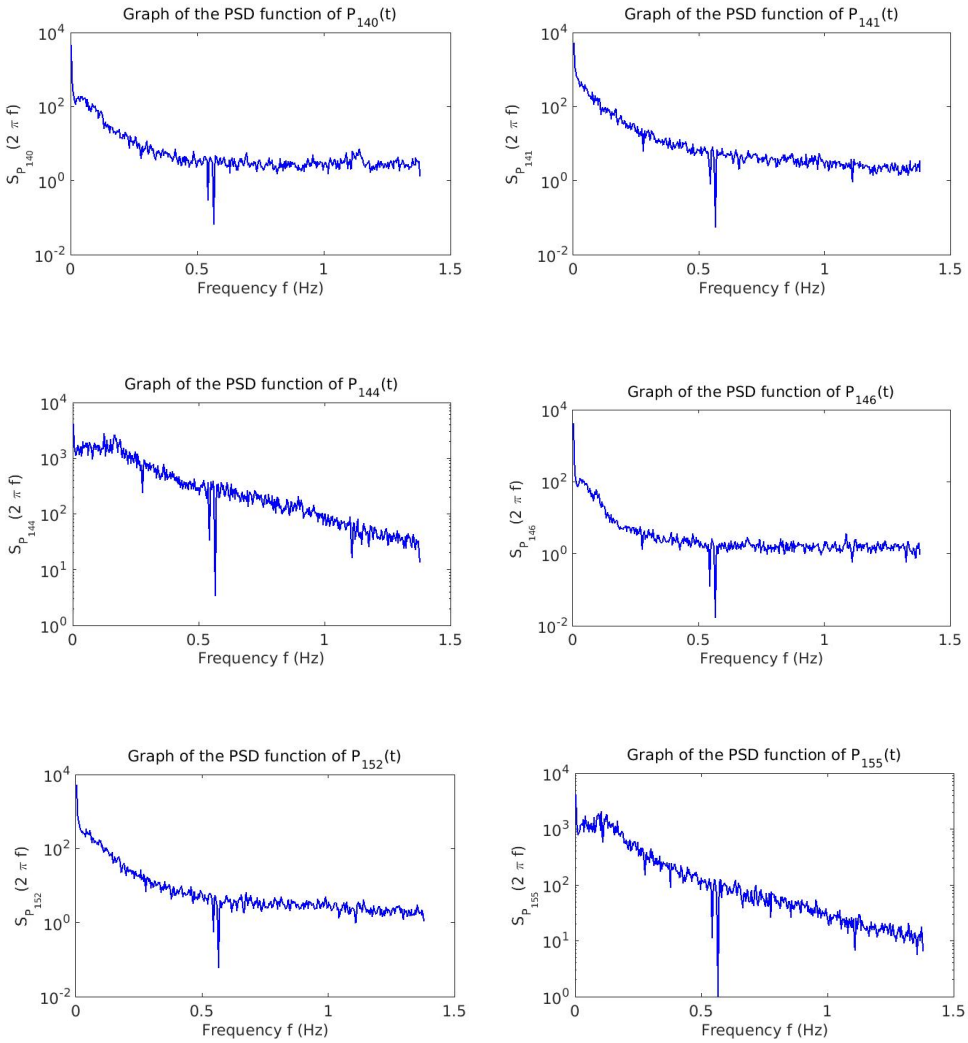


Figure 7.5: Graph of the PSD function $f \mapsto S_{P_j}(2\pi f)$ of the experimental $P_j(t)$ for $j = 140, 141, 144, 146, 152, 155$. Horizontal axis in Hz and vertical axis in $\mathrm{N}^2\ \mathrm{m}^{-4}$ s.

of extreme values, it would have been better if the experimental data basis had allow for choosing $n_p = 2{,}048$ and $n_r = 100$, what would lead us to multiplying by $8$ the time duration of wind tunnel tests.

## 7.4 Construction of the reduced-order model with the quasi-static acceleration term

As explained in Section 7.1, it is necessary to take into account the quasi-static acceleration term in the construction of the reduced-order model of the roof structure. The convergence analysis with respect to $N$ of the reduced-order model is performed by studying the graph of function $N \mapsto \|\widehat{\mathbb{h}}_N^{c,\mathrm{acc}}\|_{\mathbf{L}^2(\mathscr{B})}$ for $N = 1$ to $20$ defined by Eq. (2.32), which is plotted in Figure 7.6 (left). Figure 7.6 (right) shows the graph of function $f \mapsto \|\widehat{\mathbb{h}}_N^{c,\mathrm{acc}}(2\pi f)\|_M^2$ for $N = 12$ where $\|\widehat{\mathbb{h}}_N^{c,\mathrm{acc}}(2\pi f)\|_M^2$ is defined by Eq. (2.33). It can be seen that the convergence of the reduced-order model is reached for $N = 12$.

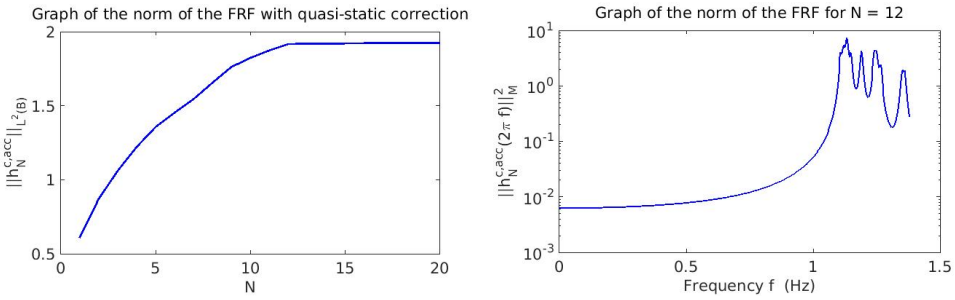


Figure 7.6: Graph of function $N \mapsto \|\widehat{\mathbb{h}}_N^{c,\mathrm{acc}}\|_{\mathbf{L}^2(\mathscr{B})}$ (left) and graph of function $f \mapsto \|\widehat{\mathbb{h}}_N^{c,\mathrm{acc}}(2\pi f)\|_M^2$ for $N = 12$ (right).

## 7.5 Generator of realizations for non-Gaussian centered process $\{\mathbf{P}(t), t \in [0,T]\}$

### 7.5.1 Statistical reduction of $\{\mathbf{P}(t), t \in [0,T]\}$

The Karhunen-Loève statistical reduction of pressure field $\{\mathbf{P}(t), t \in [0,T]\}$ is carried out with the $n_r = 24$ experimental realizations. Figure 7.7 (left) displays the square root of the eigenvalues $\mu_j$ of the eigenvalue problem defined by Eq. (4.13). Function $N_{\mathrm{KL}} \mapsto \mathrm{err}_{\mathrm{KL}}(N_{\mathrm{KL}})$ defined by Eq. (4.10) is plotted in Figure 7.7 (right). Since $n_r = 24$, the rank of the covariance operator of $\mathbf{P}$ is

24 and consequently, the eigenvalues for which their rank is larger than 24 are 0. As 24 is relatively small value, the value $N_{\text{KL}} = 24$ is retained. The $n_r$ realizations of the random vector $\mathbf{H}$ with values in $\mathbb{R}^{N_{\text{KL}}}$, whose components are defined by Eq. (4.21), are computed using the $n_r$ experimental realizations of $\{\mathbf{P}(t), t \in [0,T]\}$.

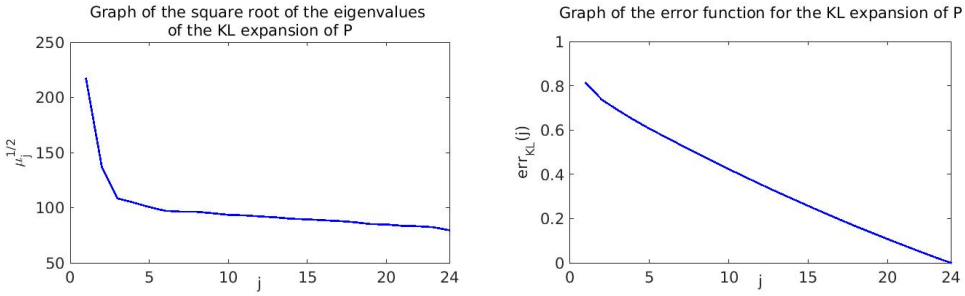


Figure 7.7: Graph of $j \mapsto \sqrt{\mu_j}$ for $j = 1, \ldots, N_{\text{KL}}$ (left) and graph of $N_{\text{KL}} \mapsto \text{err}_{\text{KL}}(N_{\text{KL}})$ related to the KL-expansion of $\{\mathbf{P}(t), t \in [0,T]\}$ (right).

### 7.5.2 Polynomial chaos expansion of random vector H

The PCE of random vector $\mathbf{H}$ is constructed by using the methodology presented in Sections 4.2 and 4.3. Figure 7.8 gives the error function $N_d \mapsto \text{err}(N_d)$ defined by Eq. (4.98) with Eq. (4.96). The convergence is reached for the degree $N_d = 4$. The coefficients of the PCE of $\mathbf{H}$ are estimated according to the method presented in Section 4.3.5.
For $\nu = 1{,}000$, the independent realizations of non-Gaussian process $\{\mathbf{P}(t),\, t \in [0,T]\}$ are generated by using the generator presented in Section 4.2.4.

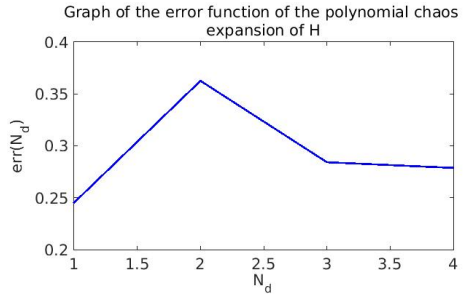


Figure 7.8: Graph of error function $N_d \mapsto \text{err}(N_d)$ of the PCE of $\mathbf{H}$.

## 7.6 Probability density functions and power spectral density functions of displacements and observations

### 7.6.1 Probability density functions of observations

For $\nu = 1000$ and for $i = 144, 145, 146, 147$, Figure 7.9 shows the PDF of $U^i$, $U^i_{\max} = \max_{t\in[0,T]} U^i(t)$, and $U^i_{\min} = \min_{t\in[0,T]} U^i(t)$. The non perfect symmetry of these PDFs is due to the non-Gaussian nature of the observations.

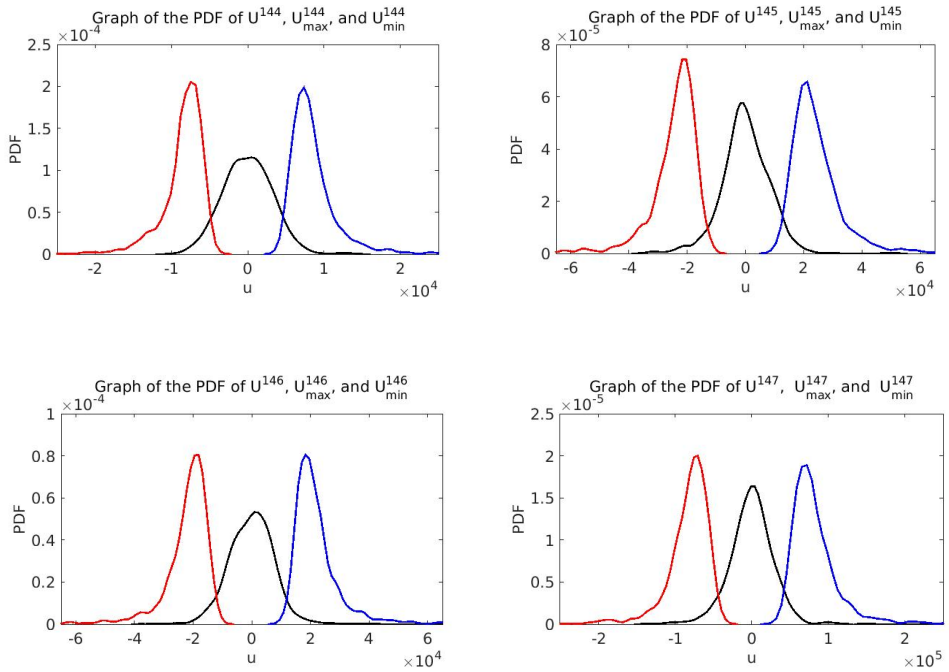


Figure 7.9: For $i = 144, 145, 146, 147$, graphs of the PDF of $U^i$ (black line, central curve), $U^i_{\max}$ (blue line, right curve), and $U^i_{\min}$ (red line, left curve). Horizontal axis in N.

### 7.6.2 Power spectral density functions of displacements and observations

For $\nu = 1{,}000$, Figure 7.10 shows the PSD functions $f \mapsto S_{X_1^{1415}}(2\pi f)$, $f \mapsto S_{X_3^{1415}}(2\pi f)$, $f \mapsto S_{X_1^{3571}}(2\pi f)$, and $f \mapsto S_{X_3^{3571}}(2\pi f)$ of the centered displacements at nodes 1415 and 3571 for DOFs 1 and 3. For $\nu = 1{,}000$ and for $i = 144, 145, 146, 147$, Figure 7.11 shows the PSD functions $f \mapsto S_{U^i}(2\pi f)$ of

centered observation $U^i$. These figures show that there is an important quasi-static contribution in the frequency band $[0\,,0.30]$ Hz.

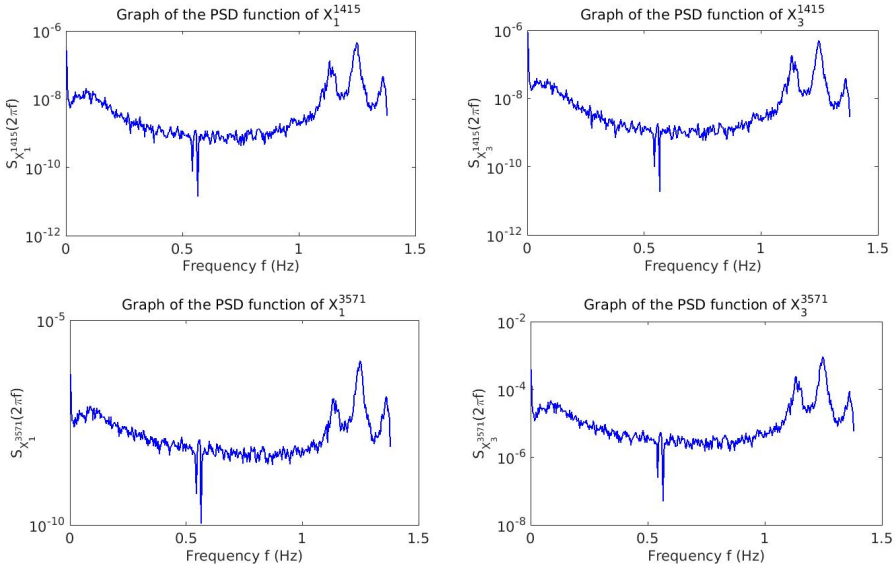


Figure 7.10: For $i = 1415, 3571$ and for $j = 1, 3$, graph of the PSD function $f \mapsto S_{X_j^i}(2\pi f)$ of displacement $X_j^i$. Horizontal axis in Hz and vertical axis in $\mathrm{m}^2$ s.

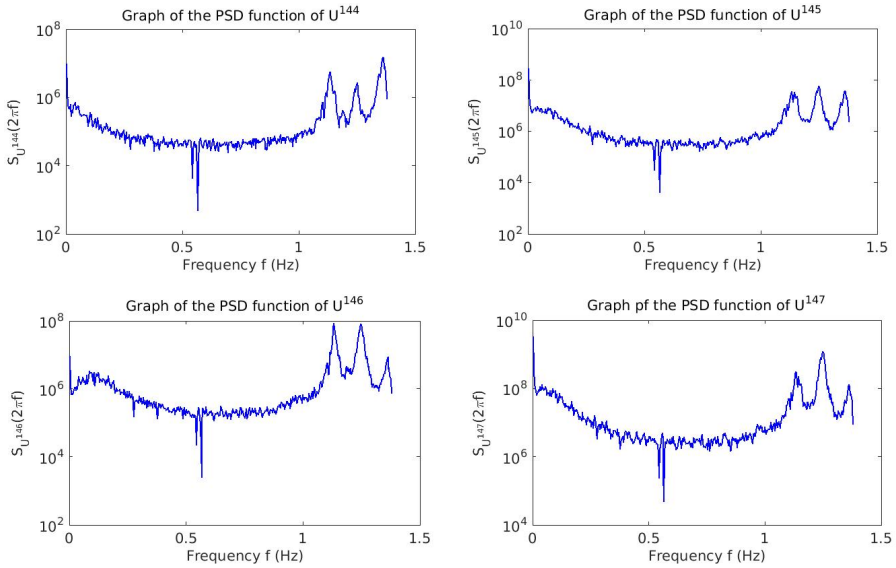


Figure 7.11: For $i = 144, 145, 146, 147$, graph of the PSD function $f \mapsto S_{U^i}(2\pi f)$ of centered observation $U^i$. Horizontal axis in Hz and vertical axis in $\mathrm{N}^2$ s.

## 7.7 Equivalent static forces

In this section, we first present the estimation of the equivalent static forces and then we present the validation of such an estimation.

### 7.7.1 Estimation of the equivalent static forces

By way of illustration, we limit the presentation of the estimation to the graphs related to the equivalent static force $\mathbf{f}^{146,e,s}$ calculated for observation $\mathbb{U}^{146}$. The 6 components (3 forces and 3 moments) of this equivalent static force are shown in Figure 7.12.

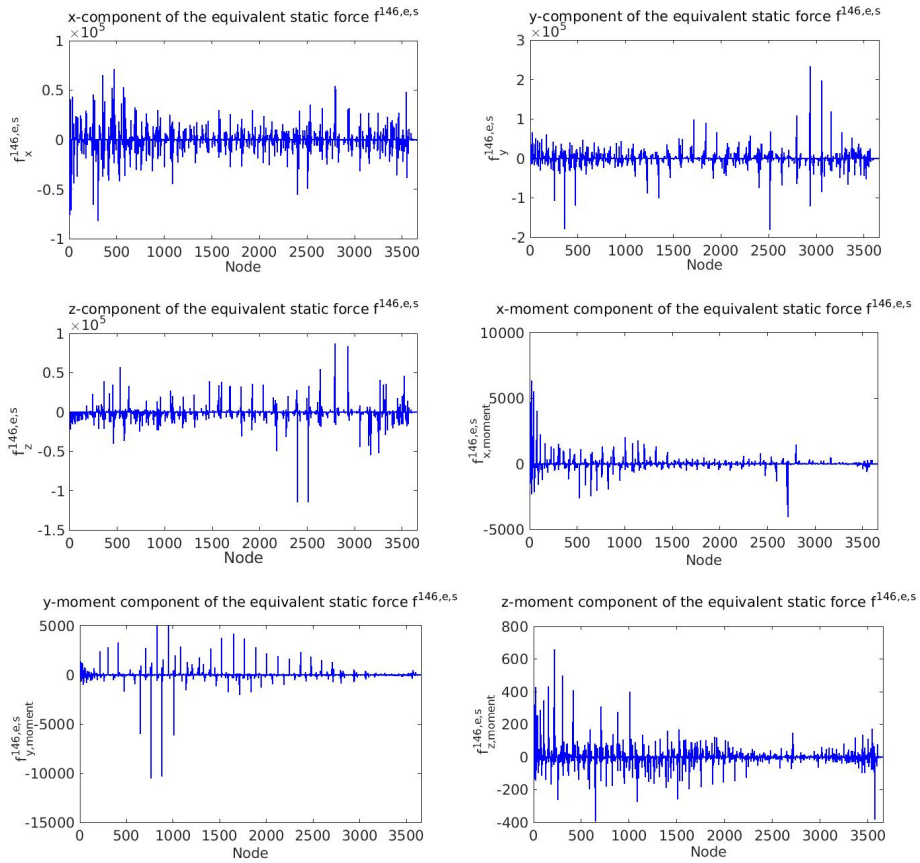


Figure 7.12: Graph of each one of the 6 components of the static equivalent force associated with observation $\mathbb{U}^{146}$ at each node of the structure mesh. Vertical axis in N for the forces and in N m for the moments.

### 7.7.2 Validation of the estimation

Following the same approach as the one presented in Section 6.6.3, the equivalent static observation are recomputed to validate the estimation of the equivalent static forces. For $i = 144, 145, 146, 147$, the mean values $\underline{u}^i$ are positive. Therefore, for these observations, the worst case corresponds to a maximum. Let $\mathbb{u}^{i,e,s}$ be the equivalent static observation $\mathbf{u}^{e,s}$ associated with $\mathbb{U}^i$, which is such that $\mathbb{u}^{i,e,s} = \underline{u}^i + u^{i,e,s}$. Let $\underline{\mathbb{U}}^i_{\max} = E\{\mathbb{U}^i_{\max}\}$ with $\mathbb{U}^i_{\max} = \max_{t\in[0\,,T]} \mathbb{U}^i(t)$. Let $\mathscr{D}^i_{\inf}$ be the lower bound of the domain associated with $\mathbb{U}^i$. The numerical values obtained are given in Table 7.1. It can be seen in Table 7.1 that $\mathbb{u}^{i,e,s}$ is effectively equal to $\underline{\mathbb{U}}^i_{\min}$ for $i = 144, 145, 146, 147$.

| Observation | $\underline{u}^i$ | $\underline{\mathbb{U}}^i_{\max}$ | $\mathscr{D}^i_{\inf}$ | $\mathbb{u}^{i,e,s}$ |
|---|---|---|---|---|
| $\mathbb{U}^{144} \times 10^4$ (N) | 0.1715 | 1.031 | 1.031 | 1.031 |
| $\mathbb{U}^{145} \times 10^4$ (N) | 0.8324 | 3.298 | 3.298 | 3.298 |
| $\mathbb{U}^{146} \times 10^4$ (N) | 0.1740 | 2.395 | 2.395 | 2.395 |
| $\mathbb{U}^{147} \times 10^4$ (N) | 0.2993 | 11.30 | 11.30 | 11.30 |

Table 7.1: Numerical values related to $\mathbb{u}^{i,e,s}$ for $i = 144, 145, 146, 147$.

### 7.7.3 Principal equivalent static forces

Using the method presented in Section 5.4.2, the algebraic basis $\{\mathbb{e}^1, \ldots, \mathbb{e}^{m_\mathbb{e}}\}$ of equivalent static forces is constructed for which the computed dimension is $m_\mathbb{e} = 37$ that is much smaller than $m_\mathbb{f} = 181$. Therefore, each one of the equivalent static force $\mathbf{f}^{e,s,i}$ can be rewritten as $\mathbf{f}^{e,s,i} = \sum_{i'=1}^{m_\mathbb{e}} f^i_{i'}\, \mathbb{e}^{i'}$. Figure 7.13 shows the $x$-, $y$-, and $z$-components of the first two principal equivalent static forces $\mathbb{e}^1$ and $\mathbb{e}^2$ at each node of the FE mesh.

## 7.8 Gust loading factors

Table 7.2 presents the gust loading factor $g_{\text{gauss}}$, computed with the Gaussian hypothesis (see Section G.2 of Appendix G), and the gust loading factors $g^+$ and $g^-$ computed with the non-Gaussian approach (see Section G.1 in Appendix G) for observation $\mathbb{U}^i$ with $i = 144, 145, 146, 147$. The values of $g_{\text{gauss}}$ are different from the values of $g^+$ and $g^-$ for the reasons given in Section 6.7. Note that the gust loading factors are not the same for all the observations (what was expected because the responses simultaneously depend on the quasi-static response and on dynamical response related to the 12 modes used in the reduced-order model).

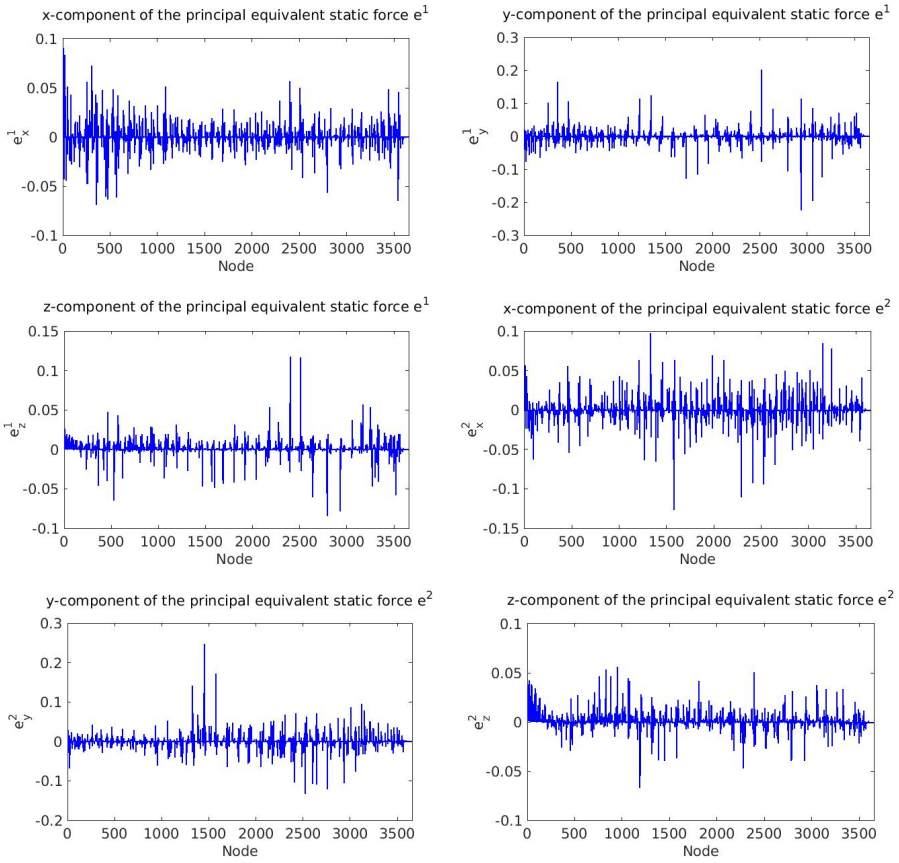


Figure 7.13: For the first two principal static equivalent forces $\mathfrak{e}^1$ and $\mathfrak{e}^2$, graph of $x$-, $y$-, and $z$-components at each node of the FE mesh.

| Observation | $g_{\text{gauss}}$ | $g^+$ | $g^-$ |
|---|---|---|---|
| $\mathbb{U}^{144}$ | 3.629 | 2.669 | 2.674 |
| $\mathbb{U}^{145}$ | 3.583 | 3.036 | 3.015 |
| $\mathbb{U}^{146}$ | 3.621 | 2.829 | 2.831 |
| $\mathbb{U}^{144}$ | 3.582 | 2.803 | 2.796 |

Table 7.2: Gust loading factors of $\mathbb{U}^i$ for $i = 144, 145, 146, 147$.

# Chapter 8

# Conclusions

## 8.1 Industrial results

- Development of a new probabilistic approach for estimating the equivalent static forces that allow for reproducing the extreme value statistics of the stochastic dynamical responses in complex structures submitted to unsteady pressure fields induced by wind, when these equivalent static forces are statically applied to structures. The pressure field induced by the wind is measured in a boundary layer wind tunnel. The method proposed avoids the use of the simplified hypotheses that are classically used in the literature.

- Development of a software written in Matlab language for computing the equivalent static wind loads in a non-Gaussian probabilistic framework for complex structures, for which the inputs are wind tunnel measurements of the unsteady pressure field and a finite element model of the structure.

- Application to a simple structure, "the Maine-Montparnasse Tower", which allows us to obtain an experimental validation of the methodology proposed and of the software developed.

- Application to a complex structure, "the roof of the Nice stadium", for which measurements have been carried out in the boundary layer wind tunnel at CSTB in Nantes.

## 8.2 Scientific results

- Development of a method that takes into account the non-Gaussianity of the unsteady pressures, that constructs an estimation of the extreme value statistics of the dynamical observations in the structure without using any

approximation, that introduces quasi-static acceleration term in order to increase the convergence rate of the reduced-order model with respect to the number of elastic modes, and that computes the static equivalent loads in a probabilistic framework by using a maximum principle of probability that allows the phases between the quantities to be kept and consequently, that avoids the use of responses envelopes.

- More precisely, the developments have consisted in

  1. constructing a generator of independent realizations of a non-Gaussian vector-valued stochastic process by using a Karhunen-Loève expansion combined with a polynomial chaos expansion that is identified by using the measurements. This vector-valued stochastic process corresponds to the spatial discretization of the unsteady pressure field applied to the structure. This generator allows for reproducing the non-Gaussianity of the unsteady pressure field and for generating a large number of independent realizations in order to be able to estimate the extreme value statistics and the probability density functions that are involved in the methodology proposed for computing the equivalent static forces.
  2. constructing a reduced-order model with a quasi-static acceleration term in time domain, which allows for accelerating the convergence of the dynamical responses with respect to retained number of the elastic modes.
  3. constructing a new probabilistic method for the computation of the equivalent static forces induced by the quasi-static and the dynamic effects of wind on structures, preserving the non-Gaussianity, not introducing the concept of a response envelope, and using a maximum principle of probability.
  4. performing an experimental validation on a simple example.
  5. demonstrating the feasibility of the proposed approach through an application to a complex structure for which unsteady pressures have been measured.

## 8.3 Perspectives

The theory and the methodology developed and presented in this thesis have a very general character but have been tested and validated only for scalar observations and with the use of a first approximation algorithm for estimating the

PCE coefficients of the non-Gaussian unsteady pressure. The thesis presents a complete mathematical development and the associated numerical methods for vector-valued observations for which their domains are separable or not. The natural perspectives for extending the work presented would therefore be:

- to test the method for vector-valued observations with a domain that can be separable or not separable.
- to test the general method that is proposed for the identification of the PCE coefficients of the non-Gaussian unsteady pressure instead of using the first approximation algorithm. For large dimensions (several tens or several hundreds of uncorrelated non-Gaussian coordinates in the Karhunen-Loève expansion of the non-Gaussian pressure field), it will then be necessary to use a partition method of the components of a non-Gaussian random vector as the union of statistically independent groups of non-Gaussian random vectors.

# Appendices

# Appendix A

# Parameterization of the domain $\mathscr{D}$ in the case of a separable domain

Domain $\mathscr{D}$ and $\mathscr{D}^c$, which are assumed to be separable, are thus written as

$$\mathscr{D} = \mathscr{D}_1 \times \ldots \times \mathscr{D}_{m_u} \quad , \quad \mathscr{D}_j = (\mathscr{D}_{\inf,j}, \mathscr{D}_{\sup,j}) \, ,$$

and

$$\mathscr{D}^c = \mathscr{D}_1^c \times \ldots \times \mathscr{D}_{m_u}^c \quad , \quad \mathscr{D}_j^c = (\mathscr{D}_{\inf,j}^c, \mathscr{D}_{\sup,j}^c) \, ,$$

with $j = 1, \ldots, m_u$. The quantities $\mathscr{D}_{\inf,j}$ and $\mathscr{D}_{\sup,j}$ are the lower and the upper bounds of $\mathscr{D}_j$, which are defined either by a given level of probability or by a direct definition. It should be noted that the definition of $\mathscr{D}_j$ by a given probability level is difficult. Indeed, for a fixed level of probability, the values of bounds depend on the number of realizations used to construct the statistical estimate of the probability density function. If this number of realizations is not sufficiently large, then the convergence is not good enough, and the values of bounds fluctuate as a function of the number of realizations. It is therefore recommended to use the direct definition defined hereinafter.

## A.1 Definition of the lower and the upper bounds by using a given level of probability

Observation $\mathbb{U}(t)$ with values in $\mathbb{R}^{m_u}$ is given by Eq. (2.42),

$$\mathbb{U}(t) = \underline{\mathbf{u}} + \mathbf{U}(t) \, ,$$

where the component $\mathbb{U}_j(t)$ with $j \in \{1, \ldots, m_u\}$ is written as

$$\mathbb{U}_j(t) = \underline{u}_j + U_j(t) \, .$$

The following notations are introduced

$$U_{\max,j} = \max_{t\in[0,T]} U_j(t) \quad , \quad \underline{U}_{\max,j} = E\{U_{\max,j}\}\,, \tag{A.1}$$

$$U_{\min,j} = \min_{t\in[0,T]} U_j(t) \quad , \quad \underline{U}_{\min,j} = E\{U_{\min,j}\}\,. \tag{A.2}$$

$$\mathbb{U}_{\max,j} = \underline{u}_j + U_{\max,j}\,, \tag{A.3}$$

$$\mathbb{U}_{\min,j} = \underline{u}_j + U_{\min,j}\,. \tag{A.4}$$

It can then be deduced that

$$E\{\mathbb{U}_{\max,j}\} = \underline{u}_j + \underline{U}_{\max,j}\,, \tag{A.5}$$

$$E\{\mathbb{U}_{\min,j}\} = \underline{u}_j + \underline{U}_{\min,j}\,. \tag{A.6}$$

Depending on the sign of $\underline{u}_j$, the following parameterization of domain $\mathscr{D}_j$ associated with $\mathbb{U}_j$ is defined as follows:

$$\text{if} \quad \underline{u}_j \geq 0 \quad , \quad \text{then} \quad \mathscr{D}_j = [E\{\mathbb{U}_{\max,j}\} + \alpha_{c,j}\sigma_{\mathbb{U}_{\max,j}}, +\infty[\,, \tag{A.7}$$

$$\text{if} \quad \underline{u}_j < 0 \quad , \quad \text{then} \quad \mathscr{D}_j = ]-\infty, E\{\mathbb{U}_{\min,j}\} - \alpha_{c,j}\sigma_{\mathbb{U}_{\min,j}}]\,, \tag{A.8}$$

in which

- $\sigma_{\mathbb{U}_{\max,j}}$ and $\sigma_{\mathbb{U}_{\min,j}}$ are the standard deviations of random vectors $\mathbb{U}_{\max,j}$ and $\mathbb{U}_{\min,j}$,
- $\alpha_{c,j}$ is a real parameter that allows for adjusting the domain, which corresponds to a level $\mathrm{Pr}_j$ of probability.

The centered domain $\mathscr{D}^c$ introduced in Section 5.1, for centered observation $\mathbf{U}(t) = (U_1(t), \ldots, U_{m_u}(t))$, is then defined as follows:

$$\text{if} \quad \underline{u}_j \geq 0 \quad , \quad \text{then} \quad \mathscr{D}_j^c = [\underline{U}_{\max,j} + \alpha_{c,j}\,\sigma_{U_{\max,j}}\,, +\infty[\,, \tag{A.9}$$

$$\text{if} \quad \underline{u}_j < 0 \quad , \quad \text{then} \quad \mathscr{D}_j^c = ]-\infty\,, \underline{U}_{\min,j} - \alpha_{c,j}\,\sigma_{U_{\min,j}}]\,, \tag{A.10}$$

in which $\underline{U}_{\max,j}$ and $\sigma_{U_{\max,j}}$ are the mean value and the standard deviation of $U_{\max,j}$, and $\underline{U}_{\min,j}$ and $\sigma_{U_{\min,j}}$ are the mean value and the standard deviation of $U_{\min,j}$. For $j = 1, \ldots, m_u$, the parameter $\alpha_{c,j}$ of centered domain $\mathscr{D}_j^c$ is computed as follows:

$$\text{si} \quad \underline{u}_j \geq 0 \quad , \quad \text{proba}\{U_j(T) > \underline{U}_{\max,j} + \alpha_{c,j}\,\sigma_{U_{\max,j}}\} \leq \mathrm{Pr}_j\,, \tag{A.11}$$

$$\text{si} \quad \underline{u}_j < 0 \quad , \quad \text{proba}\{U_j(T) \leq \underline{U}_{\min,j} - \alpha_{c,j}\,\sigma_{U_{\min,j}}\} \leq \mathrm{Pr}_j\,, \tag{A.12}$$

in which $\text{Pr}_j$ is the probability level. Practically, $\text{Pr}_j$ is given and the value of coefficient $\alpha_{c,j}$ is computed by Eq. (A.11) (or Eq. (A.12)). For information, let $U_g$ be the normalized random vector (centered and with a standard deviation equal to 1). Using $\nu$ independent realizations of $U_g$, the estimate of probability $\text{Pr} = \text{proba}\{U_g > j\,\sigma_{U_g}\}$, for $j = 1, \ldots, 4$, is given in Table A.1 (numerical values obtained with the *ksdensity* function of Matlab).

| $\nu$ | 10,000,000 | 1,000,000 | 10,000 | 5,000 | 2,000 | 1,000 | 200 |
|---|---|---|---|---|---|---|---|
| $\text{Pr}(j=1)$ | 0.1587 | 0.1595 | 0.1677 | 0.1613 | 0.1564 | 0.1677 | 0.2179 |
| $\text{Pr}(j=2)$ | 0.0229 | 0.0231 | 0.0276 | 0.0239 | 0.0211 | 0.0276 | 0.0410 |
| $\text{Pr}(j=3)$ | 0.0014 | 0.0014 | 0.0013 | 0.0018 | 0.0026 | 0.0026 | 0.0046 |
| $\text{Pr}(j=4) \times 10^{-05}$ | 3.13 | 4.58 | 0.706 | 12.3 | 3.53 | 19.6 | 13.3 |

Table A.1: For $j = 1, \ldots, 4$, $\text{Pr} = \text{proba}\{U_g > j\,\sigma_{U_g}\}$ as a function of $\nu$.

## A.2 Direct definition of the lower and the upper bounds using the statistical mean of the maximum and the minimum

For $j = 1, \ldots, m_u$ and considering the sign of $\underline{u}_j$, the values of the lower and the upper bounds of the centered domain, $\mathscr{D}^c_{\text{inf},j}$ and $\mathscr{D}^c_{\text{sup},j}$, are defined as follows:

$$\text{if} \quad \underline{u}_j \geq 0 \quad , \quad \text{then} \quad \mathscr{D}^c_{\text{inf},j} = \underline{U}_{\text{max},j} \quad , \quad \mathscr{D}^c_{\text{sup},j} = \alpha\,\underline{U}_{\text{max},j}\,, \tag{A.13}$$

$$\text{if} \quad \underline{u}_j < 0 \quad , \quad \text{then} \quad \mathscr{D}^c_{\text{inf},j} = \alpha\,\underline{U}_{\text{min},j} \quad , \quad \mathscr{D}^c_{\text{sup},j} = \underline{U}_{\text{min},j}\,, \tag{A.14}$$

in which $\underline{U}_{\text{max},j}$ is the mean value of $U_{\text{max},j}$, $\underline{U}_{\text{min},j}$ is the mean value of $U_{\text{min},j}$, and where $\alpha$ is a given positive constant (for instance $\alpha = 1{,}000$).

# Appendix B

# Numerical aspects for the convergence analysis of the reduced-order model with respect to its dimension

In this appendix, we present a numerical analysis for computing $\|\widehat{\mathbb{h}}_N^{c,\text{acc}}\|_{\mathbf{L}^2(\mathscr{B})}$ defined by Eq. (2.32) in Chapter 2,

$$\|\widehat{\mathbb{h}}_N^{c,\text{acc}}\|_{\mathbf{L}^2(\mathscr{B})} = \sqrt{\int_{\mathscr{B}} \|\widehat{\mathbb{h}}_N^{c,\text{acc}}(\omega)\|_M^2 d\omega}\,, \tag{B.1}$$

in which

$$\|\widehat{\mathbb{h}}_N^{c,\text{acc}}(\omega)\|_M^2 = \text{tr}\{[\widehat{\mathbb{h}}_N^{c,\text{acc}}(\omega)]^* \, [M] \, [\widehat{\mathbb{h}}_N^{c,\text{acc}}(\omega)]\}\,, \tag{B.2}$$

which avoids the explicit construction of the full matrix $[\widehat{\mathbb{h}}_N^{c,\text{acc}}(\omega)]$ that is defined (see Eq. (2.31)) by

$$[\widehat{\mathbb{h}}_N^{c,\text{acc}}(\omega)] = [K]^{-1}\,[A_c] + \{[\varphi_N]\,[\widehat{h}_N(\omega)]\,[\phi_N^c] - [\varphi_N]\,[\widehat{h}_N(0)]\,[\phi_N^c]\}\,. \tag{B.3}$$

Matrix $[\widehat{\mathbb{h}}_N^{c,\text{acc}}(\omega)]$ is computed by

$$[\widehat{\mathbb{h}}_N^{c,\text{acc}}(\omega)] = [A_1] + [\varphi_N]([\widehat{h}_N(\omega)] - [\widehat{h}_N(0)])[\phi_N^c]\,, \tag{B.4}$$

in which the matrix $[A_1]$, which belongs to $\mathbb{M}_{m,m_{\text{exp}}}(\mathbb{R})$, is the solution of the matrix equation, $[K]\,[A_1] = [A_c]$.

# Appendix C

# Direct and inverse fast Fourier transform

The Fourier transform $\widehat{f}(\omega)$ of a scalar-valued function $f(t)$ is defined by

$$\widehat{f}(\omega) = \int_{\mathbb{R}} e^{-i\omega t}\, f(t)\, dt\,. \tag{C.1}$$

If the support of function $f$ is the closed interval $[0\,, T]$, Eq. (C.1) is rewritten as

$$\widehat{f}(\omega) = \int_{0}^{T} e^{-i\omega t}\, f(t)\, dt\,, \tag{C.2}$$

The Fourier transform defined by Eq. (C.2) is discretized by using the sampling parameters defined in Chapter 3, which yields

$$\widehat{f}_{\widetilde{q}} = \Delta t \sum_{\widetilde{k}=0}^{n_p-1} e^{-i(\omega_c+(\widetilde{q}+\frac{1}{2})\Delta\omega)\{t_1+\widetilde{k}\Delta t\}}\, f_{\widetilde{k}}\,, \tag{C.3}$$

in which $\widetilde{k} = k - 1$, where $\widetilde{q} = q - 1$, where $f_{\widetilde{k}} = f(t_{\widetilde{k}} + 1)$, and where $f(\omega_{\widetilde{q}} + 1) = f_{\widetilde{q}}$. Equation (C.3) is computed by using the fast Fourier transform,

$$\widehat{f}_{\widetilde{q}} = \sum_{\widetilde{k}=0}^{n_p-1} e^{-\frac{2i\pi}{n_p}\widetilde{q}\widetilde{k}}\, \widetilde{f}_{\widetilde{k}} \quad , \quad \widetilde{f}_{\widetilde{k}} = \Delta t\, e^{-i(-\pi+\frac{\pi}{n_p})\widetilde{k}} f_{\widetilde{k}}\,, \tag{C.4}$$

for which the inverse fast Fourier transform is given by

$$f_{\widetilde{k}} = \frac{\Delta\omega}{2\pi} e^{i(-\pi+\frac{\pi}{n_p})\widetilde{k}}\, \widetilde{f}_{\widetilde{k}} \quad , \quad \widetilde{f}_{\widetilde{k}} = \sum_{\widetilde{q}=0}^{n_p} e^{\frac{2i\pi}{n_p}\widetilde{q}\widetilde{k}}\, \widehat{f}_{\widetilde{q}}\,. \tag{C.5}$$

# Appendix D

# Construction of the initial point of the optimization problems defined in Chapter 5

Two methods are proposed for constructing the initial point related to the optimization problem, each one can be used for the case without quasi-static acceleration term or with quasi-static acceleration term:

- initialization by using the extreme value statistics corresponding to the non-Gaussian case.
- initialization by using the Gaussian approximation.

It is recommended to use the first method for which the numerical experiments that have been done show that it is more efficient.

## D.1 Initialization by using the extreme value statistics corresponding to the non-Gaussian case

Let $\mathbf{Z}$ be the $\mathbb{R}^n$-valued random variable with $n = m_w + m_u$, which is defined as follows

$$\mathbf{Z} = (\mathbf{W}, \mathbf{U}(T)) , \tag{D.1}$$

in which $\mathbf{W}$ is the $\mathbb{R}^{m_w}$-valued random variable defined hereinafter.

1. If the quasi-static acceleration term is not taken into account, then

   $$\mathbf{Z} = (\mathbf{Q}(T), \mathbf{U}(T)) ,$$

   with $n = N + m_u$. Consequently, $\mathbf{W} = \mathbf{Q}(T)$ and $m_w = N$.

2. If the quasi-static acceleration term is taken into account, then

$$\mathbf{Z} = (\mathbf{H}, \mathbf{Q}(T), \mathbf{U}(T)) \,,$$

with $n = N_{\text{PCA}} + N + m_u$. Consequently, $\mathbf{W} = (\mathbf{H}, \mathbf{Q}(T))$ and $m_w = N_{\text{PCA}} + N$.

In the following, we consider $\mathbf{Z} = (\mathbf{W}, \mathbf{U}(T))$ with values in $\mathbb{R}^n$ such that $n = m_w + m_u$. The correlation matrix of $\mathbf{Z}$, denoted by $[r_{\mathbf{Z}}] \in \mathbb{M}_n(\mathbb{R})$, is written as,

$$[r_{\mathbf{Z}}]_{jk} = \frac{E\{(Z_j - \underline{z}_j)\,(Z_k - \underline{z}_k)\}}{\sigma_{Z_j}\,\sigma_{Z_k}} = \frac{[C_{\mathbf{Z}}]_{jk}}{\sigma_{Z_j}\,\sigma_{Z_k}} \,, \tag{D.2}$$

in which

$$\sigma_{Z_j}^2 = E\{(Z_j - \underline{z}_j)^2\} = [C_{\mathbf{Z}}]_{jj} > 0 \,, \tag{D.3}$$

where $[C_{\mathbf{Z}}] \in \mathbb{M}_n(\mathbb{R})$ is the covariance matrix of $\mathbf{Z}$. The matrix representation of Eq. (D.2) is

$$[C_{\mathbf{Z}}] = [\sigma]\,[r_{\mathbf{Z}}]\,[\sigma] \,, \tag{D.4}$$

in which $[\sigma]$ is the diagonal matrix in $\mathbb{M}_n(\mathbb{R})$ such that

$$[\sigma]_{jk} = \delta_{jk}\,\sigma_{Z_j} \,. \tag{D.5}$$

Let $\{\mathbf{z}^\ell = (\mathbf{w}^\ell, \mathbf{u}^\ell), \ell = 1, \ldots, \nu\}$ be the $\nu$ independent realizations of $\mathbf{Z}$. For constructing the initial point, we need to calculate the PCA of $\mathbf{Z}$ and consequently, to solve the eigenvalue problem related to covariance matrix $[C_{\mathbf{Z}}]$. However, the numerical values of the realizations of the components of $\mathbf{W}$ can be very different from the one of the components of $\mathbf{U}(T)$ (for instance several magnitude orders). We thus introduce a numerical scaling consisting in solving the eigenvalue problem related to correlation matrix $[r_{\mathbf{Z}}]$ instead of covariance matrix $[C_{\mathbf{Z}}]$,

$$[r_{\mathbf{Z}}]\widetilde{\Psi}^\alpha = \mu_\alpha \widetilde{\Psi}^\alpha \,. \tag{D.6}$$

The eigenvectors are orthonormal,

$$< \widetilde{\mathbf{\Psi}}^\alpha, \widetilde{\mathbf{\Psi}}^\beta >= \delta_{\alpha\beta} \,, \tag{D.7}$$

and the eigenvalues are such that $\mu_1 \geq \mu_2 \geq \ldots \geq \mu_n$. If $m_u \leq N$, it can be verified that at least $m_u$ eigenvalues are strictly positive. If $m_u > N$, the number of strictly positive eigenvalues can be less than $N$. This situation, which should not happen, would correspond to an observability matrix of $\mathbf{U}(T)$, which would have at least two rows that would be proportional. Let $[\widetilde{\mathbf{\Psi}}] = [\widetilde{\mathbf{\Psi}}^1 \ldots \widetilde{\mathbf{\Psi}}^n]$ be the

matrix in $\mathbb{M}_n(\mathbb{R})$ of the eigenvectors, which is such that $[\widetilde{\mathbf{\Psi}}]\,[\widetilde{\mathbf{\Psi}}]^T = [\widetilde{\mathbf{\Psi}}]^T\,[\widetilde{\mathbf{\Psi}}] = [I_n]$. Matrix $[r_{\mathbf{Z}}]$ can be rewritten as,

$$[r_{\mathbf{Z}}] = \sum_{\alpha=1}^{n} \mu_\alpha \widetilde{\mathbf{\Psi}}^\alpha\, \widetilde{\mathbf{\Psi}}^{\alpha T}\,. \tag{D.8}$$

Substituting Eq. (D.8) in Eq. (D.4) yields

$$[C_{\mathbf{Z}}] = \sum_{\alpha=1}^{n} \mu_\alpha \mathbf{\Psi}^\alpha\, \mathbf{\Psi}^{\alpha T}\,, \tag{D.9}$$

with

$$\mathbf{\Psi}^\alpha = [\sigma]\,\widetilde{\mathbf{\Psi}}^\alpha \in \mathbb{R}^n\,. \tag{D.10}$$

It should be noted that $\{\mathbf{\Psi}^\alpha\}_\alpha$ is a basis of $\mathbb{R}^n$ but is not orthonormal for the usual Euclidean inner product of $\mathbb{R}^n$. Otherwise, we have

$$< [\sigma]^{-2}\mathbf{\Psi}^\alpha, \mathbf{\Psi}^\beta >= \delta_{\alpha\beta}\,. \tag{D.11}$$

The PCA of $\mathbb{R}^n$-valued random variable $\mathbf{Z}$ that can be written as

$$\mathbf{Z} = \underline{\mathbf{z}} + \sum_{\alpha=1}^{n} \zeta_\alpha \sqrt{\mu_\alpha}\mathbf{\Psi}^\alpha\,, \tag{D.12}$$

where $\zeta_1, \ldots, \zeta_n$ are the uncorrelated centered random variables ($E\{\zeta_\alpha\} = 0$) with unit variances ($E\{\zeta_\alpha\,\zeta_\beta\} = \delta_{\alpha\beta}$). For $\alpha = 1, \ldots, n$, we have

$$\zeta_\alpha = \frac{1}{\sqrt{\mu_\alpha}} < [\sigma]^{-2}(\mathbf{Z} - \mathbf{z}), \mathbf{\Psi}^\alpha > \,. \tag{D.13}$$

For a question of inversibility, which will appear later, the approximation $\mathbf{Z}^{(m_u)}$ of $\mathbf{Z}$ is introduced such that

$$\mathbf{Z}^{(m_u)} = \underline{\mathbf{z}} + \sum_{\alpha=1}^{m_u} \zeta_\alpha \sqrt{\mu_\alpha}\mathbf{\Psi}^\alpha\,. \tag{D.14}$$

By introducing the decomposition $\mathbf{Z}^{(m_u)} = (\mathbf{W}^{(m_u)}, \mathbf{U}^{(m_u)}(T))$, the $\mathbb{R}^{m_w}$-valued random variable $\mathbf{W}^{(m_u)}$ can be written as,

$$\mathbf{W}^{(m_u)} = \mathbf{m}_{\mathbf{W}} + \sum_{\alpha=1}^{m_u} \zeta_\alpha \sqrt{\mu_\alpha}\mathbf{\Psi}^\alpha_{\mathbf{W}}\,, \tag{D.15}$$

and the $\mathbb{R}^{m_u}$-valued random variable $\mathbf{U}^{(m_u)}(T)$ can be written as,

$$\mathbf{U}^{(m_u)}(T) = \mathbf{m}_{\mathbf{U}(T)} + \sum_{\alpha=1}^{m_u} \zeta_\alpha \sqrt{\mu_\alpha}\mathbf{\Psi}^\alpha_{\mathbf{U}(T)}\,. \tag{D.16}$$

By identification, it can be seen that the vector $\mathbf{m}_{\mathbf{W}}$ in $\mathbb{R}^{m_w}$ and the vector $\mathbf{m}_{\mathbf{U}(T)}$ in $\mathbb{R}^{m_u}$ are such that

$$\underline{\mathbf{z}} = (\mathbf{m}_{\mathbf{W}}, \mathbf{m}_{\mathbf{U}(T)}) \in \mathbb{R}^n = \mathbb{R}^{m_w} \times \mathbb{R}^{m_u}\,, \tag{D.17}$$

and the vector $\mathbf{\Psi}^{\alpha}_{\mathbf{W}}$ in $\mathbb{R}^{m_w}$ and the vector $\mathbf{\Psi}^{\alpha}_{\mathbf{U}(T)}$ in $\mathbb{R}^{m_u}$ are such that

$$\mathbf{\Psi}^{\alpha} = (\mathbf{\Psi}^{\alpha}_{\mathbf{W}}, \mathbf{\Psi}^{\alpha}_{\mathbf{U}(T)})\,. \tag{D.18}$$

Let $[\Phi_{\mathbf{W}}]$ and $[\Phi_{\mathbf{U}(T)}]$ be the matrices in $\mathbb{M}_{m_w,m_u}(\mathbb{R})$ and $\mathbb{M}_{m_u}(\mathbb{R})$ such that

$$[\Phi_{\mathbf{W}}] = [\mathbf{\Psi}^1_{\mathbf{W}} \dots \mathbf{\Psi}^{m_u}_{\mathbf{W}}] \quad , \quad [\Phi_{\mathbf{U}(T)}] = [\mathbf{\Psi}^1_{\mathbf{U}(T)} \dots \Psi^{m_u}_{\mathbf{U}(T)}]\,. \tag{D.19}$$

Equation (D.16) can be rewritten as

$$\mathbf{U}^{(m_u)}(T) = \mathbf{m}_{\mathbf{U}(T)} + [\Phi_{\mathbf{U}(T)}]\,[\,\mu\,]^{1/2}\,\boldsymbol{\zeta}\,, \tag{D.20}$$

in which $[\,\mu\,]$ is the diagonal matrix in $\mathbb{M}_{m_u}(\mathbb{R})$ such that $[\,\mu\,]_{\alpha\beta} = \mu_\alpha\,\delta_{\alpha\beta}$ and where $\boldsymbol{\zeta} = (\zeta_1, \dots, \zeta_{m_u})$ is a centered $\mathbb{R}^{m_u}$-valued random variable such that $E\{\boldsymbol{\zeta}\,\boldsymbol{\zeta}^T\} = [I_{m_u}]$.

Let $\mathbf{u}^0$ be the vector given in $\mathbb{R}^{m_u}$ (which will be constructed in Sections D.1.1 and D.1.2). Taking into account Eq. (D.20), the deterministic vector $\mathbf{z}^0$ in $\mathbb{R}^{m_u}$ is the solution of the following optimization problem,

$$\mathbf{z}^0 = \min_{\mathbf{z}\in\mathbb{R}^{m_u}} \|\mathbf{u}^0 - \mathbf{m}_{\mathbf{U}(T)} - [\Phi_{\mathbf{U}(T)}]\,[\mu]^{1/2}\,\mathbf{z}\|^2\,. \tag{D.21}$$

As $\{\mathbf{\Psi}^{\alpha}\}_{\alpha}$ is a basis of the space $\mathbb{R}^n$, this implies that $[\Phi_{\mathbf{U}(T)}]$ is an invertible matrix. Then the square matrix $[\Phi_{\mathbf{U}(T)}]\,[\,\mu\,]^{1/2}$ is invertible. The problem defined by Eq. (D.21) is then equivalent to solve the linear equation in $\mathbf{z}$,

$$[\Phi_{\mathbf{U}(T)}]\,[\,\mu\,]^{1/2}\,\mathbf{z} = \mathbf{u}^0 - \mathbf{m}_{\mathbf{U}(T)}\,, \tag{D.22}$$

which has a unique solution $\mathbf{z}^0$. We formally write,

$$\mathbf{z}^0 = ([\Phi_{\mathbf{U}(T)}]\,[\,\mu\,]^{1/2})^{-1}\,(\mathbf{u}^0 - \mathbf{m}_{\mathbf{U}(T)})\,. \tag{D.23}$$

Eq. (D.15) is rewritten as,

$$\mathbf{W}^{(m_u)} = \mathbf{m}_{\mathbf{W}} + [\Phi_{\mathbf{W}}]\,[\,\mu\,]^{1/2}\,\boldsymbol{\zeta}\,. \tag{D.24}$$

The initial value $\mathbf{w}^0 \in \mathbb{R}^{m_w}$ is defined by

$$\mathbf{w}^0 = \mathbf{m}_{\mathbf{W}} + [\Phi_{\mathbf{W}}]\,[\,\mu\,]^{1/2}\,\mathbf{z}^0\,, \tag{D.25}$$

in which $\mathbf{z}^0$ is defined by Eq. (D.23).

### D.1.1 Construction of $\mathbf{u}^0$ in $\mathbb{R}^{m_u}$: First method

For $j = 1, \ldots, m_u$, let $\boldsymbol{\ell}_0$ be the vector in $\mathbb{R}^{m_u}$ defined as follows:

$$\text{if} \quad \underline{u}_j \geq 0 \quad , \quad \text{then} \quad \ell_{0,j} = \arg\{\max_{\ell \in \{1,\ldots,n_r\}} U_j(T;\theta_\ell)\}\,, \tag{D.26}$$

$$\text{if} \quad \underline{u}_j < 0 \quad , \quad \text{then} \quad \ell_{0,j} = \arg\{\min_{\ell \in \{1,\ldots,n_r\}} U_j(T;\theta_\ell)\}\,. \tag{D.27}$$

For $j = 1, \ldots, m_u$, let $\mathbf{r}_0$ be the vector in $\mathbb{R}^{m_u}$ defined by

$$r_{0,j} = U_j(T;\theta_{\ell_{0,j}})\,. \tag{D.28}$$

Let $j_0$ be such that

$$j_0 = \arg\{\max_{j \in \{1,\ldots,m_u\}} |r_{0,j}|\}\,. \tag{D.29}$$

Consequently, $\mathbf{u}_0$ in $\mathbb{R}^{m_u}$ is given by

$$\mathbf{u}_0 = \mathbf{U}(T;\theta_{\ell_0}) \quad , \quad \ell_0 = \ell_{0,j_0}\,. \tag{D.30}$$

### D.1.2 Construction of $\mathbf{u}^0$ in $\mathbb{R}^{m_u}$: Second method

For $j = 1, \ldots, m_u$, vector $\mathbf{u}_0$ in $\mathbb{R}^{m_u}$ is defined as follows

$$\text{if} \quad \underline{u}_j \geq 0 \quad , \quad \text{then} \quad u_{0,j} = \underline{U}_{\max,j}\,, \tag{D.31}$$

$$\text{if} \quad \underline{u}_j < 0 \quad , \quad \text{then} \quad u_{0,j} = \underline{U}_{\min,j}\,. \tag{D.32}$$

It should be noted that the second method must preferably be used instead of the first one when the lower and the upper bounds of the domain associated with observation $\mathbf{U}$ are defined by the method described in Section A.2 of Appendix A.

## D.2 Initialization by using the Gaussian approximation

For constructing the initial point corresponding to the Gaussian approximation and in order to keep the same algorithm for the Gaussian case with the non-Gaussian one, we need to generate $\nu_{\text{sim}}^{\text{gauss}}$ independent realizations $\mathbb{P}_{\text{gauss}}^{\ell'}$ defined by Eq. (4.23) using Eqs. (4.2) and (4.17) adapted to the Gaussian case. Taking $N_d = 1$, the normalized Hermite polynomial $\Psi_1(\Xi) = \Xi$ represents the normalized Gaussian random variable. Therefore, random vector $\mathbf{H}$ used in Eq. (4.2), for which the components $\{H_j\}_{j=1,\ldots,N_{\text{KL}}}$ are given by Eq. (4.84), is a Gaussian vector. Using the method proposed in Section 4.3, the $\nu_{\text{sim}}^{\text{gauss}}$ independent realizations $\widetilde{\eta}_j^{\ell'}$

of $H_j$ that we have to generate for $j \in \{1, \ldots, N_{\text{KL}}\}$ and for $\ell' \in \{1, \ldots, \nu_{\text{sim}}^{\text{gauss}}\}$, are computed by

$$\widetilde{\eta}_j^{\ell'} = \psi_1(\Xi_j(\theta'_\ell)) \,. \tag{D.33}$$

The corresponding realizations, $\{\mathbb{P}_{\text{gauss}}^{\ell'}\}_{\ell'=1,\ldots,\nu_{\text{sim}}^{\text{gauss}}}$, are thus computed by

$$\mathbb{P}_{\text{gauss}}^{\ell'} = \sum_{j=1}^{N_{\text{KL}}} \sqrt{\mu_j}\, \widetilde{\eta}_j^{\ell'}\, \mathbb{b}^j \,, \tag{D.34}$$

where $\mu_j$ and $\mathbb{b}^j$ are given by Eqs. (4.28) to (4.32). The independent realizations of the Gaussian generalized coordinates $\mathbf{Q}_{\text{gauss}}(t)$ are computed using the method described in Section 3.4.2.

### D.2.1 Case without quasi-static acceleration term

Using Eq. (5.8), the vector of the Gaussian observation $\mathbf{U}_{\text{gauss}}(T)$ is written as

$$\mathbf{U}_{\text{gauss}}(T) = [\phi_N^o]\, \mathbf{Q}_{\text{gauss}}(T) \,, \tag{D.35}$$

in which $[\phi_N^o]$ is defined by Eq. (2.40). The initial point $\mathbf{q}^0 \in \mathbb{R}^N$ for the problem defined by Eq. (5.11) is the solution of the optimization problem related to a Gaussian joint probability density function,

$$\mathbf{q}^0 = \arg\{\max_{\mathbf{q}\in\mathbb{R}^N} \int_{\mathscr{D}^c} p_{\mathbf{Q}_{\text{gauss}}(T),\mathbf{U}_{\text{gauss}}(T)}(\mathbf{q},\mathbf{u})\, d\mathbf{u}\} \,. \tag{D.36}$$

### D.2.2 Case with quasi-static acceleration term

Using Eq. (5.20), the Gaussian observation vector $\mathbf{U}_{\text{gauss}}(T)$ is written as

$$\mathbf{U}_{\text{gauss}}(T) = [\mathscr{U}_N^{oc}]\, \mathbf{P}_{\text{gauss}}(T) + [\phi_N^o]\, \mathbf{Q}_{\text{gauss}}(T) \,, \tag{D.37}$$

where $[\mathscr{U}_N^{oc}]$ is defined by Eq. (2.41). The realizations of random vector $\mathbf{H}_{\text{gauss}}$ with values in $\mathbb{R}^{N_{\text{PCA}}}$ are computed using Eq. (5.23) and the realizations of $\mathbf{P}_{\text{gauss}}(T)$ are computed by using Eq. (5.21) that is rewritten as

$$\mathbf{P}_{\text{gauss}}(T) \simeq \underline{\mathbf{p}}_T + \sum_{j=1}^{N_{\text{PCA}}} \sqrt{\Lambda_j}\, H_{\text{gauss},j}\, \mathbf{a}^j \,. \tag{D.38}$$

For the optimization problem defined by Eq. (5.37), the initial point $(\boldsymbol{\eta}^0, \mathbf{q}^0) \in \mathbb{R}^{N_{\text{PCA}}} \times \mathbb{R}^N$ is the solution of the optimization problem related to a Gaussian joint probability density function,

$$(\boldsymbol{\eta}^0, \mathbf{q}^0) = \arg\{\max_{(\boldsymbol{\eta},\mathbf{q})\in\mathbb{R}^{N_{\text{PCA}}}\times\mathbb{R}^N} \int_{\mathscr{D}^c} p_{\mathbf{H}_{\text{gauss}},\mathbf{Q}_{\text{gauss}}(T),\mathbf{U}_{\text{gauss}}(T)}(\boldsymbol{\eta},\mathbf{q},\mathbf{u})\, d\mathbf{u}\} \,. \tag{D.39}$$

# Appendix E

# Algebraic and numerical considerations to evaluate the cost functions for a separable domain

Taking into account Eq. (5.84), integral $I_\ell$ given by Eq. (5.72) can be rewritten as

$$I_\ell = \Pi_{i=1}^{m_u} \int_{\mathscr{D}^c_{\inf,i}}^{\mathscr{D}^c_{\sup,i}} \frac{1}{\sqrt{2\pi}\,\widehat{s}_n\,\widetilde{\sigma}_i} \exp\left\{-\frac{1}{2\widehat{s}_n^2}\frac{1}{\widetilde{\sigma}_i^2}(\frac{\widehat{s}_n}{s_n}u_i^\ell - u_i)^2\right\} du_i\,, \tag{E.1}$$

The term under the integral is the expression of a probability density function $p_{U_i}(u_i)$ of a Gaussian random variable $U_i$ with the mean value $\frac{\widehat{s}_n}{s_n}u_i^\ell$ and the variance $\widehat{s}_n^2\,\widetilde{\sigma}_i^2$. For $i$ fixed in $\{1,\ldots,m_u\}$, let $\xi_i$ be the normalized Gaussian random vector $(E\{\xi_i\}=0, E\{\xi_i^2\}=1)$,

$$\xi_i = \frac{1}{\widehat{s}_n\,\widetilde{\sigma}_i}(U_i - \frac{\widehat{s}_n}{s_n}u_i^\ell)\,. \tag{E.2}$$

Let $\alpha_i$ and $\beta_i$ be the parameters such that,

$$\alpha_i = \frac{1}{\widehat{s}_n\,\widetilde{\sigma}_i}(\mathscr{D}^c_{\inf,i} - \frac{\widehat{s}_n}{s_n}u_i^\ell) \quad \text{and} \quad \beta_i = \frac{1}{\widehat{s}_n\,\widetilde{\sigma}_i}(\mathscr{D}^c_{\sup,i} - \frac{\widehat{s}_n}{s_n}u_i^\ell)\,. \tag{E.3}$$

Consequently, integral $I_\ell$ is rewritten as

$$I_\ell = \Pi_{i=1}^{m_u}(F_{\xi_i}(\beta_i) - F_{\xi_i}(\alpha_i))\,, \tag{E.4}$$

in which $F_{\xi_i}$ is the cumulative distribution function of the Gaussian random variable $\xi_i$.

# Appendix F

# Generation of realizations of a Gaussian vector-valued process

For the first application devoted to Maine-Montparnasse Tower presented in Chapter 6, we need a generator of independent realization for a Gaussian vector-valued stochastic process. In this appendix, the extension proposed in [96] of Shinozuka's method [103] is used. The centered vector-valued stochastic process that models the longitudinal wind velocity $\{\mathbf{V}(t), t \in [0,T]\}$ with $\mathbf{V}(t) = (V_1(t), \ldots, V_{m_{\exp}}(t))$, is the restriction to interval $[0\,,T]$ of a Gaussian, stationary, second-order, centered, and mean-square continuous stochastic process indexed by $\mathbb{R}$ with values in $\mathbb{R}^{m_{\exp}}$. It is assumed that there is a positive-definite Hermitian matrix-valued spectral density function $[S_{\mathbf{V}}(\omega)]$ of $\{\mathbf{V}(t), t \in \mathbb{R}\}$. For all fixed $\omega$, the Cholesky decomposition of matrix $[S_{\mathbf{V}}(\omega)]$ is written as

$$[S_{\mathbf{V}}(\omega)] = [\mathscr{L}(\omega)]\,[\mathscr{L}(\omega)]^*\,, \tag{F.1}$$

in which $[\mathscr{L}(\omega)] \in \mathbb{M}_{m_{\exp}}(\mathbb{C})$ is a lower triangular complex matrix. Using the generator, $n_r$ independent realizations $\{\mathbf{V}(t,\theta^\ell), t \in [0,T]\}$ for $\ell = 1, \ldots, n_r$ of $\{\mathbf{V}(t), t \in \mathbb{R}\}$ are constructed, such that, for all $k = 1, \ldots, n_p$ and for all $j = 1, \ldots, m_{\exp}$,

$$V_j(t_k;\theta^\ell) \simeq \sqrt{2\Delta\omega}\,\mathrm{Re}\left\{\exp(-i\pi(1-\frac{1}{n_p})(k-1))\,\widetilde{V}_j(t_k;\theta^\ell)\right\}\,, \tag{F.2}$$

with

$$\widetilde{V}_j(t_k;\theta^\ell) = \sum_{q=1}^{n_p} \widehat{V}_j(\omega_q;\theta^\ell)\,\exp(\frac{2i\pi}{n_p}(k-1)(q-1))\,, \tag{F.3}$$

in which $\Delta\omega$ is the frequency step defined by Eq. (3.8) and where, for $q = 1, \ldots, n_p$ and for all $j$ and $j'$ in $\{1, \ldots, m_{\exp}\}$, we have

$$\widehat{V}_j(\omega_q;\theta^\ell) = \sum_{j'=1}^{m_{\text{exp}}} [\mathscr{L}(\omega_q)]_{jj'}\, [\Gamma(\theta^\ell)]_{j'q}\,, \tag{F.4}$$

with

$$[\Gamma(\theta^\ell)]_{j'q} = \sqrt{-\log[\mathscr{U}(\theta^\ell)]_{j'q}}\, \exp(2i\pi[\widetilde{\mathscr{U}}(\theta^\ell)]_{j'q})\,, \tag{F.5}$$

in which $[\mathscr{U}(\theta^\ell)]$ and $[\widetilde{\mathscr{U}}(\theta^\ell)]$ are realizations of random matrices with values in $\mathbb{M}_{m_{\text{exp}},n_p}(\mathbb{R})$ whose all their entries are independent random variables that are uniform on $[0,1]$ (the two random matrices are independent from all the other random variables used in the formulation and for each one of these random matrices all the entries are independent). Consequently, $\{\mathbf{V}(t;\theta^\ell), t \in [0,T]\}_{\ell=1,\ldots,n_r}$ are the $n_r$ independent realizations of Gaussian process $\{\mathbf{V}(t), t \in [0,T]\}$.

# Appendix G

# Gust Loading Factor

The notion of gust loading factor is not used in the methodology proposed for computing the equivalent static forces. Nevertheless, the gust loading factors of the responses are computed as a postprocessing from the direct estimate of extreme value statistics in order to compare the values obtained with respect to the common values that are well known for this type of quantity.

## G.1 Calculation of the gust loading factor from the direct extreme-value-statistics estimates for the general non-Gaussian case

Let $\mathbb{A}(t) = \underline{a} + A(t)$ be the stationary real-valued stochastic process (for instance $\mathbb{A}(t) = \{\mathbb{U}_j(t)$ or $Y_k(t)\}$) such that

$$\underline{a} = E\{\mathbb{A}(t)\} \quad , \quad E\{A(t)\} = 0\,. \tag{G.1}$$

Let $\mathbb{A}_{\max}$ be the random maximum and let $\mathbb{A}_{\min}$ be the random minimum of $\mathbb{A}(t)$ on $[0, T]$,

$$\mathbb{A}_{\max} = \max_{t\in[0,T]} \mathbb{A}(t) = \underline{a} + \max_{t\in[0,T]} A(t)\,, \tag{G.2}$$

and

$$\mathbb{A}_{\min} = \min_{t\in[0,T]} \mathbb{A}(t) = \underline{a} + \min_{t\in[0,T]} A(t)\,. \tag{G.3}$$

For a given duration $T$, let $g^+$ and $g^-$ be the gust loading factors for the maximum and for the minimum on $[0\,, T]$ of stochastic process $\mathbb{A}$, which are defined by the following equations

$$E\{\mathbb{A}_{\max}\} = \underline{a} + g^+\,\sigma_A\,, \tag{G.4}$$

$$E\{\mathbb{A}_{\min}\} = \underline{a} - g^-\,\sigma_A\,, \tag{G.5}$$

in which $\sigma_A$ is the standard deviation of the centered random variable $A(t)$, which is equal to the standard deviation $\sigma_{\mathbb{A}}$ of the random vector $\mathbb{A}(t)$, these standard deviations being independent of $t$. It can be deduced that

$$g^+ = \frac{E\{\mathbb{A}_{\max}\} - \underline{a}}{\sigma_A} = \frac{E\{A_{\max}\}}{\sigma_A}\,, \tag{G.6}$$

$$g^- = \frac{-E\{\mathbb{A}_{\min}\} + \underline{a}}{\sigma_A} = \frac{-E\{A_{\min}\}}{\sigma_A}\,, \tag{G.7}$$

in which

$$A_{\max} = \max_{t\in[0,T]} A(t) \quad , \quad A_{\min} = \min_{t\in[0,T]} A(t)\,. \tag{G.8}$$

## G.2 Calculation of the gust loading factor using a Gaussian approximation and the usual asymptotic hypothesis

Let us assume that the real-valued stochastic process $\{A(t), t \in \mathbb{R}\}$ is Gaussian, second-order, centered, stationary, and satisfying additional technical hypotheses [77], which are not given here. For a given duration $T$, it is assumed that the point process of upcrossings of level $a$ has an asymptotic Poisson distribution. Under these conditions, the cumulative distribution function, $F_{A_{\max}}(a)$, of $A_{\max} = \max_{t\in[0,T]} A(t)$, is written as

$$F_{A_{\max}}(a) = P(A_{\max} \leq a) = \left\{ \begin{array}{ccc} \exp\{-\mu(a)\} & \text{if} & a > 0 \\ 0 & \text{if} & a \leq 0 \end{array} \right. , \tag{G.9}$$

where $\mu(a)$ is the mean number of upcrossings by level $a$ of stochastic process $A$ on $[0\,, T]$, which, for a stationary Gaussian stochastic process, is given by the following Rice formula,

$$\mu(a) = \nu\, T\, \exp\{-\frac{a^2}{2\,\sigma_A^2}\}\,, \tag{G.10}$$

in which $\nu$ is called the apparent frequency that is given by

$$\nu = \frac{1}{2\pi}\,\frac{\sigma_{\dot{A}}}{\sigma_A}\,, \tag{G.11}$$

where $\sigma_A$ is the standard deviation of $A(t)$ and where $\sigma_{\dot{A}}$ is the standard deviation of the mean-square derivative $\dot{A}(t)$ of $A(t)$ at time $t$. The gust loading factor for the maximum, denoted by $g_{\text{gauss}}$, is thus defined by

$$g_{\text{gauss}} = \frac{E\{A_{\max}\}}{\sigma_A}\,, \tag{G.12}$$

where $E\{A_{\max}\}$ is such that

$$E\{A_{\max}\} = \int_0^{+\infty} a\, p_{A_{\max}}(a)\, da = \int_0^{+\infty} a\, d(F_{A_{\max}}(a))\,. \tag{G.13}$$

In this thesis, the right-hand side of Eq. (G.13) is computed by using the centered trapezoidal rule and not by introducing an additional approximation that allows for obtaining the very classical formula [32]

$$g_{\text{gauss}} = \sqrt{2\log(\nu T)} + \frac{\gamma}{\sqrt{2\log(\nu T)}}\,, \tag{G.14}$$

in which $\gamma \simeq 0.5772$ is the Euler constant.

# Appendix H

# Parameters and models for the Maine-Montparnasse Tower application

## H.1 Finite element model

The properties of the Timoshenko beam finite element of the computational model of the Maine-Montparnasse Tower are listed in Table H.1.

| Element | 1 | 2 | 3 | 4 | 5 | 6 | 7 | 8 | 9 | 10 |
|---|---|---|---|---|---|---|---|---|---|---|
| length (m) | 10 | 10 | 12.5 | 12.5 | 8.75 | 8.75 | 8.75 | 8.75 | 11.25 | 11.25 |
| linear mass $\times 10^3$ (Kg/m) | 2550 | 2550 | 470 | 470 | 470 | 470 | 470 | 470 | 470 | 470 |
| bending inertia ($m^4$) | 19200 | 19200 | 4525 | 4525 | 3574 | 3574 | 3574 | 3574 | 2682 | 2682 |
| Element | 11 | 12 | 13 | 14 | 15 | 16 | 17 | 18 | 19 | 20 |
| length (m) | 11.25 | 11.25 | 11.25 | 11.25 | 11.25 | 11.25 | 12.5 | 12.5 | 12.5 | 13.84 |
| linear mass $\times 10^3$ (Kg/m) | 470 | 470 | 470 | 470 | 470 | 470 | 470 | 470 | 470 | 470 |
| bending inertia ($m^4$) | 2682 | 2682 | 1744 | 1744 | 1744 | 1744 | 980 | 980 | 980 | 980 |

Table H.1: Properties of the Timoshenko beam finite element of the computational model of the Maine-Montparnasse Tower.

- Young's modulus $E = 4.3 \times 10^{10}$ Pa
- Poisson's ratio: $\nu = 0.3$
- Shear correction factor: $k_s = 5/6$
- Shear modulus: $G = E/2(1 + \nu)$ Pa
- Width of the Tower along the axis $oy = 40$
- Section area: $A = 40 \times 61.8$ m$^2$

- Constant of elasticity of the rotation around $oy$ of the foundation at node 1: $9.0909 \times 10^{12}$ N $\times$ m/rad
- Moment of inertia for the rotation around $oy$ of the foundation at node 1: $1.4 \times 10^{11}$ Kg $\times$ m$^2$ /rad

These last two values have been updated in the finite element model in order to obtain both the flexibility that was measured at the top of the Tower and the two first eigenfrequencies that were measured [16, 77].

## H.2 Model of the longitudinal velocity field of wind

Hereinafter, we describe a stochastic model of the the longitudinal velocity field $\{\mathbb{V}(z,t)\}_{(z,t)}$ in terms of its mean profile, $\{\underline{v}(z)\}_z$, and of its centered statistical fluctuations $\{V(z,t)\}_{(z,t)}$.

### H.2.1 Parameters of the mean wind profile [77]

The Maine-Montparnasse Tower is located in the roughness zone of class V (city). The numerical values of the parameters related to the mean wind profile defined by Eq. (6.2) are:

- the reference mean wind velocity: $\underline{V}_R = 17$ m/s.
- the roughness length: $z_0 = 2.5$ m.
- the terrain factor $k_r$ depending on the roughness length $z_0$: $k_r = 0.292$.
- the displacement height for the wind generation: $d_r = 35.5$ m.

### H.2.2 Cross-spectral density function of $\{V(z,t)\}_{(z,t)}$

The cross-spectral density function of stochastic field $\{V(z,t)\}_{(z,t)}$, which is stationary in $t$, is given (see for instance [7, 25, 30, 38, 77, 107]) by

$$S_V(z,z',\omega) = \sqrt{\gamma_V^2(z,z',\omega)\, S_V(z,\omega)\, S_V(z',\omega)}\,, \tag{H.1}$$

where $\gamma_V^2(z,z',\omega)$ is the spatial coherence function, which is written as

$$\sqrt{\gamma_V^2(z,z',\omega)} \simeq C \times \exp\left(-\frac{|\omega|}{2\pi \underline{V}_R} C_z |z-z'|\right). \tag{H.2}$$

The constant $C_z$ is equal to 6 and the constant $C$ is computed to take into account, in a spatial meaning, the lateral fluctuations according to the coordinate $y$, which are not taken into account in the model. By using the following spatial coherence in $y$ and $z$,

$$\sqrt{\gamma^2_{\mathbf{v}}(z,z',\omega)} = \exp\left(-\frac{|\omega|}{2\pi \underline{V}_R}\sqrt{C_y^2(y-y')^2 + C_z^2(z-z')^2}\right), \tag{H.3}$$

in which $C_y = C_z = 6$, the constant $C$ can be estimated by

$$C \times L^2 = \int_0^L \int_0^L \exp\left(-\frac{|\omega_1|}{2\pi \underline{V}_R} C_y |y-y'|\right) dy\, dy' . \tag{H.4}$$

For $\underline{V}_R = 17$ m/s, $\omega_1 = 2\pi \times 0.2$ rad/s, and $L = 61.8$ m, the calculation of $C$ given by Eq. (H.4) yields $C = 0.36$.

### H.2.3 One-sided power spectral density function of the longitudinal velocity field $\{V(z,t)\}_t$

The Harris model is used [25, 55, 77, 107]. For all fixed $z$, the one-sided power spectral density function $S_V(z,\omega)$ of process $\{V(z,t)\}_t$ that is stationary in $t$, is then given, for $\omega \geq 0$, by

$$\frac{2\,\omega\, S_V(z,\omega)}{\sigma_V^2(z)} = \lambda \frac{f}{(2+f^2)^{5/6}}, \tag{H.5}$$

in which $\lambda$ is a constant taken equal to $0.6$, where the reduced frequency $f$ is independent of $z$ and is given by

$$f = \frac{1800\,\omega}{2\pi \underline{V}_R}. \tag{H.6}$$

For fixed $z$ and fixed $t$, the standard deviation of the real random variable $V(z,t)$ is independent of $t$ (stationary) and is taken independent of $z$,

$$\sigma_V(z) = K \underline{V}_R, \tag{H.7}$$

in which $K$ is a constant taken equal to $0.234$.

## H.3 Parameters of signal processing

The parameters for the time and frequency samplings for digital signal processing are the following.

- Dimension of random vector $\mathbb{P}(t)$: $m_{\text{exp}} = 17$.
- Cutoff frequency: $\nu_c = 1.37$ Hz and $\omega_c = 8.6$ rad/s.
- Sampling frequency: $\nu_e = 2.64$ Hz.
- Sampling time step: $\Delta t = 1/\nu_e = 0.365$ s.
- Duration of the time window: $T \simeq 748$ s.
- Number of time steps in the time window: $n_p = 2048$.

## H.4 Construction of the controlability matrix

In this application, for all fixed $t$, the time-independent controlability matrix defined by Eq. (2.7), which allows for transforming the vector $\mathbb{P}(t)$ of pressures into the vector $\mathbf{F}(t)$ of external nodal forces,

$$\mathbf{F}(t) = [A_c]\,\mathbb{P}(t) \quad , \quad t \in \mathbb{R}\,, \tag{H.8}$$

is constructed by considering a uniform pressure along each finite element and consequently, the nodal force at each node is equal to this pressure multiplied by the area subjected to wind effects.

# Bibliography


[1] Andrews H, Patterson C. Singular value decomposition and digital image processing. *Transactions on Acoustics, Speech, and Signal Processing - IEEE*, 24(1):26–53, 1976.

[2] Arnst M, Ghanem R, Soize C. Identification of Bayesian posteriors for coefficients of chaos expansions. *Journal of Computational Physics*, 229(9):3134–3154, 2010.

[3] Bathe JK, Wilson EL. *Numerical Methods in Finite Element Analysis*. Prentice-Hall, New York, 1976.

[4] Bellanger M. *Traitement Numérique du Signal (Digital Signal Processing)*. Masson, Paris, 1993.

[5] Bienkiewicz B, Tamura Y, Ham HJ Ueda H, Hibi K. Proper orthogonal decomposition and reconstruction of multi-channel roof pressure. *Journal of Wind Engineering and Industrial Aerodynamics*, 54:369–381, 1995.

[6] Biétry J, Delaunay D, Conti E. Comparison of full-scale measurement and computation of wind effects on a cable-stayed bridge. *Journal of Wind Engineering and Industrial Aerodynamics*, 57(2-3):225–235, 1995.

[7] Biétry J, Simiu E, Sacré C. Mean wind profiles and charge of terrain roughness. *Journal of the Structural Division*, 104(10):1585–1593, 1978.

[8] Blaise N, Canor T, Denoël V. Reconstruction of the envelope of non-Gaussian structural responses with principal static wind loads . *Journal of Wind Engineering and Industrial Aerodynamics*, 149:59 – 76, 2016.

[9] Blaise N, Denoël V. Principal static wind loads. *Journal of Wind Engineering and Industrial Aerodynamics*, 113:29–39, 2013.

[10] Blaise N, Denoël V. Adjusted equivalent static wind loads for non-gaussian linear static analysis. In *14th International Conference on Wind Engineering*, Porto Alegre, Brazil, June 21-26 2015.

[11] Blatman G, Sudret B. An adaptive algorithm to build up sparse polynomial chaos expansions for stochastic finite element analysis. *Probabilistic Engineering Mechanics*, 25(2):183–197, 2010.

[12] Blatman G, Sudret B. Adaptive sparse polynomial chaos expansion based on least angle regression. *Journal of Computational Physics*, 230(6):2345–2367, 2011.

[13] Bowman AW, Azzalini A. *Applied Smoothing Techniques for Data Analysis*. Oxford University Press, Oxford, 1997.

[14] Byrd RH, Hribar ME, Nocedal J. An interior point algorithm for large-scale nonlinear programming. *SIAM Journal on Optimization*, 9(4):877–900, 1999.

[15] Carlin BP, Louis TA. *Bayesian Methods for Data Analysis*. Chapman & Hall / CRC Press, Boca Raton, third edition, 2009.

[16] CEBTP (Center for Research and Studies for Buildings and Public Works). Effets du vent sur la Tour Maine-Montparnasse. Technical report, 15 June 1978. Comlpementary report 1st October 1978.

[17] Chatelin F. *Eigenvalues of Matrices*. Wiley, New York, 1993.

[18] Chen X, Kareem A. Equivalent static wind loads for buffeting response of bridges. *Journal of Structural Engineering*, 127(12):1467–1475, 2001.

[19] Chen X, Kareem A. Equivalent static wind loads on buildings : New model. *Journal of Structural Engineering*, 130(10):1425–1435, 2004.

[20] Chen X, Kareem A. Proper orthogonal decomposition-based modeling, analysis, and simulation of dynamic wind load effects on structures. *Journal of Engineering Mechanics*, 131(4):325–339, 2005.

[21] Chen X, Zhou N. Equivalent static wind loads on low-rise buildings based on full-scale pressure measurements. *Engineering Structures*, 29(10):2563–2575, 2007.

[22] Clough RW, Penzien J. *Dynamic of Structures*. McGraw-Hill, New York, 1975.

[23] Congdon P. *Bayesian Statistical Modelling*. John Wiley & Sons, Chichester, second edition, 2007.

[24] Cook NJ, Mayne JR. A novel working approach to the assessment of wind loads for equivalent static design. *Journal of Wind Engineering and Industrial Aerodynamics*, 4(2):149–164, 1979.

[25] Counihan JO. Adiabatic atmospheric boundary layers: A review and analysis of data from period 1880-1972. *Atmospheric Environment (1967)*, 9(10):871–905, 1975.

[26] Cramer H, Leadbetter MR. *Stationary and Related Stochastic Processes*. John Wiley & Sons, New York, 1967.

[27] Das S, Ghanem R, Spall JC. Asymptotic sampling distribution for polynomial chaos representation from data: a maximum entropy and fisher information approach. *SIAM Journal on Scientific Computing*, 30(5):2207–2234, 2008.

[28] Dautray R, Lions JL. *Mathematical Analysis and Numerical Methods for Science and Technology*. Springer-Verlag, Berlin, 1990.

[29] Davenport AG. The application of statistical concepts of the wind loading of structures. *Proceeding of the Institution of Civil Engineers*, 19(4):449–472, 1961.

[30] Davenport AG. The spectrum of horizontal gustiness near the ground in high winds. *Quarterly Journal of the Royal Meteorological Society*, 87(372):194–211, 1961.

[31] Davenport AG. Note on the distribution of the largest value of a random function with application to gust loading. *Proceedings, Institution of Civil Engineers*, 28(2):187–196, 1964.

[32] Davenport AG. Gust loading factors. *Journal of Structural Division - ASCE*, 93(3):11–34, 1967.

[33] Davenport AG. How can we simplify and generalize wind loads? *Journal of Wind Engineering and Industrial Aerodynamics*, 54:657–669, 1995.

[34] Debusschere BJ, Najm HN, Pebay PP, Knio OM, Ghanem RG, Le Maître OP. Numerical challenges in the use of polynomial chaos representations for stochastic processes. *SIAM Journal on Scientific Computing*, 26(2):698–719, 2004.

[35] Desceliers C, Ghanem R, Soize C. Maximum likelihood estimation of stochastic chaos representations from experimental data. *International Journal of Numerical Methods in Engineering*, 66(6):978–1001, 2006.

[36] Doob JL. *Stochastic Processes*. John Wiley & Sons, New York, 1990.

[37] Doostan A, Ghanem R, Red-Horse J. Stochastic model reduction for chaos representations. *Computer Methods in Applied Mechanics and Engineering*, 196(37):3951–3966, 2007.

[38] Duchène-Marullaz P. Full-scale measurements of atmospheric turbulence in a suburban area. In *Proceedings of the Fourth International Conference on Wind Effects on Buildings and Structures*, pages 23–31, Heathrow, United Kingdom, 1975. Edited by KJ Eaton, Building Research Establishment.

[39] Ellingwood BR, Tekie PB. Wind load statistics for probability-based structural design. *Journal of Structural Engineering - ASCE*, 46(2):453–463, 1999.

[40] Ernst OG, Mugler A, Starkloff HJ, Ullmann E. On the convergence of generalized polynomial chaos expansions. *ESAIM Mathematical Modelling and Numerical Analysis*, 2(46):317–339, 2012.

[41] Flamand O, De Oliveira F, Stathopoulos-Vlamis A, Papanikolas P. Conditions for occurrence of vortex shedding on a large cable stayed bridge: Full scale data from monitoring system. *Journal of Wind Engineering and Industrial Aerodynamics*, 135:163–169, 2014.

[42] Fu J, Xie Z, Li QS. Closure to equivalent static wind loads on long-span roof structures. *Journal of Structural Engineering - ASCE*, 136(4):470–471, 2010.

[43] Fung YC. *Foundations of Solid Mecanics*. Prentice Hall, Englewood Cliffs, New Jersey, 1968.

[44] Geradin M, Rixen D. *Mechanical Vibrations, Theory and Applications to Structural Dynamics*. Wiley, Chichester, second edition, 1997.

[45] Gerbrands JJ. On the relationships between SVD, KLT and PCA. *Pattern Recognition*, 14(1-6):375–381, 1981.

[46] Ghanem R, Doostan R. Characterization of stochastic system parameters from experimental data: A bayesian inference approach. *Journal of Computational Physics*, 217(1):63–81, 2006.

[47] Ghanem R, Spanos PD. *Stochastic Finite Elements: a Spectral Approach*. Springer-Verlag, New York, 1991. See also the revised edition (2003),Dover Publications, New York.

[48] Gill PE, Murray W, Wright MH. *Practical Optimization*. Academic Press, London, 1981.

[49] Givens GH, Hoeting JA. *Computational Statistics*. Wiley, New York, second edition, 2013.

[50] Golub GH, Van Loan CF. *Matrix Computations*. The Johns Hopkins University Press, Baltimore, fourth edition, 2013.

[51] Grimmond CSB. Aerodynamic roughness of urban areas derived from wind observations. *Boundary-Layer Meteorology*, 89(1):1–24, 1998.

[52] Gu M, Huang Y. Equivalent static wind loads for stability design of large span roof structures. *Wind and Structures*, 20(1):95–115, 2015.

[53] Guikhman L, Skorkhod AV. *The Theory of Stochastic Processes*. Springer-Verlag, Berlin, 1979.

[54] Guilleminot J, Soize C. Stochastic model and generator for random fields with symmetry properties: application to the mesoscopic modeling of elastic random media. *Multiscale Modelling Simulation (A SIAM Interdisciplinary Journal)*, 11(3):840–870, 2013.

[55] Harris RI. The nature of the wind. In Institution Of Civil Engineers, editor, *Seminar in the Modern Design of Wind-Sensitive Structures*, Construction Industry Research and Information Association, pages 29–55, London, England, 1970.

[56] Heck JV. Référentiel relatif aux dispositions constructives et aux justifications en zone sismique des systèmes de revêtements muraux attachés en pierres minces à attaches disposées dans les champs verticaux des pierres. Technical Report CTMNC - CSTB-DSSF/IS 31-05-2010, CSTB, Champs-sur-Marne, France, 2010.

[57] Hillewaere J, Degroote J, Lombaert G, Vierendeels J, Degrande G. Computational aspects of simulating wind induced ovalling vibrations in silo groups. *Journal of Computational and Applied Mathematics*, 246:161–173, 2013.

[58] Hillewaere J, Degroote J, Lombaert G, Vierendeels J, Degrande G. Wind-structure interaction simulations of ovalling vibrations in silo groups. *Journal of Fluids and Structures*, 59:328–350, 2015.

[59] Holmes JD. Optimised peak load distributions. *Journal of Wind Engineering and Industrial Aerodynamics*, 41(1-3):267–276, 1992.

[60] Holmes JD. Effective static load distributions in wind engineering. *Journal of Wind Engineering and Industrial Aerodynamics*, 90(2):91–109, 2002.

[61] Horova I, Kolacek J, Zelinka J. *Kernel Smoothing in Matlab*. World Scientific, Singapor, 2012.

[62] Huang G, Chen X. Wind load effects and equivalent static wind loads of tall buildings based on synchronous pressure measurements. *Engineering Structures*, 29(10):2641–2653, 2007.

[63] Huang TS. *Picture Processing and Digital Filtering*. Springer, Berlin, 1975.

[64] Hughes TJR. *The Finite Element Method: Linear Static and Dynamic Finite Element Analysis*. Dover Publications, New York, 2000.

[65] Irwin PA. Wind engineering challenges of the new generation of supertall buildings. *Journal of Wind Engineering and Industrial Aerodynamics*, 97(7):328–334, 2009.

[66] Isakov V. *Inverse Problems for Partial Differential Equations*. Springer-Verlag, New York, 2006.

[67] Jain AK, Marty MN, Flynn PJ. Data clustering: a review. *ACM Computing Surveys (CSUR)*, 31(3):264–323, 1991.

[68] Jenkins GM, Watt DG. *Spectral Analysis and its Applications*. Holden Day, San Francisco, 1968.

[69] Jolliffe I. *Principal component analysis*. Springer-Verlag, New York, 2002.

[70] Kaipio J, Somersalo E. *Statistical and Computational Inverse Problems*. Springer-Verlag, New York, 2005.

[71] Kareem A. Dynamic response of high-rise buildings to stochastic wind loads. *Journal of Wind Engineering and Industrial Aerodynamics*, 42(1-3):1101–1112, 1992.

[72] Karhunen K. Uber lineare methoden in der wahrscheinlichkeitsrechnung. *American Academy of Science, Fennicade Series A, I*, 37:3–79, 1947.

[73] Kasperski M. Extreme wind load distributions for linear and nonlinear design. *Engineering Structure*, 14(1):27–34, 1992.

[74] Kasperski M, Niemann HJ. On the correlation of dynamic wind loads and structural response of natural-draught cooling towers. *Journal of Wind Engineering and Industrial Aerodynamics*, 30(1-3):67–75, 1988.

[75] Kasperski M, Niemann HJ. The L.R.C (load-response-correlation)-Method. A General Method of Estimating Unfavourable Wind Load. Distributions for Linear and Non-linear Structural Behaviour. *Journal of Wind Engineering and Industrial Aerodynamics*, 43(1-3):1753–1763, 1992.

[76] Katsumara A, Tamura Y, Nakamura O. Universal wind load distribution simultaneously reproducing largest load effects in all subject members on large-span cantilevered roof. *Journal of Wind Engineering and Industrial Aerodynamics*, 95(9):1145–1165, 2007.

[77] Krée P, Soize C. *Mathematics of Random Phenomena*. Reidel, New York, 1986. French version: Mécanique Aléatoire, Dunod, Paris, 1983.

[78] Kumar KS, Stathopoulos T. Wind loads on low building roofs: A stochastic perspective. *Journal of Structural Engineering - ASCE*, 126(8):944–956, 2000.

[79] Le Maître OP, Knio OM. *Spectral Methods for Uncertainty Quantification with Applications to Computational Fluid Dynamics*. Springer, Heidelberg, 2010.

[80] Leadbetter MR. On Crossings of Levels and Curves by a Wide Class of Stochastic Processes. *Annales of Mathematical Statistics*, 37, 1966.

[81] Liang SG, Zou LH, Wang DH, Huang GQ. Analysis of three dimensional equivalent static wind loads of symmetric high-rise buildings based on wind tunnel tests. *Journal of Wind and Structures*, 19(5):565–583, 2014.

[82] Loève M. Fonctions aléatoires du second ordre, supplément à P. Levy. In *Processus Stochastique et Mouvement Brownien*, Paris, 1948. Gauthier Villars.

[83] Lou W, Zhang L, Huang MF, Li QS. Multiobjective equivalent static wind loads on complex tall buildings using non-gaussian peak factors. *Journal of Structural Engineering*, 141(11):04015033, 2015.

[84] Lu CL, Huang SH, Tuan AY, Zhi LH, Su S. Evaluation of wind loads and wind induced responses of a super-tall building by large eddy simulation. *WIND AND STRUCTURES*, 23(4):313–350, 2016.

[85] Ludeman LC. *Fundamentals of Digital Signal Processing*. Harper and Row, New York, 1986.

[86] Marzouk YM, Najm HN. Dimensionality reduction and polynomial chaos acceleration of bayesian inference in inverse problems. *Journal of Computational Physics*, 228(6):1862–1902, 2009.

[87] Meirovitch L. *Dynamics and Control of Structures*. Wiley, New York, 1980.

[88] Meirovitch L. *Computational Methods in Structural Dynamics*. Sijthoff and Noordhoff, The Netherlands, 1990.

[89] Metivier M. *Nations Fondamentales de la Théorie des Probabilités*. Dunod, Paris, 1968.

[90] Nouy A, Soize C. Random field representations for stochastic elliptic boundary value problems and statistical inverse problems. *European Journal of Applied Mathematics*, 25(3):339–373, 2014.

[91] Ohayon R, Soize C. *Structural Acoustic and Vibration*. Academic Press, San Diego, London, 1998.

[92] Oppenheim AV, Schaffer RN. *Digital Signal Processing*. Prentice Hall, Englewood Cliffs, New Jersy, 1975.

[93] Papoulis A. *Signal Analysis*. McGraw-Hill, New York, 1977.

[94] Patruno L, Ricci M, de Miranda S, Ubertini F. An efficient approach to the determination of Equivalent Static Wind Loads. *Journal of Fluids and Structures*, 68:1–14, 2017.

[95] Perrin G, Soize C, Duhamel D, Funfschilling C. Identification of polynomial chaos representations in high dimension from a set of realizations. *SIAM Journal on Scientific Computing*, 34(6):A2917–A2945, 2012.

[96] Poirion F, Soize C. Numerical methods and mathematical aspects for simulation of homogeneous and non homogeneous Gaussian vector fields. In P. Krée and W. Wedig, editors, *Probabilistic Methods in Applied Physics*, pages 17–53. Springer-Verlag, Berlin, 1995.

[97] Priestley MB. *Spectral Analysis and Time Series*. Academic Press, New York, 1981.

[98] Repetto MP, Solari G. Equivalent static wind actions on vertical structures. *Journal of Wind Engineering and Industrial Aerodynamics*, 92(5):335–357, 2004.

[99] Rice SO. Mathematical Analysis of Random Noise. *Bell System Technical Journal*, 18, 1944.

[100] Rice SO. Mathematical Analysis of Random Noise. *Bell System Technical Journal*, 19, 1945.

[101] Sacré C, Moisselin JM, Sabre M, Flori JP, Dubuisson B. A new statistical approach to extreme wind speeds in France. *Journal of Wind Engineering and Industrial Aerodynamics*, 95(9):1415–1423, 2007.

[102] Serfling RJ. *Approximation Theorems of Mathematical Statistics*. John Wiley & Sons, New York, 1980.

[103] Shinozuka M. Simulation of Multivariate and Multidimensional Random Processes. *The Journal of the Acoustical Society of America*, 49(1B):357–367, 1971.

[104] Simiu E. Gust factors and alongwind pressure correlations. *Journal of the Structural Division - ASCE*, 99(4):773–783, 1973.

[105] Simiu E. Equivalent static wind loads for tall building design. *Journal of the Structural Division - ASCE*, 102(4):719–737, 1976.

[106] Simiu E, Filliben JJ, Bietry J. Sampling errors in estimation of extreme winds. *Journal of Structure Division - ASCE*, 104(3):491–501, 1978.

[107] Simiu E, Scanlan RH. *Wind Effects on Structures. Fundamentals and Applications to Design*. John Wiley & Sons, New York, third edition, 1996.

[108] Soize C. Gust loading factors with nonlinear pressure termes. *Journal of Structure division - ASCE*, 104(6):991–1007, 1978.

[109] Soize C. Oscillators submitted to squared Gaussian processes. *Journal of Mathematical Physics*, 21(10):2500–2507, 1980.

[110] Soize C. *Méthodes Mathématiques en Analyse du Signal*. Masson, Paris, 1993.

[111] Soize C. *The Fokker-Planck Equation for Stochastic Dynamical Systems and its Explicit Steady State Solutions*. World Scientific, Singapore, 1994.

[112] Soize C. Identification of high-dimension polynomial chaos expansions with random coefficients for non-Gaussian tensor-valued random fields using partial and limited experimental data. *Computer methods in applied mechanics and engineering*, 199(33-36):2150–2164, 2010.

[113] Soize C. Polynomial chaos expansion of a multimodal random vector. *SIAM/ASA Journal on Uncertainty Quantification*, 3(1):34–60, 2015.

[114] Soize C. Optimal partition in terms of independant random vectors of any non-Gaussian vector defined by a set of realizations. *SIAM/ASA Journal of uncertainty qualification* , 5(1):176–211, 2017.

[115] Soize C. *Uncertainty quantification. An Accelerated Course with Advanced Applications in Computational Engineering*. Springer, New York, 2017.

[116] Soize C. *Fundamentals of Random Signal Analysis. Application to Modal Identification in Structural Dynamics*. Course given at PUC-Rio University, Rio de Janeiro, Brazil, August 19-23, 1996, Final Edition, Paris, 1997.

[117] Soize C, Desceliers C. Computational aspects for constructing realizations of polynomial chaos in high dimension. *SIAM Journal on Scientific Computing*, 32(5):2820–2831, 2010.

[118] Soize C, Farhat C. A nonparametric probabilistic approach for quantifying uncertainties in low-dimensional and high-dimensional nonlinear models. *International Journal for Numerical Methods in Engineering*, 109(6):837–888, 2017.

[119] Soize C, Ghanem R. Physical systems with random uncertainties : Chaos representation with arbitrary probability measure. *SIAM Journal on Scientific Computing*, 26(2):395–410, 2004.

[120] Soize C, Ghanem R. Polynomial chaos representation of databases on manifolds. *Journal of Computational Physics*, 335:201–221, 2017.

[121] Solari G. Mathematical model to predict 3-D wind loading on buildings. *Journal of Engineering Mechanics - ASCE*, 111(2):254–276, 1985.

[122] Solliec C, Mary J. Simultaneous measurements of fluctuating pressures using piezoresistive multichannel transducers as applied to atmospheric wind tunnel tests. *Journal of Wind Engineering and Industrial Aerodynamics*, 56(1):71–86, 1995.

[123] Spall JC. *Introduction to Stochastic Search and Optimization*. John Wiley & Sons, Hoboken, 2003.

[124] Stuart AM. Inverse problems: A bayesian perspective. *Acta Numerica*, 19:451–559, 2010.

[125] Sun W, Gu M, Zhou X. Universal equivalent static wind loads of fluctuating wind loads on large-span roofs based on POD compensation. *Advances in Structural Engineering*, 18(9):1443–1459, 2015.

[126] Tamura Y, Suganuma S, Kikuchi H, Hibi K. Proper orthogonal decomposition of random wind pressure field. *Journal of Fluids and Structures*, 13(7):1069–1095, 1999.

[127] Tarantola A. *Inverse problem Theory and Methods for Model Parameter Estimation*. SIAM, Philadelphia, 2005.

[128] Tipireddy R, Ghanem R. Basis adaptation in homogeneous chaos spaces. *Journal of Computational Physics*, 259:304–317, 2014.

[129] Truesdell C. *Encyclopedia of Physics, Vol VIa/3, Mechanics of Solids III*. Springer-Verlag, Berlin, Heidelberg, New York, 1973.

[130] Uematsu Y, Moteki T, Hongo T. Model of wind pressure field on circular flat roofs and its application to load estimation. *Journal of Wind Engineering and Industrial Aerodynamics*, 96(6):1003–1014, 2008.

[131] Uematsu Y, Yamada M, Inoue A, Hongo T. Wind loads and wind-induced dynamic behavior of a single-layer latticed dome. *Journal of Wind Engineering and Industrial Aerodynamics*, 66(3):227–248, 1997.

[132] Vaicaitis R, Shinozuka M, Takeno M. Parametric study of wind loading on structures. *Journal of Structural Division - ASCE*, 99(3):453–468, 1973.

[133] Vaicaitis R, Simiu E. Nonlinear pressure terms and along-wind response. *Journal of the Structural Division - ASCE*, 103(4):903–906, 1977.

[134] Vickery BJ, Danveport AG. A comparison of theoretical and experimental determination of the response of elastic structures to turbulent flow. In *Proceedings of the Second Conference on Wind Effects on Buildings and Structures*, volume 1, pages 705–738, Ottawa, Canada, 1967.

[135] Vinet J, De Oliveira F. Etude aérodynamiques de dimensionnement au vent du stade de Nice. Technical Report EN-CAPE 11.056 C-V1, CSTB, Nantes, France, 2011. Rapport confidentiel.

[136] Vinet J, De Oliveira F. Etudes aérodynamiques de dimensionnement au vent du Stade Vélodrome de Marseille : nouvelles configurations. Technical Report EN-CAPE 11.114 C V2, CSTB, Nantes, France, 2011.

[137] Vinet J, De Oliveira F, Barre C, Fayette E, Consigny F, Vondiere R. Wind effects on stadium refurbishment the example of Stade Velodrome in Marseille, France. In *Proceedings of the 14th International Conference on Wind Engineering (ICWE14)*, pages 1–10, Porto Alegre, Brazil, June 21-26 2015.

[138] Walter E, Pronzato L. *Identification of Parametric Models from Experimental Data*. Springer-Verlag, Berlin, 1997.

[139] Xiu DB, Karniadakis GE. The Wiener-Askey polynomial chaos for stochastic differential equations. *SIAM Journal on Scientific Computing*, 24(2):619–644, 2002.

[140] Yang QS, Chen B, Wu Y, Tamura Y. Wind-Induced Response and Equivalent Static Wind Load of Long-Span Roof Structures by Combined Ritz-Proper Orthogonal Decomposition Method. *Journal of Structural Engineering - ASCE* , 139(6):997–1008, 2013.

[141] Yi J, Zhang JW, Li QS. Dynamic characteristics and wind-induced responses of a super-tall building during typhoons. *Journal of Wind Engineering and Industrial Aerodynamics*, 121:116–130, 2013.

[142] Zhang X, Yao M. Numerical investigation on the wind stability of super long-span partially earth-anchored cable-stayed bridges. *Wind and Structures*, 21(4):407–424, 2015.

[143] Fang M Zhi L, Li QS. Identification of Wind Loads and Estimation of Structural Responses of Super-Tall Buildings by an Inverse Method.

[144] Zhou X, Gu M. An approximation method for computing the dynamic responses and equivalent static wind loads of large-span roof structures. *International Journal of Structural Stability and Dynamics*, 10(5):1141–1165, 2010.

[145] Zhou Y, Gu M, Xiang HF. Alongwind static equivalent wind loads and responses of tall buildings. Part I: Unfavorable distributions of static equivalent wind loads. *Journal of Wind Engineering and Industrial Aerodynamics*, 79(1):135–150, 1999.

[146] Zhou Y, Gu M, Xiang HF. Alongwind static equivalent wind loads and responses of tall buildings. Part II: Effects of mode shapes . *Journal of Wind Engineering and Industrial Aerodynamics*, 79(1-2):151–158, 1999.

[147] Zienkiewicz OC, Taylor RL. *The Finite Element Method For Solid And Structural Mechanics*. Elsevier, Butterworth-Heinemann, Amsterdam, sixth edition edition, 2005.